Quantification of cooling effects and water demand of urban facade greenings

vorgelegt von
M.Sc.
Marie-Therese Hölscher
geb. in Paderborn

von der Fakultät VI - Planen Bauen Umwelt
der Technischen Universität Berlin
zur Erlangung des akademischen Grades

Doktor der Naturwissenschaften
-Dr. rer. nat.-

genehmigte Dissertation

Promotionsausschuss:

Vorsitzender: Prof. Dr. Dieter Scherer

Gutachter: Prof. Dr. Gerd Wessolek

Gutachter: Prof. Dr. Christoph Thomas

Gutachterin: Prof. Dr. Eva Nora Paton

Tag der wissenschaftlichen Aussprache: 17. November 2017

Berlin 2018

I dedicate this dissertation to my late mother GERTRUD BERNHARDINE HÖLSCHER

(* 29th July 1959; † 7th February 2016)

Preface

Bioclimate in urban areas is altering due to global climate change, so that the already higher air and surface temperatures in cities (urban heat island effect, UHI) are increasing. Climate change leads to an increase of summer days ($T_{max} \geq 25$ °C), hot days ($T_{max} \geq 30$ °C) and tropical nights ($T_{min} \geq 20$ °C) (SENSTADT 2011). Extreme events such as heat periods occur more often and become longer and more intensive. Long heat periods in summer are a problem even for healthy people, but highly vulnerable persons, such as sick or elderly people, are especially at risk. Thus, the identification and implementation of suitable adaptation and mitigation measures are current significant challenges to address.

The research presented in this thesis was conducted within the framework of the interdisciplinary DFG research unit 1736 "urban climate and heat stress in mid-latitude cities in view of climate change (UCaHS)" (www.UCaHS.org). The research unit dealt with complex scientific questions related to urban heat stress. Outdoor and indoor heat-stress hazards, heat-related health risks for humans as well as reduction and adaptation strategies were investigated and controversially discussed. In this context, urban facade greenings were experimentally examined because they are often discussed as a promising countermeasure against heat stress.

Facade greening is the complete or partial covering of vertical surfaces with plants (KRUPKA 1992, KÖHLER 1993). After a first hype in the 70s and 80s, facade greening has become popular again in recent years, in particular propagated by the French garden designer PATRICK BLANC. It could be applied nearly everywhere in the city, especially on buildings in which people suffer from heat stress, mainly during the night. Facade greening is expected to reduce air temperatures because of its potential high transpiration per horizontal base area. However, so far, there is a lack of sufficient data on water demand and transpiration rates of urban facade greenings which is necessary for a general model on the cooling effects and the water demand.

This thesis quantifies cooling effects of urban facade greenings for the building and the outdoor human bioclimate. It quantifies the underlying thermal processes and required amounts of water for the climbing plants. Therefore, measurement techniques for the quantification of transpiration rates (xylem sap flow, lysimeter) are extended and adjusted to the situation of urban facade greenings. Finally, facade greenings are compared with other countermeasures and assessed whether and to what extent they are suitable for the reduction of indoor and outdoor heat stress.

Berlin, June 2017

MARIE-THERESE HÖLSCHER

Acknowledgments

I would like thank all the people who supported me towards the completion of this dissertation:

First of all, I would like to express my sincere gratitude to PROF. DR. GERD WESSOLEK for supervising and supporting my dissertation. I want to thank him for his great expertise and anecdotes and for the space he gave me for my own development.

PROF. DR. CHRISTOPH THOMAS and PROF. DR. EVA NORA PATON for being my second and third reviewer of this thesis.

My mentor DR. THOMAS NEHLS for the enriching discussions, his work experience and wisdoms. His motivating words and commitment helped me substantially to conduct this research.

NIKOLA SCHWARZER for her great manual dexterity and her active commitment, making the measurement campaigns possible. I also want to thank her for good talks, lots of inspiration and her company during the overnight measurements.

All the MEMBERS OF THE DFG RESEARCH UNIT UCAHS for the interesting discussions and collaborations. Special thanks go to PROF. DR. DIETER SCHERER, who coordinated the research unit, DR. BRITTA JÄNICKE, OLIVER BUCHIN and DR. NADINE WALIKEWITZ.

All my COLLEAGUES from the department of soil conversion for the pleasant working atmosphere and for good talks and suggestions. I would like to thank DR. MORITZ WERKENTHIN for enriching discussions and teatimes; DR. STEFFEN TRINKS for his help with the measurement setup, his patience and helpfulness with technical problems, chocolate and other nourishment for my nerves; DR. BJÖRN KLUGE and JOACHIM BUCHHOLZ for their help and great support during the measurement campaigns; REINHILD SCHWARTENGRÄBER for her caring way and HELENA SCHMIESCHEK for all the organisational matters.

MARTIN ANDREAS KERN from the department of soil science for his performance and help with the sap flow experiments, great ideas and motivating words.

CHRISTINE HILDEGARD BEUSCH for correcting this dissertation and relaxing breaks.

COLIN JAMES SANDERS, PHILIP SANDERS and MAHOMET NJOYA for their English corrections and language expertise.

I also want to thank my FAMILY and my FRIENDS for being there for me. Special thanks go to my mother GERTRUD BERNHARDINE HÖLSCHER, who always had an open ear for my worries and fears, to my life partner MARC-THOMAS BERGER and to my son JONATHAN DAVID HÖLSCHER.

This dissertation, as a part of the Research Unit 1736 “urban climate and heat stress in mid-latitude cities in view of climate change (UCaHS)” (www.UCaHS.org), was funded by the DEUTSCHE FORSCHUNGSGEMEINSCHAFT (DFG).

Abstract

Higher air temperatures in cities lead to increased heat stress for the urban population, especially during the night in hot summer periods. Facade greening is often discussed as a promising mitigation strategy as it can be applied on building surfaces where the heat stress is mainly caused. It reduces the stored energy in the building mass through shading and transpirative cooling and additionally influences the heat distribution within the street canyon.

In previous studies, it was hardly differentiated between shading and transpiration effects because no studies are available on transpiration rates and water demand of climbing plants. This thesis quantifies water demand and cooling effects of facade greenings for the building and the urban street canyon. Therefore, methods for the quantification of transpiration rates are extended and adjusted to urban facade greening settings.

Several experiments were conducted in summer on three building facades in the city centre of Berlin, Germany. Transpiration rates (xylem sap flow, lysimeter) were determined for three typical facade greening species: *Parthenocissus tricuspidata*, *Hedera helix* and *Fallopia baldschuanica*. Furthermore, surface temperatures of greened walls, bare walls and plant leaves as well as different meteorological parameters were measured. Finally, facade greenings were evaluated concerning their hazard reduction potential and compared with other countermeasures.

Only minor cooling effects were detectable for the urban street canyon. In contrast, the effect for the building was clearly measurable: surface temperatures of the exterior and the interior building walls were decreased by up to 15.5 K and 1.7 K, respectively. A risk analysis shows that already a mean T_{air} reduction of 0.8 K can reduce the number of heat-related deaths. Thus, facade greening has up to medium potential to reduce indoor heat-stress hazards and is generally more effective to cool buildings than other vegetation, such as parks, street trees or green roofs.

Provided cooling effects on hot summer days mainly depended on shading, while only a lower proportion was due to transpiration. Nevertheless, facade greening must be sufficiently irrigated with up to 3.0 L d^{-1} m^{-2} per wall area in order to realise its maximum cooling performance.

Zusammenfassung

Höhere Lufttemperaturen in Städten führen insbesondere nachts während heißer Sommerperioden zu verstärktem Hitzestress für die urbane Bevölkerung. Fassadenbegrünung wird oft als eine vielversprechende Minderungsstrategie diskutiert, da sie an Gebäudeoberflächen angebracht werden kann, wo der Hitzestress hauptsächlich entsteht. Sie reduziert die gespeicherte Energie in den Gebäudemassen durch Beschattung senkrechter Oberflächen sowie Verdunstungskühlung und beeinflusst zudem die Wärmeverteilung in der Straßenschlucht.

In vergangenen Untersuchungen wurde kaum zwischen Beschattungswirkung und Transpirationskühlung differenziert, weil es bisher kaum Aussagen zur Transpiration von Fassadengrün und damit zur benötigten Wassermenge gibt. In der vorliegenden Arbeit werden Wasserbedarf und Kühlungseffekte von Fassadenbegrünungen für das Gebäude und die urbane Straßenschlucht quantifiziert. In diesem Rahmen werden auch Methoden für die Quantifizierung von Transpirationsraten (Xylemsaftfluss, Lysimeter) auf die Situation urbaner Fassadenbegrünungen erweitert und angepasst.

Eine Vielzahl von Experimenten wurde im Sommer an drei verschiedenen Gebäudefassaden in der Innenstadt von Berlin durchgeführt. Dabei wurden Transpirationsraten von drei typischen Kletterpflanzen für Gebäudebegrünungen bestimmt: *Parthenocissus tricuspidata*, *Hedera helix* und *Fallopia baldschuanica*. Außerdem wurden Oberflächentemperaturen von begrünten Fassaden, unbegrünten Fassaden und Pflanzenblättern sowie verschiedene meteorologische Parameter gemessen. Letztendlich wurden Fassadenbegrünungen mit anderen Gegenmaßnahmen verglichen und bewertet.

Der Kühlungseffekt für die Straßenschlucht war nur geringfügig nachweisbar. Im Gegensatz dazu war der Effekt für das Gebäude klar zu quantifizieren: Die Oberflächentemperaturen der begrünten Außen- und Innenwand waren um bis zu 15.5 K bzw. 1.7 K reduziert. Die Ergebnisse einer Risikoanalyse zeigen, dass bereits eine durchschnittliche Senkung der Lufttemperatur um 0.8 K die Anzahl von Hitzetoten reduzieren kann. Fassadenbegrünung hat daher ein bis zu mittleres Potential die Hitzestressgefahr im Innenraum zu mildern und ist generell effektiver für die Gebäudekühlung als andere urbane Vegetationsformen wie Parks, Straßenbäume oder Dachbegrünungen.

Die Kühlungseffekte an heißen Sommertagen beruhten hauptsächlich auf der Beschattungswirkung, während ein geringerer Anteil auf die Transpirationskühlung zurückzuführen war. Nichtsdestotrotz müssen die Kletterpflanzen ausreichend bewässert werden, um die Kühlleistung voll auszuschöpfen. Bis zu 3.0 Liter pro m² Wandfläche und Tag und sind nötig.

Table of contents

List of figures

List of tables

Abbreviations

CET	Central European Time
c_w	specific heat of water
ΔT	temperature difference
$e_{(a)}$	(actual) vapour pressure
e_s	saturation vapour pressure
E	evaporation
$ET_{(a)}$	(actual) evapotranspiration
ET_0	potential evapotranspiration
FAO	Food and Agriculture Organization of the United Nations
G	soil heat flux density
$K\downarrow_b$	incoming short-wave radiation behind the greenery
$K\downarrow_f$	incoming short-wave radiation in front of the greenery
K_c	crop coefficient
LA	leaf area
LAD	leaf area density
LAI	leaf area index
MAD	mean absolute deviation
MD	mean deviation
NVS	night value subtraction
P	recorded power input to the heater
Q_{fic}	fictitious water flux
Q_S	sap flow
Q_t	total recorded heat input from the sap flow logger
RH	relative humidity
RMSD	root-mean-square deviation
R_n	net radiation
SHB	stem heat balance
S	shading effect
SVF	sky view factor
S_{str}	mean radiant flux density
T	transpiration
T_{max}	maximum air temperature of the day
T_{air}	air temperature
T_{mrt}	mean radiant temperature
u	wind speed
UHI	urban heat island
VPD	vapour pressure deficit
WA	wall area
WLAI	wall leaf area index (leaf area corresponding covered wall area)

1 General introduction

1.1 Context - urban climate and heat stress

Urban areas usually have higher air temperatures (T_{air}) than their rural surroundings (IMHOFF et al. 2010), a phenomenon called urban heat island (UHI) effect. The differences mainly occur during the night. For instance, nocturnal T_{air} in the densely built-up inner-city of Berlin (Alexanderplatz) is up to 8 K higher than the one in the Grunewald forest on a hot low-exchange radiation day (SENSTADT 2011, Fig. 1.1). During the day, however, T_{air} is not extraordinary higher or is partially even lower (PARLOW et al. 2014).

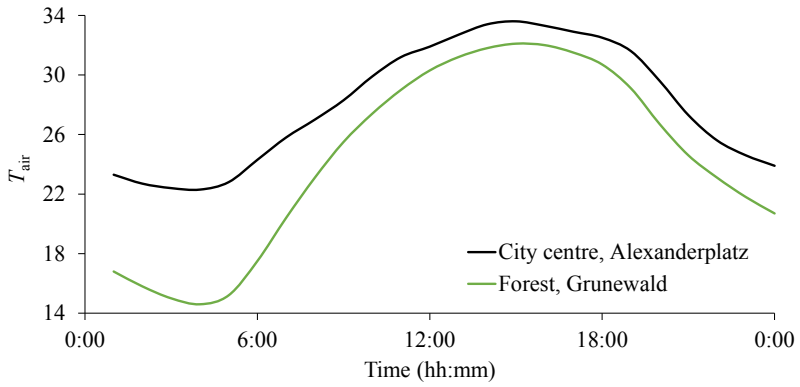

Fig. 1.1 Air temperature (T_{air}) in a height of 2 m at two locations in Berlin, Germany on a hot low-exchange radiation day (8th July 1991), own figure, using data from SENSTADT (2001).

The main reason for the UHI phenomenon is the increased absorption of solar radiation by the city's surface compared to the natural landscape (TAKEBAYASHI and MORIYAMA 2007). That is the result of the city's high surface area due to its vertical structure. In the inner-city of Berlin, the ratio of vertical to horizontal area exceeds the factor three (NEHLS 2010). It is expected to be much higher for other cities, such as Frankfurt am Main, London or Tokio. For instance, MANKIEWICZ (2017) estimated a factor of 10 for New York City. Furthermore, sealed and built structures have higher heat storage than vegetated surfaces because of their higher heat capacity and density (ALEXANDRI and JONES 2004). The higher heat capacity leads to higher long-wave emission during nighttime (SHAM et al. 2012), which results in a higher T_{air} inside and outside the buildings. Other reasons for the UHI are increased anthropogenic heat emissions (MONTÁVEZ et al. 2008) as well as limited evapotranspiration and shading due to the absence of vegetation (WANG and XU 2008). The increase of extreme temperatures as a result of global climate change further escalates these higher temperatures.

During hot summer seasons, the higher temperatures lead to amplified heat stress for the urban population (MAYER and HÖPPE 1987). This means at the individual level, they restrict

the human body to balance the heat flows by its thermoregulation system. This leads to heat-related health risks such as rash, cramps, exhaustion and stroke or, in extreme cases, to death and may be reinforced by pre-existing health problems like lung or heart diseases (BUCHIN et al. 2015). Thus, especially elderly people are highly vulnerable to heat stress (STAFOGGIA et al. 2008, SCHERER et al. 2014) and the relevance of heat stress will increase not only by external driving factors (UHI, climate change), but also by the demographic change in many mid-latitude cities (BUCHIN et al. 2015).

People can adapt their behaviour during the day easier than during the night. That might be the reason why GABRIEL and ENDLICHER (2011) could provide a better explanation on the excess mortalities of 1994 in Berlin by daily minimum T_{air} above 20 °C than by daily maximums above 30 °C. Typical daytime strategies are searching for shade, drinking or going into the park, pool or lake. In contrast, people have only limited adaptation possibilities during the night, where they usually stay and sleep in their residential buildings (FRANCK et al. 2013). Nocturnal heat stress is particularly associated with sleep disturbance and reduced recreation (LIBERT et al. 1991, OKAMOTO-MIZUNO et al. 2004), whereby these problems are intensified with the duration of the heat period (GABRIEL and ENDLICHER 2011).

1.2 Countermeasures to urban heat islands

Tab. 1.1 Classification of countermeasures to UHI, clustered into the spatial scale of implementation (city scale, building scale, room scale), according to BUCHIN et al. 2015.

Countermeasures		
City scale	*Building scale*	*Room scale*
(pavement and urban green)	*(roof and facade)*	*(passive and active cooling)*
Cool pavements	Cool roof	Overhangs and shutters
Trees	Green roof	Curtains
Grass	Facade greening	Night ventilation
		Vapour compression air-conditioning
		Absorption based air-conditioning
		Evaporative cooling

Countermeasures are mitigation strategies to reduce absorption of radiation and storage of heat (e.g. cool roofs) or to increase evapotranspiration and biomass production (e.g. facade greening) (BUCHIN et al. 2015). They contribute to change the conditions in the urban canopy layer and therefore promote the reduction of heat-stress related health risks, indoors and / or outdoors. Because people and especially vulnerable groups spend their majority of time (> 80 %) indoors (KLEPEIS et al. 1995, KRAUSE and SCHULZ 1998), the impact on the indoor climate is particularly relevant. Nevertheless, a countermeasure should not have a negative effect on the outdoor climate.

Some often discussed countermeasures are listed in Tab 1.1. For a detailed description of the individual measures see chapter 5.

1.3 Facade greening as a countermeasure to UHI and urban heat stress

Several studies show the potential of urban vegetation to reduce ambient T_{air} (e.g. LU et al. 2012, DUGORD et al. 2014), but space for horizontal vegetation is limited in cities. BOWLER et al. (2010) further discussed the spatially limited effectiveness of horizontal green areas such as parks for adjacent quarters. Vertical green is often discussed as a promising countermeasure against urban heat stress. For instance, it is mentioned in 15 of 24 mitigation and adaptation plans in Germany as an adaptation strategy to improve microclimatic conditions (DONNER et al. 2015).

Facade greening can be applied nearly everywhere in the city, especially on buildings where the heat stress is mainly caused and in which people suffer from it (FRANCK et al. 2013). Building surfaces constitute a largely unused application potential and underlie a low utilisation pressure. According to DEBUS (2009), about 67 % of the building facades in Berlin (structural type the Imperial-Era) can be potentially vegetated. That results in a ratio of greenable vertical area to horizontal ground area of 1.2 (DEBUS 2009). BARTFELDER and KÖHLER (1987), who made extensive investigations on urban facade greenings in Berlin (West), calculated a similar value of 1.3. Moreover, vertical green is expected to reduce ambient T_{air} because of its high amount of leaves and corresponding high transpiration rate per horizontal base area. Lianas in a tropical rainforest for example make up only 4.5 % of the total above-ground biomass but account for 19 % of the leaf area (PUTZ and MOONEY 1992).

Furthermore, facade greening offers a wide range of other ecosystem services such as noise reduction, habitat creation for wildlife or filtering of air pollutants (e.g. BARTFELDER and KÖHLER 1987, THÖNNESSEN 2002, SCHLÖßER 2003). In contrast, ecosystem disservices are the often mentioned damage of the building substance, insects in flats, foliage in autumn, annoying birds in spring mornings as well as problems with the preservation of historical monuments. Most of these disadvantages can be avoided by a careful planning and maintenance (e.g. SENSTADT 2011, PFOSER et al. 2013).

1.3.1 Plant species

In this thesis, facade greening only refers to the classic soil-bound variants with woody climbing plants, also referred to as lianas. HUNTER et al. (2014) further differ between “direct green facades” with self-clinging climbers, attaching themselves directly on the wall surface, and “double-skin green facades” with additional climbing support structures in front of the building wall to assist the climbers’ upward growth.

Climbing plants reach their highest global abundance in tropical rain forests (PUTZ and MOONEY 1992). In central Europe, however, only few native species occur naturally (i.e. in riparian forests) (KÖHLER 1993). Facades in central European cities are greened with only a few native plants species. *Parthenocissus tricuspidata* is a well-examined (e.g. BARTFELDER and KÖHLER 1987, KÖHLER 2008, HUNTER et al. 2014) and the most used climbing plant in Germany (THÖNNESSEN 2002). For instance, more than half of the facade greenings in Berlin (59 %) are planted with it (Fig. 1.2). *P. tricuspidata* is originally distributed in Asia and North America and was introduced to Europe in the middle of the last century (KÖHLER 1993). It is a self-clinging climber which directly climbs on the building surface with its adhesive pads. *Hedera helix* is also widely used (16 % of the facade greenings in Berlin) and an evergreen native liana with its natural habitat in European woodlands and meadows. It is also self-clinging, climbing with its adventitious roots. The rest of the greened facades in Berlin is divided in *Parthenocissus quinquefolia* (6 %), *Fallopia baldschuanica* (3 %), *Vitis venifera* (6 %), *Wisteria sinensis* (3 %) and others (7 %). *F. baldschuanica* is a deciduous rambling plant originating from Asia that needs additional climbing structures for its upward growth. Besides *P. tricuspidata* and *H. helix*, it was selected in this work because of its rapid growth, relatively small habitat requirements and expected high transpiration rates (HOELSCHER 2013).

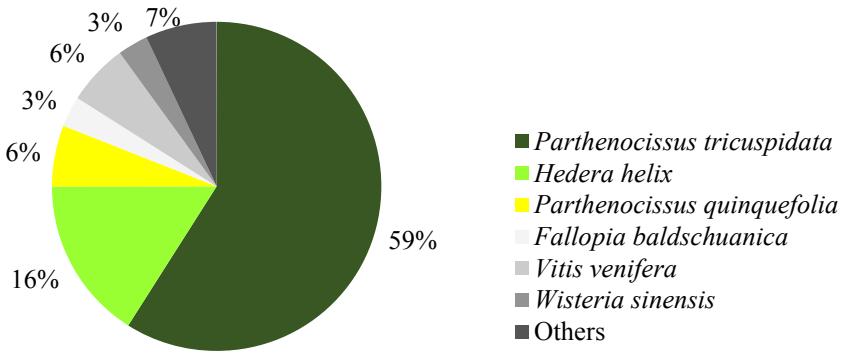

Fig. 1.2 Overview about the used climbing plant species for facade greening of parts of Berlin, Germany, own figure, using data from KÖHLER (1993).

1.3.2 Cooling potential and water balance of facade greenings

Facade greening cools building walls through shading, evapotranspirative cooling and thermal insulation (PÉREZ et al. 2011, HUNTER et al. 2014). Furthermore, it influences the heat distribution within the street canyon: it absorbs and converses solar radiation into photochemical energy and latent heat which otherwise would be absorbed elsewhere and cools the surrounding air, which induces air flow in the canyon.

Special site conditions of urban facade greenings

Site conditions on facades are modified compared to free open spaces. Facade greenings in cities often have little root space due to sealing and compaction of the soils. Water quality and availability are also restricted, which could be a supply problem, especially during hot summer periods if the plants are not additionally irrigated. Water deficits may reduce the cooling potential by transpiration (e.g. HSIAO 1973, ESCALONA et al. 2013).

The exposition of the facade has a great influence on the absorbed solar radiation. In the northern hemisphere, the incoming solar radiation generally decreases from the south to the north. Surrounding buildings further influence the lighting conditions on the facade. They may partially or completely shade the facade (reduced sky view factor, SVF) but sunlight reflections from glass and mirrored surfaces may act as additional light sources (PFOSER et al. 2013). Lighting conditions also change with the height and the lateral position on the facade, which is for sure a challenge for modelling facade greening's transpiration.

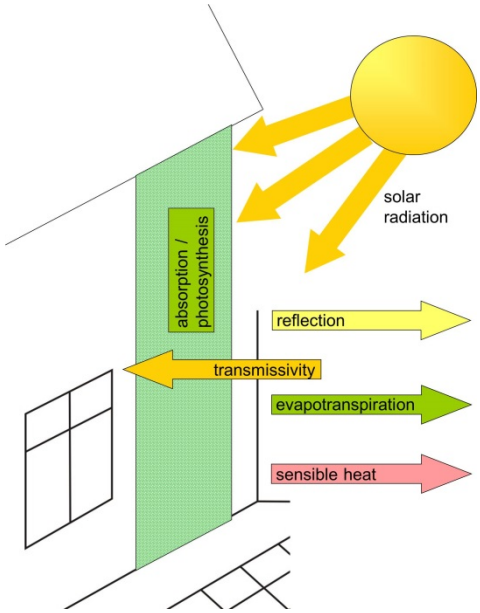

Fig. 1.3 Individual components of the energy balance for facade greenings. For the quantification of the fluxes see 7.2.1 and Fig. 7.1.

Shading, thermal insulation and evapotranspiration

Shading is reflection and absorption of solar radiation (HUNTER et al. 2014). It reduces energy consumption for air-conditioning systems by up to 19 % (STEC et al. 2005) and is therefore required for newly constructed buildings in Germany (ENEV 2015). Shading by plants depends on plant traits, such as number of leaf layers, leaf solar transmittance and percentage of coverage (IP et al. 2010, KOYAMA et al. 2013) (Fig. 1.3). For instance, one layer of leaves (*P. quinquefolia*) reduced incoming solar radiation by 37 %, while it was 86 % for five layers (IP et al. 2010). According to PÉREZ et al. (2011), *H. helix* provides the highest shading effect.

Facade greening can also insulate building walls by changing the temperature and the humidity in the space between building wall and greening (PERÉZ et al. 2011). This insulation effect depends on the size of the air space, foliage density and facade greening design (PERÉZ et al. 2011). It can be effective in both summer and winter for evergreen climbing plants and in summer for deciduous plants.

Plants take up water and inorganic ions over their roots from the soil solution. The different water potentials of soil and atmosphere induce a transpiration pull (= cohesion-tension theory), whereby the water is transported within the xylem of the plant to the leaves. Plants mainly transpire through their stomata and marginally through the cuticle (HEß 2008). Transpiration through stomata is controlled by some plant species and is influenced by a variety of factors, such as radiation, temperature, ambient CO_2 concentration, leaf water potential and water vapour pressure deficit of the surrounding air (*VPD*) (JARVIS 1976, JONES 2000). Water can also evaporate from the soil or substrate surface which is called evaporation. The transition of water from the liquid into vapour state requires an energy amount of 2450 J g^{-1} (at $T_{air} = 20°C$) which becomes effective as evapotranspirative cooling (SCHOPFER and BRENNICKE 2010). Evapotranspirative cooling (latent heat) reduces the proportion of direct warming of the air (sensible heat) in the energy balance.

The cooling potential of facade greening has been examined in many studies (e.g. BARTFELDER and KÖHLER 1987, STEC et al. 2005, SUSOROVA et al. 2013). Most of them focus on surface wall temperatures and partly on T_{air}, whereas studies quantifying the influence on the mean radiant temperature (T_{mrt}) are rare. Wall temperatures are clearly reduced by greenery. So far, the highest differences between a greened and a bare wall were measured by MAZZALI et al. (2013) with differences of up to -20 K. In contrast, the effect on the ambient air was found to be low to negligible (PÉREZ et al. 2011, GROSS 2012, DJEDJIG et al. 2013). T_{mrt} was reduced by 2 to 13 K in a tropical urban environment (TAN et al. 2014). However, these are results of case studies and most of them concentrate on the shading effect.

There are first approaches to differentiate between shading and transpiration (CAMERON et al. 2014, KOYAMA et al. 2015). However, the experiments and thus the results are questionable: plants in pots stood in front of a wall, not attached to it as common for facade greenings. Shading and transpiration were distinguished by cutting the plant stems or sealing the foliage to prevent transpiration, thus not allowing long-term measurements.

Until now, no studies has existed on transpiration rates and water demand of urban facade greenings, although it is necessary for the process understanding and a general model on the cooling effects as well as a sufficient watering of the climbing plants. Whether and to what extent facade greening is a suitable adaptation strategy, could not be sufficiently assessed.

1.4 Measuring transpiration of facade greenings

1.4.1 Sap flow measurements

Sap flow measurements are indirect methods to determine water demand and transpiration rates of single plants or plant stands. They use heat as a tracer for sap movement in the xylem of plant stems. In contrast to other instruments (e.g. porometer, deuterium tracing), sap flow techniques can be installed without great effort and automated easily with a continuous recording and a high temporal resolution (SMITH and ALLEN 1996). However, they could also lead to inaccuracies in the determination of transpiration. According to RAVEN et al. (2005), there is a temporal shift between water transported in the xylem and water release in the plants' leaves, which might be substantial for the diurnal variation of transpiration of high facade greenings. Furthermore, about 1 % of the transported water is stored in the production of biomass (RAVEN et al. 2005). Nonetheless, sap flow measurements are often applied in forestry, agriculture, horticulture and ecology (e.g. PERTIERRA et al. 2002, MATYSSEK et al. 2009, RODRIGUEZ-DOMINGUEZ et al. 2012) and could be useful for studying water balance of urban facade greenings as well. Whether and how this method could be suited to facade greenings in urban situations is discussed in chapter 4 of this thesis.

1.4.2 Lysimeter measurements

Weighing lysimeters are measuring instruments for the direct water flux determination of a unvegetated or vegetated soil body by weighing the system in regular intervals. Surface runoff, infiltration and precipitation are often additionally recorded to calculate its actual evaporation or evapotranspiration, respectively. Although lysimeters are laborious and expensive in their installation, they allow very precise measurements.

In order to assess transpiration rates of urban climbing plants, we developed a new and modified lysimeter system (SCHWARZER 2015) (Fig. 1.4). Twelve individuals of *Fallopia baldschuanica* were planted into two containers with a volume of about 1 m^3 for each, which were buried into the ground to minimise edge effects. The plants grew in a hydroponic system of coarse sand (0.063 to 2 mm) and were supplied with nutrient solution from a constant standing water table in a depth of 0.6 m. Water table was replenished using a pump from a reservoir which stood on a balance (Sartorius Signum1, Sartorius Weighing Technology GmbH, Germany) and was automatically filled up when the water fell below a certain level. Excess water in the container was flowing back into the water reservoir through a separate drainage (outflow).

Container and refillable water reservoir were sealed in order to prevent infiltration of precipitation and to minimise evaporation from the substrate. Thus, transpiration (T) of the climbing plants can be calculated as follows:

$$T = \Delta S - E\,, \qquad \text{(eq. 1.1)}$$

where ΔS is the change in storage in the refillable reservoir and E is the evaporation from the substrate. E was at most 0.013 L h^{-1} and negligible in relation to transpiration rates. With the lysimeter system, T can be calculated in a resolution of at least 30 min and with an accuracy of 0.01 mm related to the ground area. The whole setup is described in detail in the diploma thesis of NIKOLA SCHWARZER (2015).

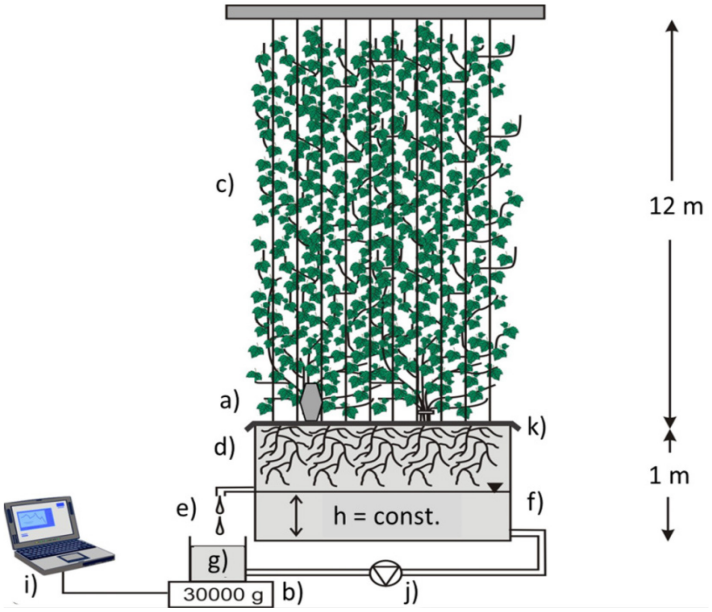

Fig. 1.4 Experimental design of the lysimeter system for transpiration measurements of facade greenings: a) sap flow sensor with radiation shield, b) balance measuring the water uptake, c) climbing plants (*Fallopia baldschuanica*), d) rooting zone in the hydroponic system (coarse sand), e) free outflow, f) intake, g) water reservoir refilled automatically, h) constant water level, i) data logger, j) pump, k) cover, published in HOELSCHER et a. 2018.

Fig. 1.5 Picture of the lysimeter system: west exposed building facade greened with *Fallopia baldschuanica* at the campus of the Technische Universität Berlin (August 2014).

1.5 Research objectives

The aim of this thesis is to quantify water demand and cooling effects of urban facade greenings for the building and the urban street canyon. Facade greenings are compared with other countermeasures and are assessed whether and to what extent they are a suitable strategy for the reduction of indoor and outdoor heat stress hazards.

The following research objectives are addressed in detail:

Studying the effects of an urban facade greening on the outdoor human bioclimate (chapter 2)

- quantify the effect of an urban facade greening on T_{mrt}

Quantification of cooling effects of urban facade greenings for the building and the urban street canyon (chapter 3)

- quantify cooling effects for the building and the ambient urban air
- distinguish between transpiration and shading effects, discuss insulation effects
- quantify water demands of three typical facade greening species: *Parthenocissus tricuspidata*, *Hedera helix* and *Fallopia baldschuanica*

Development of a new practical calibration method in order to derive transpirations rates of urban climbing plants from sap flow measurements (chapter 4)

- develop a new practicable calibration method for deriving valid transpiration data from sap flow measurements using the stem heat balance method
- assess the applicability of different calibration approaches based on simultaneous weight measurements

Application of a heat-related risk concept which differentiates between indoor and outdoor hazards as well as the evaluation of different countermeasures to UHI (chapter 5)

- evaluate and compare different countermeasures (including urban facade greenings) concerning their hazard reduction potential for indoor and outdoor conditions.

Modelling evapotranspiration of urban facade greening (chapter 6)

- determine evapotranspiration by lysimetry and compare the results with those calculated by the FAO grass reference evapotranspiration
- derive simple relationships (like crop factors)

2 Evaluating the effects of facade greening on human bioclimate in a complex urban environment[1]

BRITTA JÄNICKE[a,*], FRED MEIER[a], MARIE-THERESE HOELSCHER[b] and DIETER SCHERER[a]

[a] Department of Ecology, Climatology, Technische Universität Berlin

[b] Department of Ecology, Soil Conservation, Technische Universität Berlin

*corresponding author; e-mail address: britta.jaenicke@tu-berlin.de

Abstract

The evaluation of the effectiveness of countermeasures for a reduction of urban heat stress, such as facade greening, is challenging due to lacking transferability of results from one location to another. Furthermore, complex variables such as the mean radiant temperature (T_{mrt}) are necessary to assess outdoor human bioclimate. We observed T_{mrt} in front of a building facade in Berlin, Germany, which is half-greened while the other part is bare. T_{mrt} was reduced (mean 2 K) in front of the greened compared to the bare facade. To overcome observational shortcomings, we applied the microscale models ENVI-met, RayMan and SOLWEIG. We evaluated these models based on observations. Our results show that T_{mrt} (MD = -1.93 K) and downward short-wave radiation (MD = 14.39 W m^{-2}) were sufficiently simulated in contrast to upward short-wave and long-wave radiation. Finally, we compare the simulated reduction of T_{mrt} with the observed one in front of the facade greening, showing that the models were not able to simulate the effects of facade greening with the applied settings. Our results reveal that facade greening contributes only slightly to a reduction of heat stress in front of building facades.

2.1 Introduction

Heat stress risk in cities threatens human health (SCHERER et al. 2014) and effective countermeasures are not clearly identified. Even though many measures to reduce outdoor urban heat stress are proposed from various disciplines and at different spatial scales (RIZWAN et al. 2008), their effectiveness is still disputed. Assessing the effectiveness of

[1] Published: JÄNICKE, B., F. MEIER, M.-T. HOELSCHER and D. SCHERER (2015). Evaluating the effects of façade greening on human bioclimate in a complex urban environment. *Advances in Meteorology* 2015, Article ID 747259: 15 pp. https://dx.doi.org/10.1155/2015/747259.

countermeasures is challenging for many reasons. For example, the transferability of results from one location to another is limited due to the complexity of the urban system and various climates (GEORGESCU et al. 2014). Moreover, the impact of a countermeasure on outdoor human bioclimate cannot be described sufficiently by simple climate elements, such as surface or air temperature. The mean radiant temperature (T_{mrt}) is an important variable for the assessment of human bioclimate in urban environments because it includes long-wave and short-wave radiation that reaches the human body (THORSSON et al. 2007, KÁNTOR and UNGER 2010).

Facade greening is a promising countermeasure to reduce urban heat. It can be attached to a large area in cities (KÖHLER 2008) and features several cobenefits, such as insulating buildings (EUMORFOPOULOU and KONTOLEON 2009, PÉREZ et al. 2011, PULSELLI et al. 2014) or serving as habitat for wildlife (KÖHLER 2008). The knowledge about the effectiveness of facade greening to reduce outdoor heat stress risks, however, is still incomplete due to limits in transferring of results to other sites (HUNTER et al. 2014). The cooling effects of facade greening regarding surface and air temperature depend on solar irradiance, vegetation properties and the particular greening system (DJEDJIG et al. 2013, KOYAMA et al. 2013, CAMERON et al. 2014). Also the mechanisms of cooling (e.g. through shadowing or transpiration) vary between different plant species (CAMERON et al. 2014). The effects of facade greening on air temperature were found to be small to negligible (PÉREZ et al. 2011, GROSS 2012, DJEDJIG et al. 2013). Wall temperatures decreased more strongly (GROSS 2012, TAN et al. 2014) as well as the emitted long-wave radiation (BERRY et al. 2013). T_{mrt} was reduced by 2 K to 13 K in the tropics (TAN et al. 2014), but the effects for other locations are unknown. Studies that quantify the influence of facade greening on T_{mrt} are rare because so far architecture and engineering disciplines are dominant with a focus on air and surface temperature and its influence on the building (HUNTER et al. 2014).

Microclimate models can be applied to expand the knowledge of the effects of facade greening on human bioclimate. Microclimate models, such as ENVI-met, RayMan or SOLWEIG, are often used in different disciplines. Particularly over the last few years, the number of studies applying ENVI-met and RayMan has grown rapidly. This is an encouraging trend as it may present an increasing awareness of the topic of human bioclimate in cities and may accelerate the implementation of countermeasures. Nevertheless, the reliability and the uncertainty of the results from studies solely based on simulations may vary appreciably. The deviations between observations and simulations have sparsely been evaluated in a comprehensive way. Thus, the inaccuracies in simulating countermeasures or real case situations are insufficiently known even apart from the special case of facade greening. A comparison of T_{mrt} simulated by ENVI-met, RayMan and SOLWEIG under the same conditions was so far performed by CHEN et al. (2014). Other variables, such as short-wave and long-wave radiation, did not undergo an intercomparison (YANG et al. 2013).

So far, the models have not been applied to simulate facade greening and we are not aware of other models that are able to simulate facade greening with regard to outdoor human bioclimate. ENVI-met, RayMan and SOLWEIG include plants, but specific vegetation types, such as facade greening, are not explicitly declared to be supported. Nevertheless, all of the models should be able to consider some aspects of facade greening. RayMan supports

different trees with a specific emissivity and albedo as well as changes due to vegetation in the sky view factor (SVF). Thus, albedo and emissivity are modified due to facade greening. SOLWEIG considers vegetation in SVF and reduction of short-wave radiation through transmissivity and sets sunlit leaf temperatures to air temperature. Hence, especially long-wave radiation is expected to alternate in front of a building with facade greening. ENVI-met moreover simulates evapotranspiration. Thus, several effects of facade greening are expected to be reproduced, such as changes in SVF, increased water-vapour fluxes, decreased long-wave radiation or modified shortwave radiation.

In order to study the effects of facade greening on outdoor human bioclimate, we will firstly use observational data to answer the following question: (i) how large is the reduction of T_{mrt} in front of a greened facade compared to a bare one at a study site? Afterwards, we will apply the models ENVI-met, RayMan and SOLWEIG to the same site in order to (ii) evaluate the general performance of the models in simulating T_{mrt} and other variables relevant to assess human bioclimate. Thereby, we will contribute to the intercomparison and evaluation of these models in a complex urban environment. Finally, we investigate (iii) if the models are able to simulate the observed alteration of T_{mrt} in front of the facade greening. In a wider sense, the last question addresses if microclimate models are able to represent specific types of urban vegetation such as facade greening.

2.2 Materials and methods

2.2.1 Study site

In order to observe and simulate the effects of facade greening on T_{mrt}, we chose a south-southwest oriented building facade, which is half-covered with *Parthenocissus tricuspidata* while the other part is bare. The facade is located at the campus of the Technische Universität Berlin, Germany, Hardenbergstraße 38 (lat. 52°51 'N, long. 13°32' E, 31 to 35 m above sea level), in a compact midrise zone (Local Climate Zone 2) (STEWART and OKE 2012). *P. tricuspidata* covers the building wall from the bottom to the top (9 m) and nearly half of the building width (11 m). The plants are attaching themselves to the facade without technical climbing support. They rooted in a raised bed on the west oriented side of the building (unsealed area about 6 m^2). The substrate consists of loamy sand. The plants are irrigated in irregular intervals, but we irrigated the cavity before the measurement campaign to guarantee sufficient water supply. The albedo (calculated from observations on the 23rd July 2013, 10:00-16:00 Central European Time, CET) is 0.36 in front of the bare building wall, 0.28 in front of the facade greening and 0.18 for the ground surface. The mean depth of the vegetation layer is 0.27 ± 0.08 m (Tab. 2.1). The average leaf area density (LAD) of the facade greening is 1.85 $m^2\,m^{-3}$ according to our measurements at one vertical transect of 1 m × 9 m. On the 19th August 2013, we harvested all leaves at this vertical transect and measured the depth of the vegetation layer and the size of all leaves with an area meter (Model 3100, LI-COR, Inc.).

Tab. 2.1 Leaf area density (LAD) and depth of the facade greening based on a vertical transect of 1 m × 9 m.

Height (m)	0-1	1-2	2-3	3-4	4-5	5-6	6-7	7-8	8-9	*Mean*
LAD ($m^2\ m^{-3}$)	1.91	2.52	2.02	1.90	1.88	1.81	1.77	1.51	1.32	*1.85*
Depth (m)	0.34	0.36	0.30	0.26	0.30	0.34	0.22	0.18	0.13	*0.27*

2.2.2 Observation

We measured on the 23rd July 2013 (00:00-23:00 CET) in front of the building facade. This day was characterised by clear sky conditions and high air temperatures (Fig. 2.1). The measurements comprised mobile integral radiation measurements as well as wind speed, relative humidity, air temperature and several other variables to initialise ENVI-met, such as soil and indoor temperature (Fig. 2.2).

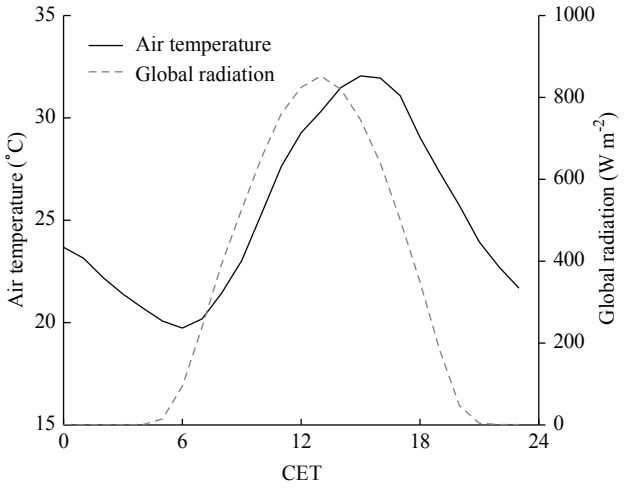

Fig. 2.1 Air temperature in front of the facade and global radiation during the measurement campaign (23rd July 2013).

The mobile measurements quantified T_{mrt} using integral radiation measurements based on three ventilated net radiometers (CNR4, Kipp & Zonen Corp., accuracy ±10 % for daily totals) and the calculation of angular factors with the formula by THORSSON et al. (2007) (eq. 2.1 and 2.2). Equation 2.1 summarises the long- and short-wave radiations from the bottom, the top and the four cardinal points. The variables were weighted according to the angular factors in order to estimate the shape of a standing person. Afterwards, T_{mrt} was calculated from mean radiant flux density (S_{str}) with the STEFAN-BOLTZMANN law (eq. 2.2). The net radiometers were oriented along the facade, which means towards north-northeast (NNE) and not towards the main cardinal points:

$$S_{str} = \alpha_\kappa \int_{i=1}^{6} K_i F_i + \varepsilon_p \int_{i=1}^{6} L_i F_i , \qquad \text{(eq. 2.1)}$$

$$T_{\mathrm{mrt}} = \sqrt[4]{\frac{S_{\mathrm{str}}}{\varepsilon_p \sigma}} - 273.15\,, \qquad \text{(eq. 2.2)}$$

where F_i = angular factors for weighting the radiation fluxes (0.06 for up- and downward and 0.22 for the cardinal points), K_i = short-wave radiation (W m^{-2}), L_i = long-wave radiation (W m^{-2}), α_κ = absorption coefficient of short-wave radiation (0.07), ε_p = the emissivity of the human body (0.97) and σ = the STEFAN-BOLTZMANN constant (5.67 10^{-8} W m^{-2} K^{-4}).

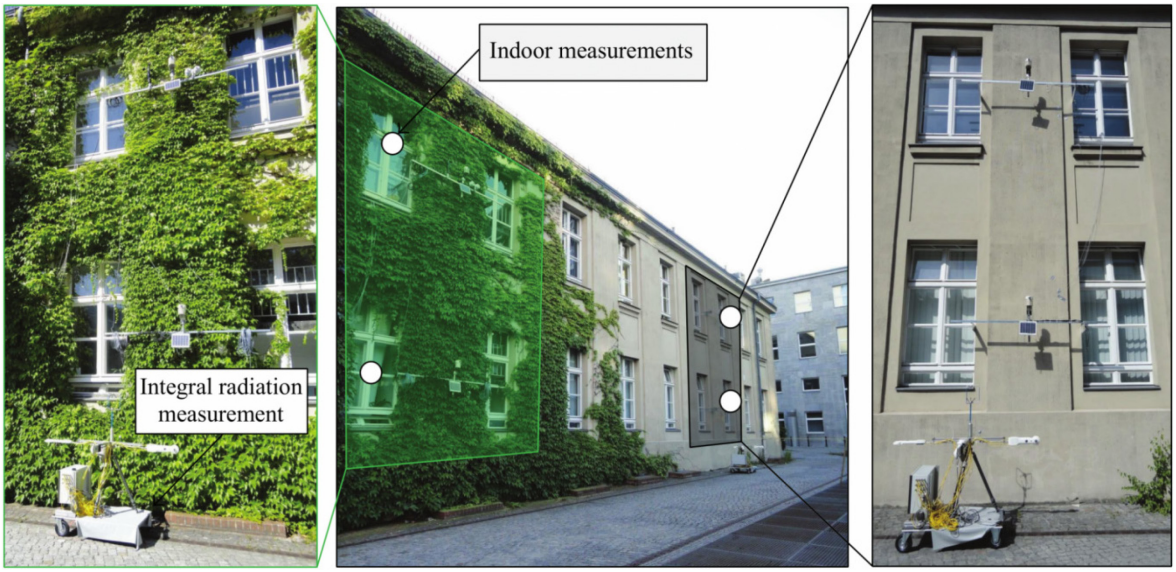

Fig. 2.2 Measurement arrangement and study site in Berlin, Germany.

The mobile station also included a ventilated temperature and relative humidity sensor (CS215, Campbell Scientific Inc., accuracy ±0.4 °C for +5 to +40 °C and ±4 % for 0 to 100 %). The station was set up at a distance of 1.2 m to the building. The measurement height was 1.1 m. We moved the station every 15 min between the greened and the bare site and aggregated the observed data afterwards from a minutely to an hourly resolution for each site (Fig. 2.2).

Additional measurements especially for initialising ENVI-met comprised soil temperatures at a depth of 0.3 m, 0.2 m and 0.1 m (analog mercury thermometers), soil humidity (TDR probes) with a resolution of 10 min and indoor air temperatures averaged over four rooms (Testo 174H, Testo AG, accuracy ±0.5 °C for -20 to +70 °C) with a 5 min resolution. Furthermore, short-wave transmissivity through the leaves was measured at two heights, each with two pyranometers, one behind and the other one in front of the greening (SP 110, Apogee). Mean transmissivity was 0.28. Off-site observations of global radiation and wind speed were carried out above roof level at the department of ecology (lat. 52°46 'N, long. 13°32' E) with a distance of about 6 km to the study site.

2.2.3 Models and simulation

For the same day (23rd July 2013, 00:00-23:00 CET), we applied the microclimate models: ENVI-met Version 3.1 Beta 5, ENVI-met Version 4.0 Preview (BRUSE and FLEER 1998, HUTTNER 2012), SOLWEIG 2013a (LINDBERG et al. 2008, LINDBERG and GRIMMOND 2011) and RayManPro (MATZARAKIS et al. 2007, 2010). The facade greening was introduced into the models as a flat plant in front of the building with leaves from ground to top. Furthermore, we specified plant parameters (albedo, transmissivity, LAD, etc.) to represent the facade greening as later described for the different models.

In order to analyse the influence of predefined meteorological data from observations and to compare them to the calculations by the models, we performed seven experiments (Tab. 2.2). The current version of ENVI-met 3 (E0a) does not support forcing of air temperature and relative humidity and thus additionally the unreleased version 4.0 Preview was applied (E0 unforced and E1 forced). The new version has already been used in other publications (WONG et al. 2010, CHEN et al. 2014, PENG and JIM 2013). SOLWEIG and RayMan require predefined values of air temperature and relative humidity. Both models can calculate short-wave downward radiation internally, which is the maximum short-wave downward radiation that can be derived at the specific date and location without clouds. These estimated values are used as global radiation to create experiments (R0 and S0) without measurement data of global radiation.

Building data for the input files were generated from the 3D city model of Berlin, which are available in the CityGML data format (http://www.citygml.org). We derived the spatial distribution and the height of vegetation from the Urban and Environmental Information System by the Senate Department for Urban Development and the Environment, Berlin. Terrain is neglected in all simulations because ENVI-met 3 does not support it. Furthermore, we assume its effects to be negligible due to the flat terrain at the study site. Meteorological data for the simulation were derived from onsite observations averaged between the greened and the bare sites in front of the facade for all variables with the exceptions of wind speed, wind direction and global radiation. To initialise ENVI-met, daily mean values were applied.

ENVI-met

ENVI-met is a CFD model for simulating surface-plant-air interactions from micro- to local scale with a focus on urban environments (BRUSE and FLEER 1998, BRUSE 1999, HUTTNER 2012). It requires intensive computational resources of a personal computer as each of the experiments lasted over 10 days. ENVI-met is, in contrast to RayMan and SOLWEIG, able to simulate the physiological processes of vegetation and to describe vegetation not only as a porous obstacle.

Tab. 2.2 Overview of the input parameters and model settings in the seven experiments. "X" represents input of times series of meteorological data.

Input parameter	Name	E0a	E0	E1	R0	R1	S0	S1
	Model	ENVI-met 3	ENVI-met 4		RayMan		SOLWEIG	
Meteorological data: initial	Unit							
Wind speed (10 m)	m s^{-1}	2.3	2.3	2.3	-	-	-	-
Wind direction (10 m)	deg	57.0	57.0	57.0	-	-	-	-
Potential air temperature (2500 m)	°C	24.85	24.85	24.85	-	-	-	-
Specific humidity (2500 m)	g kg^{-1}	8.56	8.56	8.56	-	-	-	-
Relative humidity (2 m)	%	45.8	45.8	-	-	-	-	-
Meteorological data								
Air temperature (1.1 m)	°C	-	-	X	X	X	X	X
Relative humidity (1.1 m)	%	-	-	X	X	X	X	X
Global radiation	W m^{-2}	-	-	-	-	X	-	X
Soil data								
Initial soil temperature (0-50 cm)	°C	23.1-25.7	23.1-25.7	23.1-25.7	-	-	-	-
Relative soil humidity (0-50 cm)	%	25.0	25.0	25.0	-	-	-	-
Environmental parameter								
Albedo surroundings	-	-	-	-	0.30	0.30	0.36	0.36
Albedo (wall)	-	0.36	0.36	0.36	-	-	-	-
Albedo (ground)	-	0.20	0.20	0.20	-	-	-	-
Albedo (plant)	-	0.28	0.28	0.28	0.28	0.28	-	-
Transmissivity of vegetation	-	-	-	-	-	-	0.28	0.28
Emissivity (ground)	-	-	-	-	-	-	0.95	0.95
Emissivity (walls)	-	-	-	-	-	-	0.90	0.90
BOWEN ratio	-	-	-	-	1.00	1.00	-	-
Solar adjustment factor	-	0.85	0.85	0.85	-	-	-	-

The domain in ENVI-met had a spatial resolution of 1 m × 1 m and consisted of 110 × 80 grid points after removing 30 nesting grid points at each border. The domain size in ENVI-met was limited. Thus, the model domain is smaller than in SOLWEIG and RayMan. We used telescoping grids (factor 15 %) starting at 2 m to include the highest building (43 m) because vertical grids were limited to 30 layers. In ENVI-met, the wind field and turbulent heat flux were simulated as well. Therefore, the model domain needed to be rotated by 30° to avoid unrealistic roughness at the edges of the building walls (Fig. 2.3).With the high resolution vegetation data, we introduced new vegetation classes based on the default plant database of ENVI-met to account for vegetation heights with a resolution of 1 m. The facade greening was also introduced as a new class with the measured LAD values (Tab. 2.1). We interpolated the 9 measured levels to 10 relative height levels to adapt to the structure of ENVI-met's plant database (see Tab. 2.3). According to on-site experiences, soils beneath vegetation were classified as loamy sand, streets as asphalt, areas beneath buildings as pavement and nonstreet areas as light brick roads.

Tab. 2.3 Measured leaf area density (LAD) profile of facade greening (italic) and assumed parameter for the plant database in ENVI-met.

Plant	Type	Albedo	Height	Root zone	Leaf area density at level										Root area density, all levels
			(m)	(m)	1	2	3	4	5	6	7	8	9	10	
Trees	Deciduous trees	0.28	6-31		0	0	0	0.2	0.7	2.2	2.2	2.0	1.7	0.4	0.1
Facade greening	Deciduous trees	0.28	9		*1.9*	*2.5*	*2.1*	*1.9*	*1.9*	*1.9*	*1.8*	*1.7*	*1.5*	*1.3*	0.1

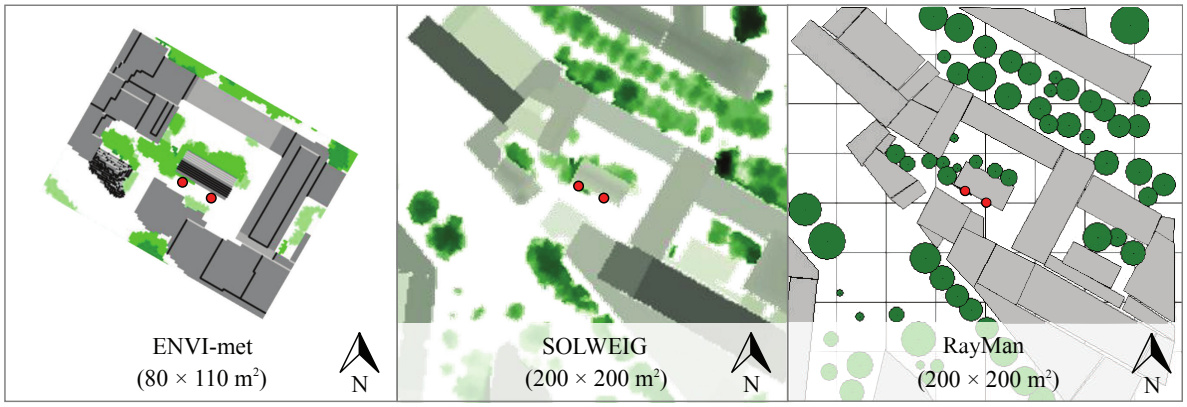

Fig. 2.3 Model domains of the different models. In the domain of SOLWEIG, dark colours represent taller buildings and vegetation compared to pale colours. Red circles indicate the greened and the bare site of observation and analyses.

SOLWEIG

SOLWEIG simulates radiation fluxes and T_{mrt} based on digital surface models (LINDBERG et al. 2008, 2011). In contrast to ENVI-met and RayMan, SOLWEIG calculates shadow patterns and consequently T_{mrt} for the middle of an hour; thus meteorological input was averaged accordingly. Vegetation and building data were also compiled with a resolution of 1 m. SOLWEIG uses trunk zones to calculate shadow patterns of vegetation, which were about 30 % of the vegetation height at the study site. The facade greening was represented as a flat plant without a trunk characterised by the observed values of albedo and transmissivity. In order to generate a SOLWEIG run (S0) without measurement data of global radiation, SOLWEIG1D was used. SOLWEIG1D calculates the maximum global radiation for the geographical location, which SOLWEIG2013a is not able to do.

RayMan

MATZARAKIS et al. (2007) developed the model RayMan (RayMan Pro 2.2) to calculate T_{mrt} and biometeorological indices in complex environments. The building and vegetation data were created manually with the supplied editor on the basis of the digital surface models. Due to this approach, buildings had a flat roof in RayMan. In contrast to SOLWEIG and ENVI-met, RayMan calculates fluxes only for one point of interest. Thus, two obstacle files were used with different centre points. Similar to SOLWEIG, RayMan can calculate global radiation itself. Consequently, we did experiments with calculated (R0) and measured global radiation (R1). The facade greening was represented as series of plants in front of the building with a diameter of 1 m, a trunk length of 0 m and an albedo of 0.28.

2.2.4 Analyses

The analyses of the simulation results refer to two points in front of the facade in each model domain, the greened site and the bare site (Fig. 2.3). For the model evaluation (Section 2.3.2), time series plots are only presented for the greened site, but the statistical analysis includes both sites.

The models that did not calculate a specific climate element (e.g. air temperature) were excluded for the section. Long-wave radiation from RayMan and ENVI-met was calculated from surface temperatures using the STEFAN-BOLTZMANN law (with an emissivity of 0.95).

The selected statistical measures for the model evaluation are a combination of generally recommended ones (WILLMOTT et al. 1985, SCHLÜNZEN and SOKHI 2008) and the ones mostly found in former studies (e.g. coefficient of determination, r^2). Root-mean-square deviation (RMSD), mean deviation (MD) and mean absolute deviation (MAD) were calculated as described by SCHLÜNZEN and SOKHI (2008). For all statistical analyses, we used IDL 8.2.2 (2007-2012 ExelisVisual Information Solutions, Inc.) and the library "Coyote" (1996-2014 Fanning Software Consulting, Inc.).

2.3 Results

2.3.1 Measuring the effects of facade greening on T_{mrt}

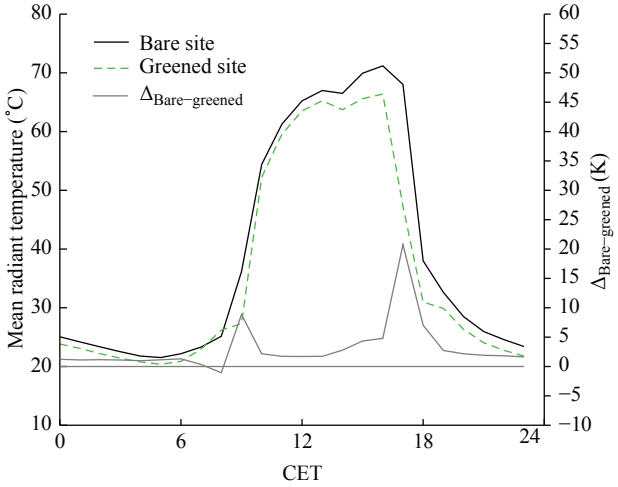

Fig. 2.4 Mean radiant temperature observed at the bare and the greened site in front of the building on the 23rd July 2013.

T_{mrt} decreased by 2.13 K (10:00-16:00 CET, 23rd July 2013) in front of the greened facade compared to the bare one (Fig. 2.4). The components for calculating T_{mrt} varied slightly between both sites and not only the short-wave radiation reflected and the long-wave radiation emitted from the facade from NNE (Fig. 2.5). Thus, the sums of short-wave and

long-wave radiation downward, upward and from the cardinal points differed between the bare and the greened site (Tab. 2.4). Nevertheless, long-wave radiation emitted from the greened site is clearly lower compared to the bare one.

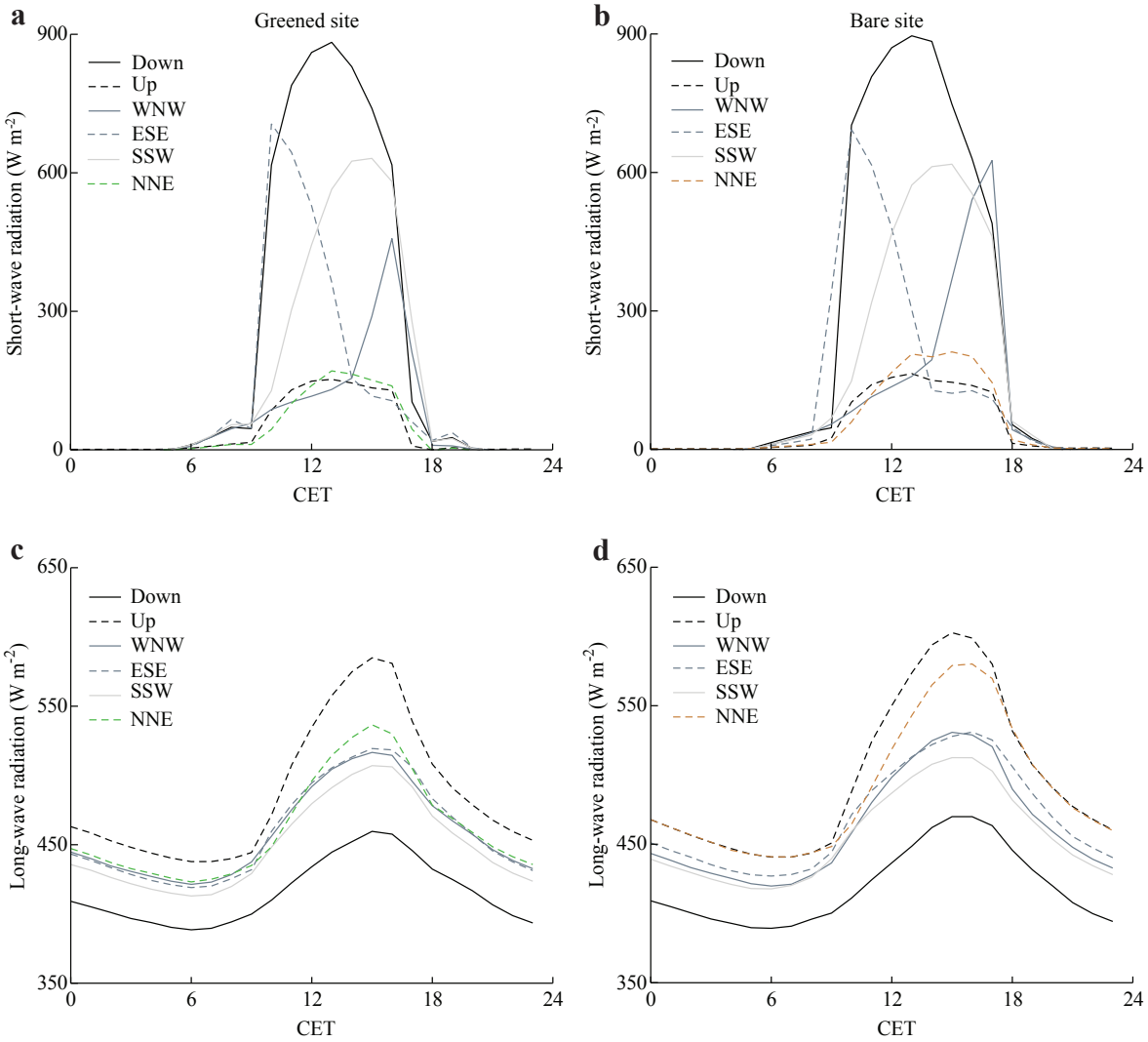

Fig. 2.5 Short-wave radiation at the greened a) and the bare b) site and long-wave radiation at the greened c) and the bare d) site on the 23rd July 2013. All components used to calculate mean radiant temperature are represented, which are up- and downward radiation (up, down) and radiation from the cardinal points (west-northwest (WNW), east-southeast (ESE), south-southwest (SSW) and north-northeast (NNE) (direction from the facades)).

2.3.2 Evaluation of ENVI-met, RayMan and SOLWEIG

Mean radiant temperature

The models simulated T_{mrt} reasonably well in pattern and amplitude compared to the observations (Fig. 2.6 a and b). Experiments with SOLWEIG showed the lowest normalised standard deviation (Fig. 2.6 b) and high r^2 (Tab. 2.5). Despite high absolute errors in RMSD and MAD, experiments with ENVI-met produced the lowest MD (Tab. 2.5).

Long- and short-wave radiation

Short-wave downward radiation in front of the greened and the bare site was simulated with high r^2 and low MD. RMSD showed larger deviation, especially in experiments with ENVI-met. Larger deviation also occurred in the morning and in the evening, which are the transition times between direct sun and shadow (Fig. 2.7 a, Tab. 2.6). Simulated short-wave upward radiation differed much more from observations than short-wave downward radiation (Fig. 2.7 b, Tab. 2.6). ENVI-met and SOLWEIG are able to compute short-wave upward radiation in contrast to RayMan. ENVI-met produced the amplitude more precisely than SOLWEIG, but SOLWEIG simulated the duration of intensive short-wave downward radiation closer to the observations (Fig. 2.7 a).

Concerning the long-wave downward radiation, SOLWEIG (S0 and S1) was the closest to the observations (Fig. 2.7 c and d). Long-wave upward radiation was underestimated during the night in all models. During the day, the differences between the simulations and observations decreased (Fig. 2.7 c).

Tab. 2.4 Sum (00:00-23:00 CET) of long- and short-wave radiation at the greened and the bare site up- and downward (up, down) and from the cardinal points (west-northwest (WNW), east-southeast (ESE), south-southwest (SSW) and north-northeast (NNE) (direction from the facades)) on the 23rd July 2013. F_i is the angular factor used in calculation of mean radiant temperature (0.06 for up- and downward radiation and 0.22 for radiation from the cardinal points).

Direction	Sum of short-wave radiations (MJ d^{-1})				Sum of long-wave radiations (MJ d^{-1})			
	Bare	Greened	$^{\Delta}$Bare-greened	$^{\Delta}$Bare-greened x F_i	Bare	Greened	$^{\Delta}$Bare-greened	$^{\Delta}$Bare-greened x F_i
Down	22.36	20.12	2.24	0.13	36.20	35.88	0.31	0.02
Up	4.35	3.57	0.78	0.05	43.02	42.04	0.99	0.06
WNW	8.67	6.11	2.56	0.56	39.92	39.60	0.33	0.07
ESE	10.93	10.39	0.54	0.12	40.49	39.62	0.87	0.19
SSW	14.27	13.44	0.83	0.18	39.36	38.81	0.55	0.12
NNE	5.03	3.54	1.49	0.33	42.29	39.92	2.37	0.52

Tab. 2.5 Overview of the performance of the experiments (EXP) in simulating mean radiant temperature on the 23rd July 2013, regarding root-mean-square deviation (RMSD), mean deviation (MD), mean absolute deviation (MAD) and coefficient of determination (r^2).

EXP	Mean radiant temperature (K)			
	RMSD	MD	MAD	r^2
E0a	7.98	-1.26	6.72	0.95
E0	8.30	0.99	6.90	0.94
E1	8.18	1.16	6.87	0.95
R0	7.11	-3.35	5.85	0.90
R1	7.35	-5.53	6.17	0.94
S0	4.63	-2.40	3.40	0.96
S1	4.81	-3.13	3.48	0.96
Mean	*6.91*	*-1.93*	*5.63*	*0.94*

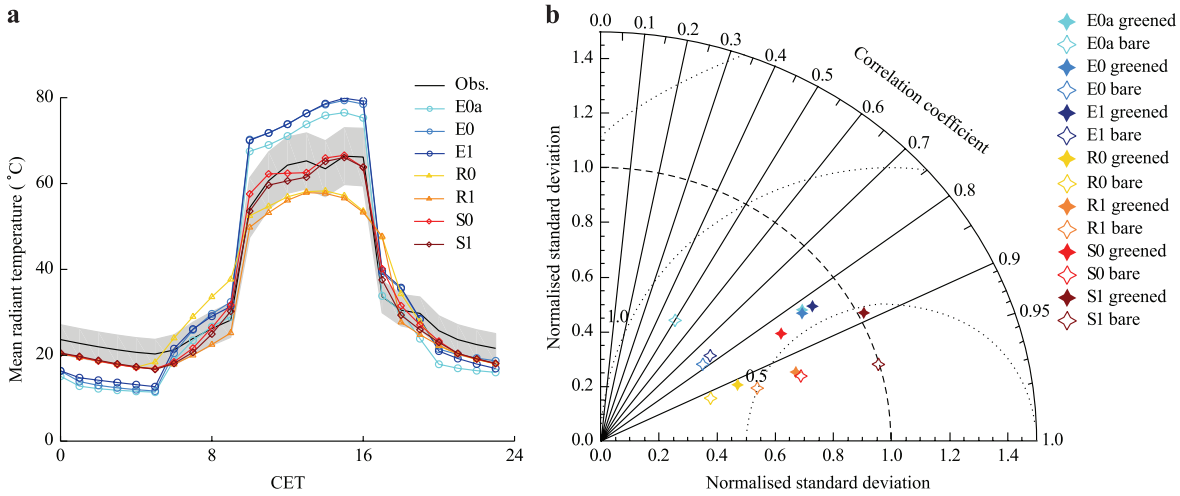

Fig. 2.6 Mean radiant temperature on 23rd July 2013, as observed and simulated a) at the greened site and b) TAYLOR-Diagram for the experiments with ENVI-met 3 (E0a), unforced (E0) and forced ENVI-met 4 (E1), RayMan without (R0) and with global radiation from observation (R1) and SOLWEIG without (S0) and with global radiation from observation (S1). The grey area indicates the accuracy range of the observations.

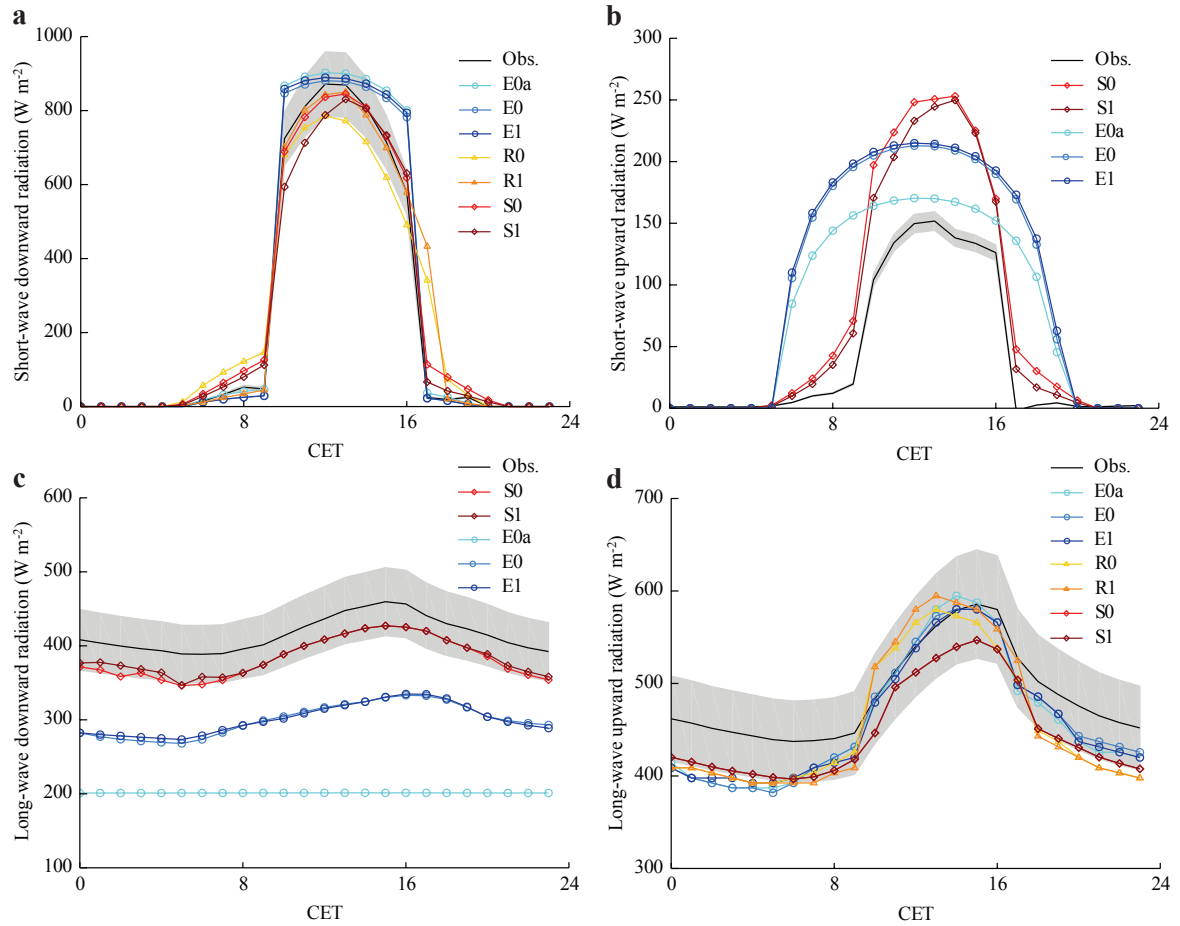

Fig. 2.7 Comparison of simulated and observed a) short-wave downward radiation, b) short-wave upward radiation, c) long-wave downward radiation and d) long-wave upward radiation on 23rd July 2013, for the greened site in front of the facade simulated with ENVI-met 3 (E0a), unforced (E0) and forced ENVI-met 4 (E1), RayMan without (R0) and with global radiation from observation (R1) and SOLWEIG without (S0) and with global radiation from observation (S1). The grey areas indicate the accuracy range of the observations.

Tab. 2.6 Overview of the performance in simulating downward a) and upward b) short-wave and long-wave radiation on the 23rd July 2013. For further explanations refer to table 2.5.

a)

Short-wave downward radiation (W m^{-2})				
EXP	RMSD	MD	MAD	r^2
E0a	130.46	46.31	50.33	0.91
E0	124.44	36.96	47.12	0.91
E1	128.17	40.46	49.70	0.91
R0	82.33	-6.15	54.06	0.96
R1	70.50	3.19	25.59	0.96
S0	54.65	-3.20	29.36	0.98
S1	65.86	-16.86	34.64	0.97
Mean	93.77	*14.39*	*41.54*	*0.94*
Long-wave downward radiation (W m^{-2})				
EXP	RMSD	MD	MAD	r^2
E0a	209.60	-208.03	208.03	0.01
E0	116.32	-115.83	115.83	0.82
E1	115.27	-114.85	114.85	0.86
R0	-	-	-	-
R1	-	-	-	-
S0	34.89	-34.31	34.31	0.95
S1	31.66	-31.16	31.16	0.95
Mean	*101.44*	*-100.71*	*100.71*	*0.71*

b)

Short-wave upward radiation (W m^{-2})				
EXP	RMSD	MD	MAD	r^2
E0a	61.86	38.34	39.84	0.60
E0	84.76	58.55	60.04	0.60
E1	87.12	60.50	62.00	0.60
R0	-	-	-	-
R1	-	-	-	-
S0	56.55	32.74	35.11	0.95
S1	51.36	27.94	30.57	0.95
Mean	*68.33*	*43.61*	*45.51*	*0.74*
Long-wave upward radiation (W m^{-2})				
EXP	RMSD	MD	MAD	r^2
E0a	35.19	-26.89	30.96	0.91
E0	33.28	-23.81	27.62	0.92
E1	31.70	-24.88	27.19	0.93
R0	46.23	-35.65	42.69	0.83
R1	46.62	-33.10	43.46	0.86
S0	43.28	-42.09	42.09	0.97
S1	43.30	-42.12	42.12	0.97
Mean	*39.94*	*-32.65*	*36.59*	*0.91*

Air temperature and specific humidity

Simulations with RayMan and SOLWEIG are based on predefined air temperatures and specific humidity; only ENVI-met computes these variables itself. ENVI-met captured the diurnal cycle of air temperature, but specific humidity was reproduced with low deviations from observations only in the forced run (E1) (Fig. 2.8 a and b). E1 showed lower deviations than E0a and E0 in simulating air temperatures, especially in the early morning (Fig. 2.8 a, Tab. 2.7). E1 was the closest to the observation for specific humidity as well (Fig. 2.8 b, Tab. 2.7). The unforced experiments E0a and E0 overestimated specific humidity by 1.5 g kg^{-1} (RMSD).

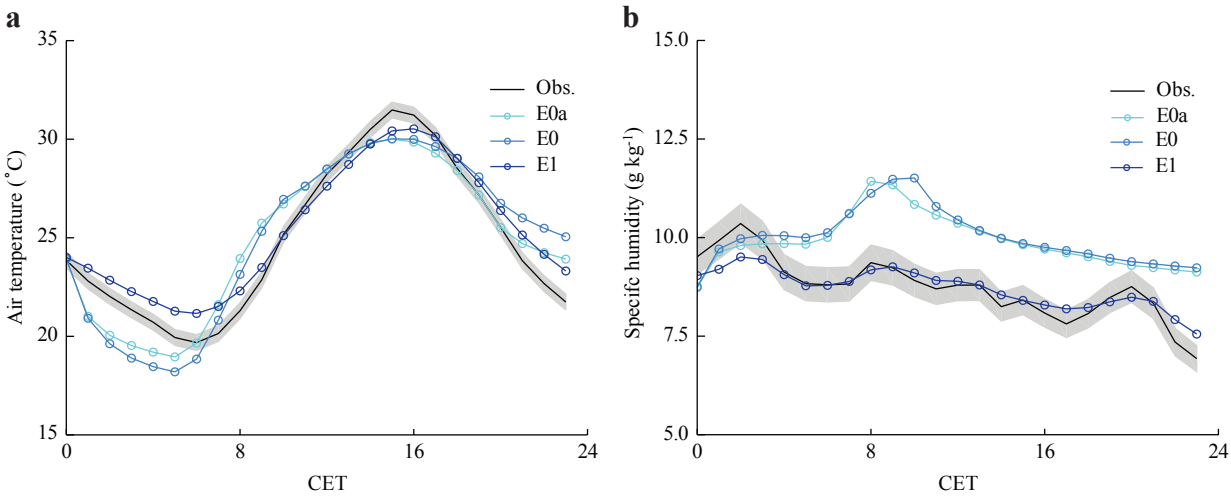

Fig. 2.8 Comparison of simulated and observed a) air temperatures and b) specific humidity of the experiments with ENVI-met 3 (E0a) and unforced and forced ENVI-met 4 (E0 and E1) on 23rd July 2013. The grey area indicates the accuracy range of the observations.

Tab. 2.7 Overview of ENVI-met's performance in simulating air temperatures and specific humidity on the 23rd July 2013. For further explanations refer to table 2.5.

EXP	RMSD	MD	MAD	r^2
Air temperature (K)				
E0a	1.39	0.00	1.13	0.87
E0	1.68	0.06	1.43	0.83
E1	0.96	0.40	0.86	0.98
Mean	*1.35*	*0.16*	*1.14*	*0.89*
Specific humidity (g kg^{-1})				
E0a	1.44	1.17	1.31	0.10
E0	1.54	1.28	1.40	0.10
E1	0.35	-0.03	0.25	0.91
Mean	*1.11*	*0.81*	*0.99*	*0.37*

2.3.3 Comparison of the observed and simulated effects of facade greening

The observed differences between the bare and the greened site were not well reproduced by the models (Fig. 2.9, Tab. 2.8). The peaks in the transition times were simulated in all models to different extent. The cooling effect of facade greening, however, was only simulated by S0 and S1, although too small. The experiments with ENVI-met showed a higher T_{mrt} in front of the greened site than in front of the bare site, while R0 and R1 produced no differences between the sites (Tab. 2.8). Emitted long-wave radiation from the greened site was reduced in the experiments with ENVI-met and SOLWEIG (Fig. 2.10 a), but to a smaller extent (Fig. 2.10 b).

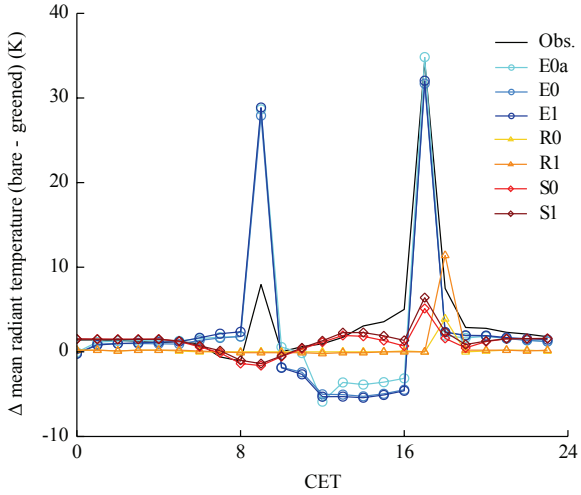

Fig. 2.9 Differences between the bare and greened site in observation and simulations (23rd July 2013) in experiments with ENVI-met 3 (E0a), unforced (E0) and forced ENVI-met 4 (E1), RayMan without (R0) and with global radiation from observation (R1) and SOLWEIG without (S0) and with global radiation from observation (S1).

Tab. 2.8 Mean (± standard deviation), minimum and maximum difference in T_{mrt} between bare and greened site in observation (OBS) on the 23rd July 2013 (10:00-16:00 CET) and experiments (EXP) with ENVI-met 3 (E0a), ENVI-met 4 (E0 and E1), RayMan (R0 and R1) and SOLWEIG (S0 and S1).

EXP	T_{mrt} (Bare-Greened) (K)		
	Mean	Minimum	Maximum
OBS	2.13±1.81	0.02	5.02
E0a	-2.81±2.25	-5.89	0.57
E0	-4.14±1.41	-5.56	-1.82
E1	-4.32±1.44	-5.42	-1.88
R0	0.01±0.04	0.00	0.10
R1	-0.09±0.07	-0.20	0.00
S0	0.96±0.88	-0.57	1.94
S1	1.30±1.01	-0.49	2.28

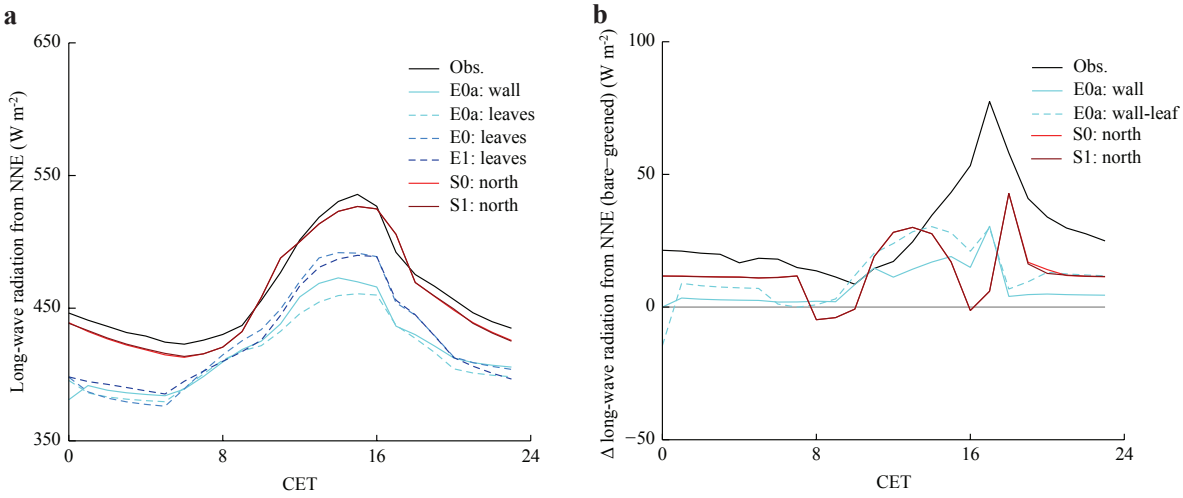

Fig. 2.10 Simulated long-wave radiation a) emitted from the greened site (wall or leaves) and b) differences between bare and greened facade in simulations and observation for the experiments with ENVI-met 3 (E0a), unforced (E0) and forced ENVI-met 4 (E1) and SOLWEIG without (S0) and with global radiation from observation (S1) (23rd July 2013).

2.4 Discussion

2.4.1 Measuring the effects of facade greening on T_{mrt}

The observed differences in T_{mrt} of 2 K were distinct but lower than the measurement accuracy of about 4 K. TAN et al. (2014) detected larger differences of 2 to 13 K between sites with and without facade greening in a tropical environment. They only detected a reduction of T_{mrt} when the facade greening was opposed to direct sunlight and not shaded. In addition, the reduction depended on the distance to the facade and was mainly limited to 1 m. Thus, the small observed differences in this study can be partly explained with the larger distance of the measurement to the facade of 1.2 m. Furthermore, the effects of facade greening on air temperature were found to be small (1.5 K, DJEDJIG et al. (2013), 1 K, BERRY et al. (2013), 0.25 K, GROSS (2012) and negligible, PÉREZ et al. (2011)). In this case study, facade greening was only attached to one facade wall. Hence, the impact on modified long- and short-wave radiation from the greened facade accounts to only 22 % in calculating T_{mrt} (eq. 2.1). Therefore, the impact on T_{mrt} was limited, even though emitted long-wave radiation was clearly reduced in front of the greened facade. The albedo also interferes with T_{mrt} because the light bare wall with its higher albedo reflected more short-wave radiation than the darker greened facade.

Furthermore, the differences in T_{mrt} cannot be reduced to the effects of facade greening exclusively. Boundary conditions were different between both sites regarding times of shadowing (Tab. 2.4). The opposing building structure is higher in front of the bare site than in front of the greened site (Fig. 2.3), which leads to different shadowing times. In the evenings, at around 17:00 CET, the greened facade was completely shadowed while the bare site still received direct sunlight for another half an hour. In the morning, at around

09:00 CET, when the sunlight appeared at the facade, some differences existed as well. Furthermore, the opposing building might also have an influence regarding the reflection of short-wave radiation. With respect to short-wave and longwave radiation, the greened site received less energy from all directions than the bare one. Consequently, the cooling effect of T_{mrt} was overestimated in the observations. This demonstrates shortcomings in the case study as both sites were not identical regarding the radiation characteristics, which introduces uncertainties when interpreting deviations between the sites. The problem of comparability and usability of case studies to observe the effects of facade greening occurs often as criticised by HUNTER et al. (2014). Specifically in complex urban environments optimal study sites are difficult to find. Elaborated assessments (e.g. integral radiation measurements) can reveal such problems in contrast to simple single-variable measurements (e.g. air temperature). Our findings further support the need of reliable model tools in combination with observations to study the effects of facade greening for specific sites and climates.

2.4.2 Evaluation of ENVI-met, RayMan and SOLWEIG

Mean radiant temperature

Simulated T_{mrt} deviated about 7 K (mean RMSD) from the observation in this and about MD 2 to 8 K and 2 to 15 K RMSD in former studies (Tab. 2.9). This uncertainty range is reasonable compared to the average accuracy in measurements of about 4 K. The uncertainty, however, varies largely depending on the selected model and study design (Tab. 2.9). KRÜGER et al. (2013) concluded for RayMan that the uncertainty in calculating T_{mrt} depends on different factors, such as morphology, meteorological conditions and surface properties. For example, correlation coefficients were much higher in this study compared to the investigations of CHEN et al. (2014). Such deviations are caused by model specific parameterisations.

Other reasons for deviations in all applied models were discrepancies in building or plant shapes. All experiments produced larger deviations during the transition between shadow and direct radiation, which was also reported by THORSSON et al. (2007) and MATZARAKIS et al. (2010). Such deviations are caused by inaccuracies in building shapes due to the spatial resolution of 1 m or by errors in the basic data of building shapes.

Simulated T_{mrt} differed hardly between the computed and predefined meteorological input data. Consequently, calculated global radiation by RayMan and SOLWEIG was sufficient for simulating T_{mrt} and observations of global radiations did not enhance the model performance considerably, at least for this nearly cloud-free day. In ENVI-met, the forcing of air temperature and relative humidity showed only minor effects on simulating T_{mrt} as well.

In SOLWEIG, the transmissivity is of importance for calculating T_{mrt} beneath vegetation (LINDBERG and GRIMMOND 2011). We applied an averaged value for the whole model domain because we measured transmissivity only at two points of the facade greening and SOLWEIG does not allow any spatial variations. Nevertheless, the range of deviations in

this study is similar to findings by LINDBERG and GRIMMOND (2011), who detected a RMSD of 3.1 K and a MAD of 2.74 K. RayMan underestimated T_{mrt} in this study probably as a consequence of too low short-wave downward radiation. On the contrary, KRÜGER et al. (2013) examined an overestimation for various cloudiness conditions (RMSD 14.93 K, MAD 12.88 K). Additionally, they detected a higher agreement with observations on clear sunny days compared to cloudy ones (KRÜGER et al. 2013). During sunny days, the accuracy of SVF has a high influence on the uncertainty in simulating T_{mrt} (KRÜGER et al. 2013). Hence, inaccuracies in the building and vegetation shape had a large impact in this study. The deviation in RayMan varies remarkably in this study and other ones (MATZARAKIS et al. 2007, THORSSON et al. 2007, HWANG et al. 2011) (Tab. 2.9).

Tab. 2.9 Overview of deviations in mean radiant temperature between simulations and observations in other studies concerning root-mean-square deviation (RMSD), mean deviation (MD), mean absolute deviation (MAD) and coefficient of determination (r^2). Standard deviations (±) are stated, if more than one analysis is performed per study.

	Mean radiant temperature (K)			
Reference	RMSD	MD	MAD	r^2
		ENVI-met		
CHEN et al. (2014)	-	-	-	0.09±0.1
HUTTNER (2012)	4.13±0.4	-	-	-
E1	8.18	1.16	6.87	0.95
		RayMan		
CHEN et al. (2014)	-	-	-	0.82±0.0
HWANG et al. (2011)	-	-	-	0.88
KRÜGER et al. (2013)	14.93±3.5	-	12.88±3.5	0.37±0.2
LIN et al. (2010)	-	-	-	0.85
THORSSON et al. (2007)	-	8.45±1.7	-	-
MATZARAKIS et al. (2007)	-	-	-	0.77
MATZARAKIS et al. (2010)	1.7±0.5	-	-	0.96±0.5
Mean	*8.32±2.0*	*8.45±1.7*	*12.88±3.5*	*0.74±0.23*
R1	7.35	-5.53	6.17	0.94
		SOLWEIG		
CHEN et al. (2014)	-	-	-	0.32
LINDBERG et al. (2008)	4.8	2.00±0.3	-	0.94
LINDBERG and GRIMMOND (2011)	3.1	-	2.74	0.91
Mean	*3.95*	*2.00±0.3*	*2.74*	*0.72*
S1	4.81	-3.13	3.48	0.96

The uncertainty also differs strongly between different studies with ENVI-met. ALI-TOUDERT (2005) detected an underestimation of T_{mrt} during the day and an overestimation during the night. In this study, however, the overestimation of short-wave radiation led to an overestimation of T_{mrt}. YANG et al. (2011) also detected an overestimation in ENVI-met due to an overestimation of short-wave downward radiation (without statistical values).

Overall, SOLWEIG simulated T_{mrt} closest to the observation both in this study and in former ones (Tab. 2.9). ENVI-met showed the largest deviations in this study. Furthermore, shortcomings in the evaluation of all three models become visible regarding the amount of studies and in comparability due to different statistics to evaluate models uncertainty.

Long- and short-wave radiation

Short-wave downward radiation showed less deviations compared to other radiation components. ENVI-met did not capture the amplitude of global radiation well, partly because only water vapour alternates short-wave radiation (YANG et al. 2011). Additionally, ALI-TOUDERT (2005) detected problems in simulating global radiation with ENVI-met and consequently a radiation adjustment factor was introduced to ENVI-met. Here, short-wave downward radiation in ENVI-met was reduced in advance by 25 % to match the amplitude of observations (Tab. 2.2). Additional deviations in short-wave downward radiation were produced by the resolution of grid points and by inaccuracies of the input data of buildings and vegetation as discussed for T_{mrt}. The small deviation in short-wave downward radiation was a main driver for the sufficient simulation of T_{mrt}.

Short-wave upward radiation has less impact on T_{mrt} due to the generally smaller energy flux density and low F_i in the calculation of T_{mrt}. Thus, the overestimation in all experiments was less decisive for simulating T_{mrt}. ENVI-met overestimated the duration of intense shortwave upward radiation because shadowing effects of the surface are neglected. SOLWEIG captured the duration but overestimated the amplitude of short-wave upward radiation due to a higher albedo. SOLWEIG cannot consider different albedo values of ground surfaces and walls. In future, this problem might be fixed because LINDBERG and GRIMMOND (2011) proposed for the next SOLWEIG version the possibility to specify albedo and emissivity spatially.

Long-wave downward radiation was underestimated. The overestimations of short-wave upward radiation and longwave downward radiation compensate each other and thus the total impact of the inaccuracies on T_{mrt} was reduced. ENVI-met 3 (E0a) failed to simulate the diurnal variation of long-wave downward radiation as it uses averaged emissivity values and surface temperatures to calculate it.

Long-wave upward is underestimated during the night because the models do not consider heat storage of the buildings sufficiently (ENVI-met 4) or not at all (ENVI-met 3, SOLWEIG and RayMan). HWANG et al. (2011) and LIN et al. (2010) discussed these shortcomings in ENVI-met 3 and detected the fact that daytime surface temperature was overestimated and night-time surface temperature was underestimated. ENVI-met 4 should be able to consider these effects in principle but failed in this case study. Possibly, the heat storage was insufficiently parameterised or the spin-up time was too short. Follow-up studies might acquire a more suitable description of heat storage in the walls. During the night, the underestimation of emitted long-wave radiation also led to undervalued T_{mrt} in all experiments.

Overall, the individual terms of the radiation balance were, with the exception of short-wave downward radiation, not plausibly simulated by all models. Short-wave downward radiation

may also show much higher inaccuracies under cloudy conditions as KRÜGER et al. (2013) detected for RayMan. Furthermore, the lack of model evaluation is more apparent for the individual terms of the radiation balance than for T_{mrt} as we detected only three other studies (Tab. 2.10), which leads to a high uncertainty regarding the reliability in simulating these variables.

Tab. 2.10 Overview of deviations in short-wave downward radiation between simulation and observation in other studies. For further explanation refer to table 2.9.

	Short-wave downward radiation (W m^{-2})			
Reference	RMSD	MD	MAD	r^2
		ENVI-met		
SRIVANIT and HOKAO (2013)	-	-289.15±8.8	-	-
E1	128.17	40.46	49.70	0.91
		SOLWEIG		
LINDBERG et al. (2008)	42.1	-	-	0.97
LINDBERG and GRIMMOND (2011)	43.3	-	-	0.97
Mean	*42.2*	-	-	*0.97*
S1	65.86	-16.86	34.64	0.97

Air temperature and specific humidity

ENVI-met reproduced air temperature close to the observations with a RMSD between 0.9 and 1.6 K and MD between 0.0 and 0.4 K in this case study and with a mean RMSD of 1.9 K and MD -0.65 K in former studies (Tab. 2.11). During the day, ENVI-met tended to underestimate air temperature but overestimated it during the night (LIN et al. 2010, ALI-TOUDERT 2005). BERKOVIC et al. (2012), who compared simulations and observations qualitatively, found larger differences during the evenings for air temperatures and relative humidity (about 3 K, 15 %). Forcing in E1 clearly decreased the uncertainty compared to E0 especially during the day but showed only minor effects on T_{mrt}.

The uncertainty in simulating air temperature with ENVI-met varies between different studies remarkably (Tab. 2.11). A high agreement was achieved by SKELHORN et al. (2014) and SRIVANIT and HOKAO (2013) after optimisation and calibration efforts of different parameters and with a longer spin-up time. Air temperature has been evaluated in several studies. Thus, the simulation seems to be reliable, with an uncertainty of about 1.88 K (RMSD). Specific humidity was evaluated by CHEN et al. (2014) with a RMSD of 0.82 g kg^{-1}, which is higher than in this study (RMSD = 0.35 g kg^{-1}). Forcing (E1) improved the simulation of specific humidity compared to the unforced runs (E0a, E0).

2.4.3 Comparison of the observed and simulated effects of facade greening

The applied models were not able to reproduce the observed effects of facade greening. SOLWEIG was the only model that simulated at least a small reduction of T_{mrt}. The reductions cannot be related to transpirative effects of the plants because such effects are not considered in SOLWEIG. Thus, the decrease in T_{mrt} was produced by radiation changes. Simulated long-wave radiation emitted from the wall was clearly reduced in front of the facade greening (S0, S1).

Tab. 2.11 Overview of deviations in air temperature and specific humidity between simulation and observation in other studies. For further explanations refer to table 2.9.

	Air temperature (K)			
Reference	RMSD	MD	MAD	r^2
CHOW and BRAZEL (2012)	2.79±0.0	0.66±0.1	2.40±0.1	0.70±0.0
CHOW et al. (2011)	1.45±0.1	-1.29±0.0	1.29±0.0	-
EMMANUEL and FERNANDO (2007)	1.95±0.4	-	-	-
HEDQUIST and BRAZEL (2014)	2.91±0.9	-0.62±1.3	2.45±0.7	0.90±0.1
HUTTNER (2012)	1.37±0.4	-	-	-
MIDDEL et al. (2014)	1.74±0.3	-	-	-
MÜLLER et al. (2014)	-	-	-	0.97
NG et al. (2012)	-	-	-	0.70±0.1
PENG and JIM (2013)	-	-3.50±0.5	-	0.95±0.0
SKELHORN et al. (2014)	-	0.64±0.3	-	0.94
SRIVANIT and HOKAO (2013)	-	-0.56±0.9	-	-
SRIVANIT and HOKAO (2013)	-	0.10	-	-
YANG et al. (2013)	0.93±0.1	-	-	0.95±0.0
Mean	*1.88±0.4*	*-0.65±0.53*	*2.05±0.3*	*0.87±0.4*
E1	0.96	0.40	0.86	0.98
	Specific humidity (g kg^{-1})			
YANG et al. (2013)	0.82±0.0	-	-	0.54±0.0
E1	0.35	-0.03	0.25	0.91

ENVI-met, which is able to simulate transpiration, reproduced higher T_{mrt} in front of the greened site compared to the bare site. Emitted long-wave radiation was reduced in front of the greened facade, but the effect was not permeated to T_{mrt}. Increasing the spin-up time in ENVI-met might amplify the generation of effects of facade greening. Specifically in ENVI-met and RayMan, the inabilities in simulating a reduction of T_{mrt} in front of the greened facade could not be easily traced back because they do not return all relevant components for T_{mrt}. To conclude, the models showed a limited applicability to facade greening in this study. The small alterations of long and short-wave radiation due to facade greening were indistinct. Thus, specific types of urban green cannot be included in these models without further adaptations. Restrictions must be made, however, regarding the complex real-case study site. Moreover, modification of model parameters and settings (e.g. spin-up time)

especially for ENVI-met could lead to other results but would go beyond the scope of this study.

2.5 Conclusions

The effect of facade greening on outdoor human bioclimate was limited in this case study because only a small reduction T_{mrt} in front of the facade greening was detected. Hence, facade greening has only a minor effect in reducing outdoor heat stress. With a facade greening attached to more than one facade in a street canyon or court yard the effect on T_{mrt}, however, might be enlarged.

The general ability of ENVI-met, RayMan and SOLWEIG to simulate T_{mrt} was reasonable as expected for well-established models. Nevertheless, the deviations from observations vary largely between different studies. Additionally, the deviations from observations for other variables (specific humidity, long-wave downward or short-wave upward radiation) were higher and might impede the models' ability in assessing heat stress. When considering the large differences in complexity and computational time, the good performance of the simple SOLWEIG and RayMan models contrary to the elaborate ENVI-met model is encouraging. ENVI-met, however, offers more opportunities for various issues, such as studies of plant-air interactions or effects of changes in albedo of individual surfaces. It also provides more options for tuning and modifications by the users, which were not completely exhausted in this study. Moreover, we recognised a lack of model evaluations regarding the amount of evaluation studies and the considered variables. An explicit statement of model uncertainties for interpreting the results should be included in every study and not only in rare exceptional cases.

The applied models are helpful for assessing human bioclimate in general due to the acceptable uncertainty in simulating T_{mrt}. In the specific case of facade greening in a complex urban environment, however, their usability is limited in the current set-up. Generic studies or simple environments combined with modified parameterisations might improve the usability. Specific types of vegetation besides trees should not be incorporated in these models without modifications and extensive evaluation. Therefore, new simulation tools or advancements in existing models are desirable to complement observational case studies. The combination of biometeorological microclimate models and observations is helpful in order to complement benefits of each method. More effort in bridging the gaps between case studies and large-scale applications of countermeasures is needed to detect an effective countermeasure against heat stress risks in cities.

Conflict of interests

The authors declare that there is no conflict of interests regarding the publication of this paper.

Acknowledgments

The authors wish to thank their colleagues for the great support during the measurement campaign and the enriching discussions. The study is part of the Research Unit 1736 “urban climate and heat stress in mid-latitude cities in view of climate change (UCaHS)” (www.UCaHS.org) funded by the Deutsche Forschungsgemeinschaft (DFG) under the codes SCHE 750/8-1, SCHE 750/9-1 and WE 1125/30-1.

3 Quantifying cooling effects of facade greening: shading, transpiration and insulation[2]

MARIE-THERESE HOELSCHER[a,*], THOMAS NEHLS[a], BRITTA JÄNICKE[b] and GERD WESSOLEK[a]

[a] Department of Ecology, Soil Conservation, Technische Universität Berlin

[b] Department of Ecology, Climatology, Technische Universität Berlin

*corresponding author; e-mail address: marie-therese.hoelscher@tu-berlin.de

Abstract

Facade greening is expected to mitigate urban heat stress through shading, transpiration cooling and thermal insulation. This study quantifies cooling effects of facade greenings for the building and the street canyon and distinguishes between transpiration and shading effects. Additionally it discusses insulation effects.

Outdoor experiments were conducted during hot summer periods on three building facades in Berlin, Germany. We determined transpiration rates (sap flow) and surface temperatures of greened and bare walls as well as of plant leaves (temperature probes) of three climbing plants: *Parthenocissus tricuspidata*, *Hedera helix* and *Fallopia baldschuanica*. Furthermore, air temperature, relative humidity and incoming short-wave radiation were measured.

No cooling effect was detectable for the street canyon. Surface temperatures of the greened exterior walls were up to 15.5 °C lower than those of the bare walls, while it was up to 1.7 °C for the interior wall (measured during nighttime). The cooling effects mainly depended on shading, whereas a lower proportion was due to transpiration. Insulation of the direct greenings reduced radiation during nighttime. We conclude that greening can be an effective strategy to mitigate indoor heat stress as long as the plants are sufficiently irrigated with up to 2.5 L d^{-1} m^{-2} per wall area.

Keywords

Cooling, vertical greening, climbing plants, transpiration, shading, insulation, building, urban context

[2] Published: HOELSCHER, M.-T., T. NEHLS, B. JÄNICKE and G. WESSOLEK (2015). Quantifying cooling effects of facade greening: Shading, transpiration and insulation. *Energy and Buildings* 114 (2016): 283-290.

3.1 Introduction

Cities often have higher air temperatures than their rural surroundings (ARNFIELD 2010) which is called urban heat island (UHI) effect. Especially at night, these differences are high (BUYANTUYEV and WU 2010). For instance, measured air temperatures in the densely built-up city centre of Berlin were up to 8 °C higher than the ones of the Grunewald forest in medium low-exchange, nocturnal radiation periods (SENSTADT 2001).

The UHI phenomenon is mainly caused by the increased absorption of solar radiation by a city surface compared to a natural landscape (TAKEBAYASHI and MORIYAMA 2007). It is the result of (i) the city's high surface area due to its vertical structure and (ii) the higher heat storage due to the higher density and higher heat capacity of the built structures compared to natural vegetated surfaces (ALEXANDRI and JONES 2004). The higher heat capacity leads to higher long-wave emission of the built structures during the night (SHAM et al. 2012). Further reasons are increased anthropogenic heat emissions (MONTÁVEZ et al. 2008) and limited evapotranspiration due to the lack of vegetation (WANG and XU 2008). Global climate change is increasing these already higher temperatures in the mid-latitudes cities, which leads to increased heat stress outdoors as well as indoors for the urban population (MAYER and HÖPPE 1987).

Heat stress threatens human health and leads to higher mortalities, especially of elderly people (≥ 65 years) (SCHERER et al. 2014, BUCHIN et al. 2015). GABRIEL and ENDLICHER (2011) could better explain excess mortalities in Berlin by daily minimum air temperatures above 20 °C than by daily maximum air temperatures above 30 °C. This shows the impact of high nocturnal temperatures on sleep disturbances, thus on human well-being and health (FRANCK et al. 2013).

Several studies show that urban vegetation reduces the ambient air temperature (e.g. LU et al. 2012). However, space for horizontal urban vegetation is restricted and its effectiveness is spatially limited for adjacent quarters (BOWLER et al. 2010). Vertical greening seems to be a promising countermeasure to urban heat stress, as it can be applied nearly everywhere in the city, particularly on buildings, the structures in which people mainly suffer from heat stress (FRANCK et al. 2013). Moreover, it is expected to reduce ambient air temperatures because of its high evapotranspiration rate per horizontal base area.

Facade greening provides cooling towards the greened structures through shadowing, transpiration cooling and thermal insulation (PÉREZ et al. 2011). Additionally, it influences the heat distribution in the street canyon by: (i) absorption and conversion of solar radiation into photochemical energy and latent heat which otherwise would be absorbed elsewhere and (ii) cooling the air in the vicinity of the greening, which induces air flow in the canyon.

In the last years, the cooling potential of facade greening has been considered in numerous studies (STEC et al. 2005, SUSOROVA et al. 2013, JÄNICKE et al. 2015), whereas most of them have concentrated on surface wall temperatures. For instance, WONG et al. (2010) found maximum differences in surface wall temperatures between a greened and a bare wall of -11.6 °C. The highest differences so far were measured by MAZZALI et al. (2013) with differences of up to -20 °C. Most of these studies focus on the shading effect which depends

on plant traits, such as number of leaf layers, percentage of coverage and leaf solar transmittance (IP et al. 2010, KOYAMA et al. 2013). Shading reduces energy consumption for air-conditioning systems by up to 19 % (STEC et al. 2005). However, these are results of case studies. So far, no studies are available on water demand and transpiration rates of urban facade greenings, although such information is necessary for a general model on the cooling effects and the sufficient watering of the plants. One opportunity to measure transpiration rates are sap flow measurements, as successfully applied for climbing plants by LEUZINGER et al. (2011).

Furthermore, there is no sufficient differentiation between shading and transpiration. A first approach was recently started by CAMERON et al. (2014), who separated these two cooling effects for some plant species including one climbing plant. According to that, *Hedera helix* reduced surface wall temperatures by an average of 7.3 °C, for which shading accounted for 60 %. However, the plants were potted and standing in front of a wall, not attached to it as usual for facade greenings. Shading and transpiration were differentiated by cutting the stems or sealing the foliage to prevent transpiration, thus not allowing long-term measurements.

In our study, we focus on three typical facade greening species in their typical settings inside the city, attached to the walls: *Parthenocissus tricuspidata*, *Hedera helix* and *Fallopia baldschuanica*. We (i) quantify the cooling effects of facade greening for the building and the ambient urban air and (ii) distinguish between transpiration and shading effects. Additionally we discuss insulation effects. Finally, we (iii) quantify the water demands of the investigated facade greening species as a prerequisite for an effective cooling.

3.2 Materials and methods

3.2.1 Plant species

Three different climbing plants were investigated: *Parthenocissus tricuspidata*, *Hedera helix* and *Fallopia baldschuanica*.

P. tricuspidata is originally distributed in Asia and North America. *H. helix* is an evergreen climbing plant with its natural habitat in European woodlands. Both, *P. tricuspidata* and *H. helix*, are self-clinging climbers which climb directly on the building surface with their adhesive pads and their adventitious roots, respectively. They are well-examined (e.g. BARTFELDER and KÖHLER 1987, STERNBERG et al. 2011, HUNTER et al. 2014) and also widely used as facade greening plants in mid-latitude cities.

F. baldschuanica is a deciduous rambling plant originating from Asia that needs climbing aids for its upward growth. It is a very fast-growing and relatively undemanding climbing plant.

3.2.2 Study sites

In order to study the cooling effects of facade greenings, measurement campaigns were carried out on three building facades at the campus of the Technische Universität Berlin, in the city centre of Berlin, Germany (lat. 52°51'N, long. 13°32'E). In each case, the investigated facades were greened on one half, while the other half was bare.

The following facades were investigated:

(a) Site A (Fig. 3.1 a): a south south-west exposed facade of a building greened with *P. tricuspidata* which clung directly on the wall ("direct facade greening" according to HUNTER et al. (2014)). The plants rooted in a raised bed filled with humic sand (unsealed area about 6 m^2) and were supplied with water in irregular intervals. The measurement campaign on this building facade was carried out from 19th July to 16th August 2013.

(b) Site B (Fig. 3.1 b): an east exposed facade with a dark coloured wall surface which was greened with *H. helix* (adult type). As described for the first site, the plants were attaching themselves on the building facade without technical climbing support. During the experiment, the plants were additionally supplied with water. The measurement campaign lasted from 1st August to 6th August 2014.

(c) Site C (Fig. 3.1 c): a west exposed facade (a 12 m high gable wall of a large hall, with only one big room inside, heated in winter but not air conditioned in summer) greened with *F. baldschuanica*. The plants had additional climbing support structures 0.3 m in front of the wall, leaving an air cavity of about 0.2 m ("double-skin green facade" according to HUNTER et al. (2014)). They were planted in containers with humic sand and supplied with nutrient solution from a constant standing water table in 0.45 m depth. Thus, they were perfectly irrigated except of a drought experiment taking place from 16th to 20th September 2014. In that period, no irrigation took place, only the water stored in the substrate was left for the plants. Measurements on this facade were carried out since August 2013.

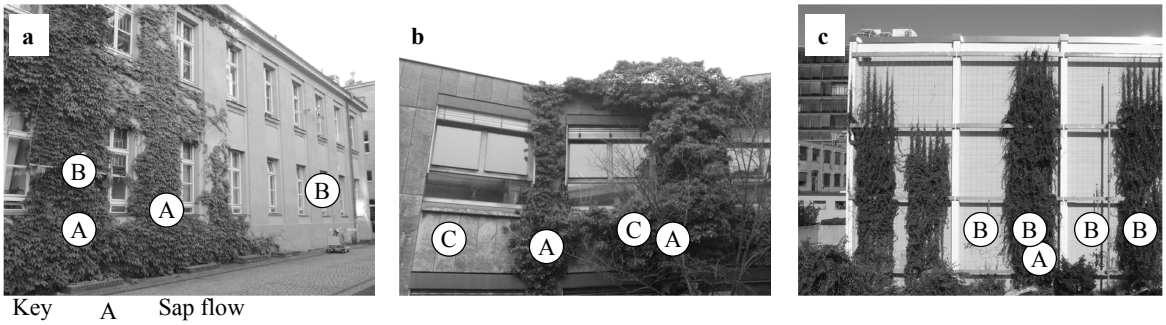

Key
A Sap flow
B Surface temperature, short-wave radiation, air temperature, relative humidity
C Surface temperature

Fig. 3.1 Three investigated building facades and the experimental designs: a) south south-west exposed facade greened with *Parthenocissus tricuspidata*, b) east exposed facade greened with *Hedera helix* and c) west exposed facade greened with *Fallopia baldschuanica*.

To calculate the wall leaf area index (WLAI, mean leaf area corresponding covered wall area) of the whole facade greenings, we harvested the leaves of at least 2 m^2 vertical area in different heights for every facade greening at the end of the measurement campaign. WLAI of the investigated facades was 1.9 for *P. tricuspidata*, 3.0 for *H. helix* and 3.0 for *F. baldschuanica*. We also determined the area of the leaves on the stems used for sap flow measurements (see below) to calculate the transpiration rate based on leaf area (LA) and wall area (WA).

3.2.3 Meteorological measurements

At each site, we measured the surface temperatures of the bare exterior wall (n = 3), the exterior wall behind the greening (n = 3) and of the plant leaves (n = 5) (SKTS 200/U 10K Thermistor, Umweltanalytische Produkte, Germany) (Fig. 3.1 a-c). At site C, additionally the surface temperatures of the interior building wall were measured for the vegetated and bare segments (n = 3 each), which both belonged to the same room. No further indoor climate parameters were measured.

For building facade A and C, meteorological measuring stations were installed 0.4 m in front of the bare and the greened facade at approximately 2.8 m above the ground. Air temperature, relative humidity (RFT-325, Driesen + Kern, Germany; HC2-S3, Rotronic Messgeräte, Germany) and incoming short-wave radiation reaching the facade (SP-110, Apogee Instruments, Inc., USA; LP02-05, Hukseflux Thermal Sensors B.V., the Netherlands) were measured in five minute intervals. Incoming radiation is given in W m^{-2}, while its cumulative sum for the whole day is given in J m^{-2}. Due to the distance between the greened and the bare station at facade A (Fig. 3.1 a), the diurnal cycles of the incoming short-wave radiation at both stations were slightly time-shifted. On a daily basis, however, the differences between both positions were less than 0.2 % of the total radiation and consequently negligible.

The accuracy of the temperature probes was 0.1 °C while the uncertainty of the radiation measurements was 0.15 x 10^{-6} V W^{-2} m^{-2}.

3.2.4 Quantifying shading

In order to calculate the cooling effect through shading, another short-wave radiation sensor was installed behind the greening at site A and C. Shading effect S (W m^{-2}) was calculated by the following equation:

$$S = K\downarrow_{f} - K\downarrow_{b}, \qquad \text{(eq. 3.1)}$$

where $K\downarrow_f$ (W m^{-2}) is the incoming short-wave radiation in front and $K\downarrow_b$ (W m^{-2}) the incoming short-wave radiation behind the greenery.

3.2.5 Quantifying transpiration

Transpiration rates of the climbing plants were determined by sap flow gauges (Sap flow module EMS 62, EMS Brno, Czech Republic) based on the stem heat balance method, with external heating and internal temperature sensing, described in detail by LINDROTH et al. (1995). For every facade greening, several main stems were instrumented, wrapped with insulation foam and shielded against direct solar radiation and precipitation. Sap flow Q_S, measured in a one minute resolution, is expressed on a volume base, assuming a water density of 1 g cm^{-3}. It was calculated by the following equation (LINDROTH et al. 1995):

$$Q_S = \frac{P}{\Delta T\, c_w} - Q_{fic}, \qquad \text{(eq. 3.2)}$$

where P (J s^{-1}) is the recorded power input to the heater, ΔT (°C) is the adjusted constant temperature difference between the two needles, c_w (J kg^{-1} K^{-1}) the specific heat of water and Q_{fic} (L s^{-1}) a fictitious flux of water, caused by the heat loss from the sensor. Q_{fic} was determined as the lowest measured sap flow during nighttime, assuming that actually no transpiration occurred in these periods (LINDROTH et al. 1995). In order to estimate the cooling effect through transpiration as energy equivalent (W m^{-2}), we assumed an evaporation heat of 2,450 J g^{-1} water (20 °C).

All measured data were aggregated to a half hourly resolution afterwards.

3.2.6 Quantifying the emitted energy during nighttime

We assume that the stored heat from the wall is emitted completely into the street canyon during the night. That is because of the higher temperature gradient in the street-canyon direction compared to the interior building direction in the summer. The emitted energy $Q\uparrow$ (W m^{-2}) from the walls was calculated as follows:

$$Q\uparrow_{green} = \Delta T_{green} * c_p * m, \qquad \text{(eq. 3.3)}$$

$$Q\uparrow_{bare} = \Delta T_{bare} * c_p * m, \qquad \text{(eq. 3.4)}$$

where the subscripts green and bare indicate the greened and bare walls; ΔT (°C) is the difference of the exterior wall surface temperatures between calendrical dusk and dawn, c_p (J kg^{-1} K^{-1}) the specific heat capacity of the wall, set to 836 J kg^{-1} K^{-1}; m (kg m^{-2}) is the mass of the wall per m^2 WA. It was calculated to be 295 kg m^{-2}, based on the following information about the wall at site C: it was 0.29 m thick in total, consisting of a 0.24 m thick masonry (specific density assumed 1,120 kg m^{-3}) plus 0.01 m tiles (1,900 kg m^{-3}) and 0.04 m wood wool insulation (155 kg m^{-3}). In order to compare the results, we assumed that the walls at all sites are identical.

3.3 Results and discussion

3.3.1 Diurnal variations in irradiation and transpiration

Figures 3.2 a and b display the meteorological conditions and the sap flow, exemplarily shown for *P. tricuspidata*, on a hot (2nd August) and on a cold summer day (14th August).

On the hot day, the sky was practically cloud-free. Air temperature and relative humidity varied from 21.2 to 37.4 °C and from 46.4 to 68.1 %, respectively. In front of the greened wall, we measured a cumulative incoming short-wave radiation of 13,761,000 J m^{-2}. The diurnal cycle of $K\downarrow_f$ is characteristic for a vertical structure like a facade. Right after sunrise, $K\downarrow_f$ increased slowly due to indirect radiation. When the sunlight reached the facade directly at about 10:00, $K\downarrow_f$ increased strongly. The cycle also demonstrates the typical situation of facades in an urban setting, namely the impact of surrounding buildings. They were shading the facades (reduced sky view factor), leading to reduced total insolation and very sharp increases and decreases of $K\downarrow_f$ when the building was no longer shaded or was shaded again. However, reflections from buildings can also lead to increased irradiation compared to non-urban situations. With sufficient temporal resolution, several reflections from buildings opposite to the wall are visible (Fig. 3.3). This reflected radiation accounted for up to 105 W m^{-2} and caused detectable sap flows.

On the cold summer day, air temperature and relative humidity varied from 12.0 to 24.4 °C and from 37.7 to 88.0 %, respectively. Cumulative incoming short-wave radiation was reduced by about 37 % compared to the hot day (8,634,000 J m^{-2}).

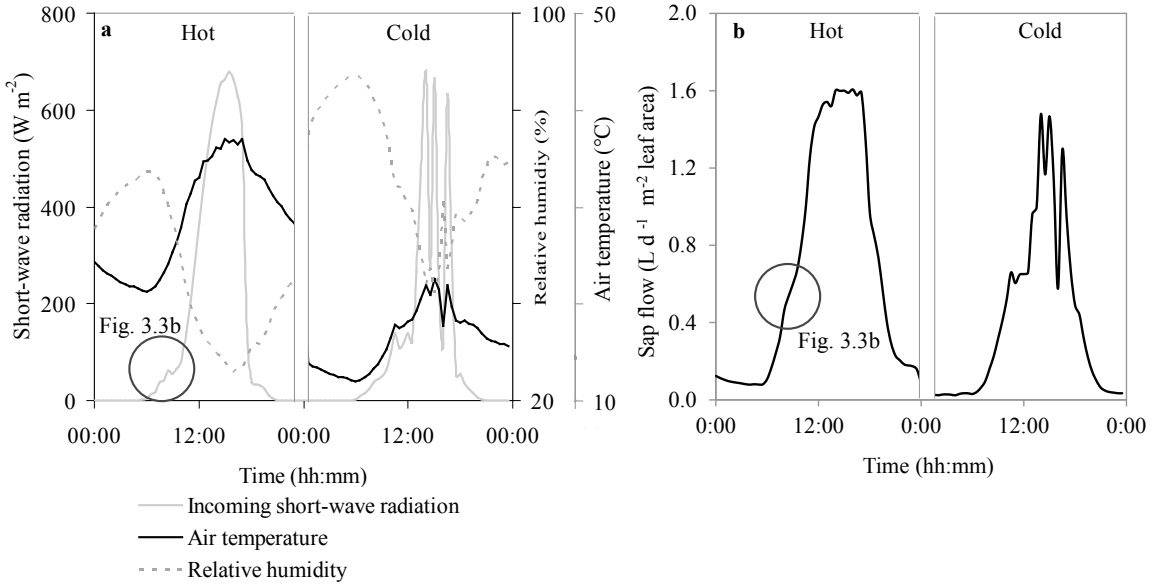

Fig. 3.2 a) Meteorological conditions in front of the greened wall on a hot (2nd August 2013) compared to a cold summer day (14th August 2013). b) Mean diurnal sap flow (*Parthenocissus tricuspidata*) on these two days. All results are for a south south-west oriented facade in Berlin, Germany.

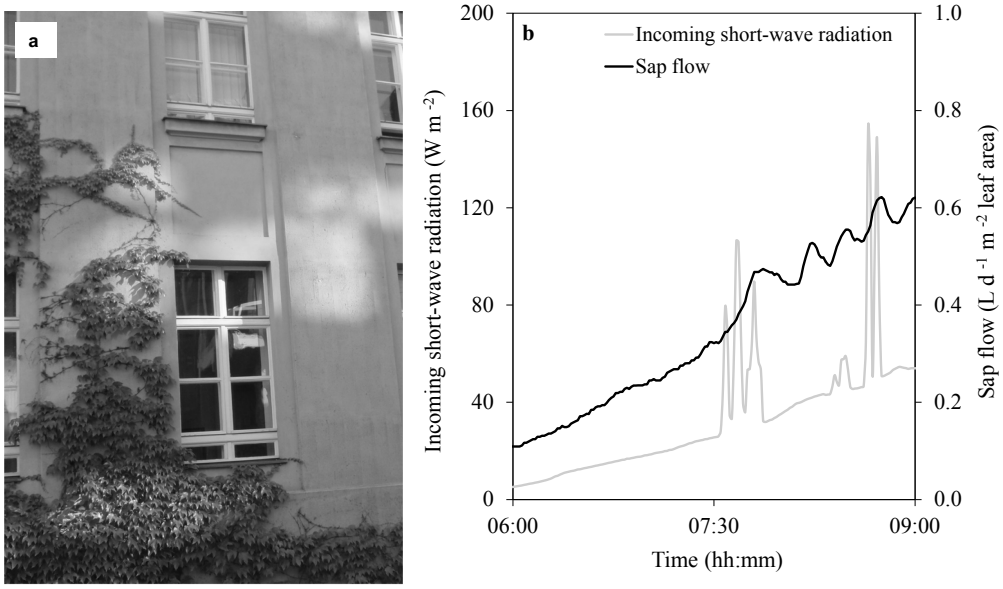

Fig. 3.3 a) Window reflections of a facing building. b) Indirect incoming short-wave radiation with peaks due to window reflections of a facing building and sap flow reactions of *Parthenocissus tricuspidata* on the 2nd August 2013.

Sap flow rates were almost similar for all investigated plant stems at each facade (data not shown). Thus, mean values are discussed in the following. The diurnal cycle of the sap flow was strongly influenced by incoming short-wave radiation, air temperature and relative humidity, with the first being the most influencing factor. With 0.1 and 0.03 L d^{-1} m^{-2} (LA) on the hot and on the cold day, sap flow was low during the night and increased with the first detectable incoming short-wave radiation in the morning (Fig. 3.2 b). Moreover, similar to short-wave radiation, it rose sharply from the point when the sun shone directly on the facade. On the hot day at noon, the sap flow curve is flattened and oscillated. The potential transpiration rate of the plant was probably reached, which may have been caused by three different phenomena: very high radiation can lead to narrowing to up to closing of the stomata for some plant species (JARVIS 1976). A second reason could be that despite irrigation, there was not enough water available fulfilling the highest water demands. A corresponding wilting of the leaves was not observed. Therefore, it is more probably that the transpiration demand exceeded the maximum water conductivity of the plant system.

3.3.2 Cooling effects of facade greening

When comparing ambient air temperatures in front of the greenings with those in front of the bare walls, no differences were found over the diurnal cycle for all investigated sites (Fig. 3.4 a and b). The detected differences were 0.03 (Site A) and 0.2 °C (Site C) which is in the range or at least near to the measuring uncertainty. At site A, at noon, the air temperature in front of the greened wall was slightly higher than in front of the bare wall, whilst in the evening it was reverse. This is due to the fact, that the greened wall receives the sunlight earlier than the bare wall, as described above. Mixing air, due to large-scale weather

pattern induced winds or micro-scale facade-greening induced air parcels in front of the greening, is probably the main reason for no clear differences in ambient air temperature. Facade-greening induced mixing air can be caused by density differences of air parcels with different temperatures and humidities as hypothesised by KRAWINA and LOIDL (1990).

While we could not measure a cooling effect for the ambient air in the street canyon, the effect for the building was clearly detectable (Fig. 3.5 a-c). Mean surface temperature of the greening with *P. tricuspidata* (Site A) was reduced by 0.1 to 11.3 °C (average $\Delta T = 3.3$ °C) compared to the surface of the bare exterior wall for a hot summer day (28th July 2013). Similar results were found for the greening with *H. helix* (Site B) (0.0 to 12.3; avg. 3.7), while it was weaker pronounced at the greening with *F. baldschuanica* (Site C) (-0.8 to 6.6; avg. 2.4).

Greening also decreased the surface temperatures of the exterior side of the building wall at all three sites (Fig. 3.6 a-c). The highest temperature reduction was reached for site A, the south south-west exposed facade: the bare wall was heated up to 51.5 °C on a hot summer day at 16:30 (2nd August), while in contrast, it was only 38.3 °C at 16:00 on the wall surface behind the greening. The maximum difference between the greened and bare wall occurred in the late afternoon at 18:00 with -15.5 °C. For the other building facades, the maximum temperature difference reached up to -13.9 °C (Site B) and -10.5 °C (Site C). On the daily average, the greened walls were cooler, with a difference of -4.4 °C (Site A), -2.2 °C (Site B) and -2.2 °C (Site C).

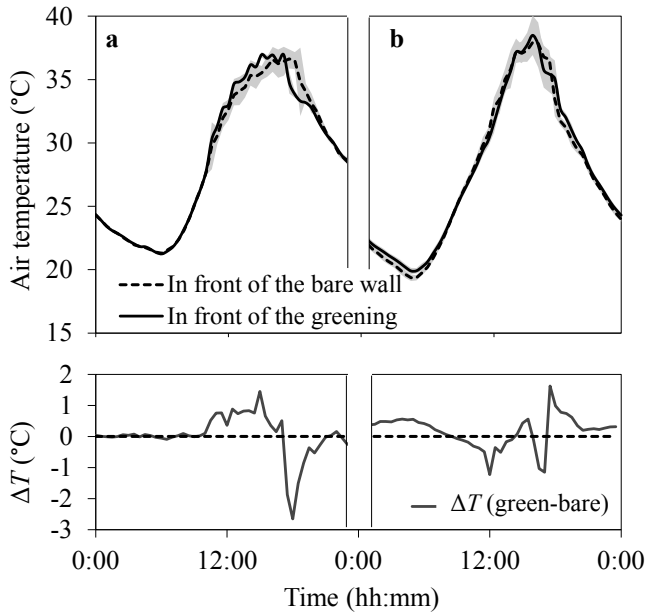

Fig. 3.4 Mean air temperatures in front of the greenings and the bare building walls (at the top) as well as temperature differences between both of them (at the bottom) on hot summer days, a) south south-west exposed facade greened with *Parthenocissus tricuspidata* (2nd August 2013) and b) west exposed facade greened with *Fallopia baldschuanica* (19th July 2014). The grey area indicates the standard deviation of the given mean values.

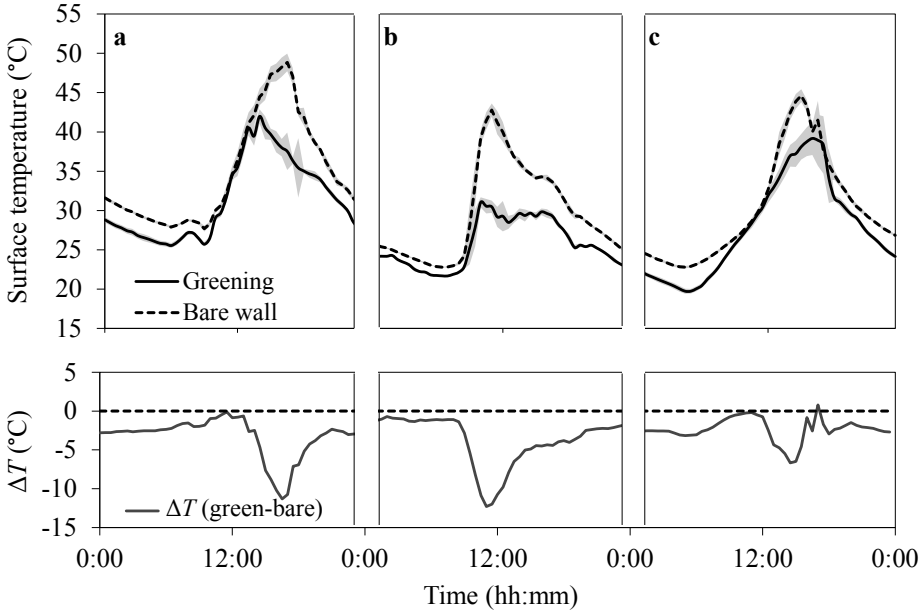

Fig. 3.5 Mean surface temperatures of the greenings (leaves) and the bare exterior building walls on the three investigated facades (at the top) as well as temperature differences between both of them (at the bottom) on hot summer days, a) south south-west exposed facade greened with *Parthenocissus tricuspidata* (28th July 2013), b) east exposed facade greened with *Hedera helix* (3rd August 2014) and c) west exposed facade greened with *Fallopia baldschuanica* (19th July 2014). The grey area indicates the standard deviation of the given mean values.

Interestingly, SUSOROVA et al. (2013) found average and maximum differences of only -1.1 and -7.9 °C for *P. tricuspidata* at a south exposed facade in Chicago, USA (lat. 41°50' N). Ambient air temperatures ranged from 20.7 to 38.8 °C, which were very much in the same range as in our experiment. As in both experiments the maximum vegetated wall temperatures were similar (37.4 °C in Berlin and 38.3 °C in Chicago), the lower differences measured in Chicago might be due to a higher albedo of the building envelope. This envelope was assembled from glass, steel and light coloured tiles and led to a maximum surface temperature of the bare wall of only 41.5 °C, compared to the 51.5 °C in Berlin. The same phenomenon could be observed in Berlin at site C, where we have a similar envelope to Chicago and where we detected the lowest maximum difference. We conclude that the cooling effect of facade greening is even more effective for surface wall temperature reduction than the best architectonical practice for the bare wall case, a light wall with glossy surfaces and a high solar reflectance.

Due to insulation of the vegetation cover, the bare walls cooled down much faster than the greened walls and were actually cooler during the night (Fig. 3.6 a-c). This insulation effect increases with increasing leave area density and thickness of the greenery for direct facade greenings. While the difference between the greened and the bare wall was up to 0.8 °C at site A, where the plants had a WLAI of 1.9, it was up to 1.6 °C on site B, where WLAI was 3.0. The difference for the well ventilated double-skin facade at site C was only up to 0.3 °C, although having a comparable high WLAI of 3.0.

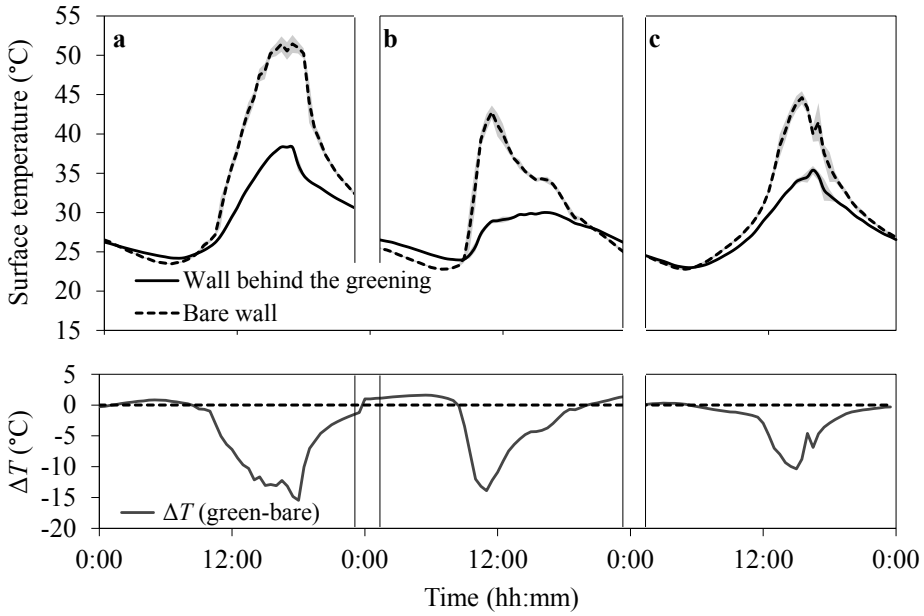

Fig. 3.6 Mean surface temperatures of the greened and bare exterior building walls on the three investigated facades (at the top) as well as temperature differences between both of them (at the bottom) on hot summer days, a) south south-west exposed facade greened with *Parthenocissus tricuspidata* (2nd August 2013), b) east exposed facade greened with *Hedera helix* (3rd August 2014) and c) west exposed facade greened with *Fallopia baldschuanica* (19th July 2014). The grey area indicates the standard deviation of the given mean values.

The insulation effect might be a disadvantage of facade greenings concerning the cooling effect for the individual building, especially because people mainly suffer from heat stress at night. However, for cooling the quarter and the street canyon, the insulation effect of direct facade greening is positive. At site A (2nd August 2013 21:40 to 3rd August 2013 04:50) and B (3rd August 2014 21:40 to 4th August 2014 04:50), the bare walls emitted 64.5 and 43.9 W m^{-2} while the greened walls emitted 36.5 and 34.1 W m^{-2}, respectively. The bare wall at site C heated the canyon with 50.4 W m^{-2} during nighttime (19th July, 22:05 to 20th July, 04:25), while the greened surface emitted only 41.3 W m^{-2} at site C.

These findings demonstrate the high impact of the design of facade greenery on the cooling effectiveness for the building. While the air could circulate behind the plants at site C, the greeneries at sites A and B stopped air circulation or at least reduced air velocities in front of the wall (PERINI et al. 2011). The design at site C was favourable to reduce the insulation effect at night, demonstrated by the highest nocturnal emission of energy of the three greened facades.

Beside the air cavity between wall and greening, it had a free lateral access to moving air as not the whole wall was greened but only some strips (Fig. 3.1 c). In conclusion, for the building cooling, it would be most effective if the greenery could be oriented in parallel during the day and perpendicular to the wall during the night (that aspect can discussed differently for winter times). However, the insulation effect of facade greening on the overall building cooling effect can only be discussed based on interior wall surface temperatures.

As expected, the cooling effect through the greenery was also detectable on the interior building wall, shown for the west exposed facade at site C greened with *F. baldschuanica* (Fig. 3.7 a-c). The interior wall of the greened facade heated up to max 27.5 °C, whereas it was max 28.8 °C for the bare wall. The greened facade was always cooler (average ΔT = -0.9 °C) with a maximum difference of -1.7 °C. Altogether, the reduction potential of the greening on interior wall temperature is not extraordinary great, but BUCHIN et al. (2015) revealed that already a mean air temperature reduction of 0.8 °C can reduce the numbers of heat-related deaths.

It is remarkable that the peaks of the interior surface temperature occurred around midnight and were timely shifted to the peaks of the exterior surface temperature. This time lag amounts to 6 to 8 hours for the 0.29 m thick wall.

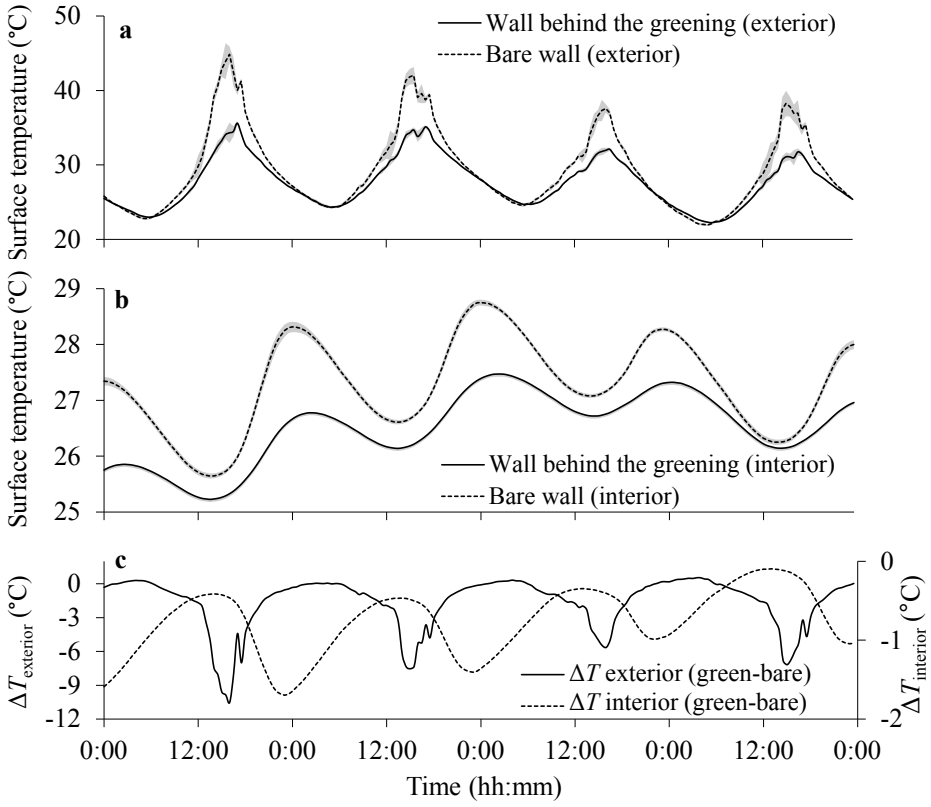

Fig. 3.7 Mean surface temperatures of the greened and bare a) exterior building wall, b) interior building wall as well as c) temperature differences between the greened and the bare walls in a hot summer period (19th to 22nd July 2014). All results are for a west exposed facade greened with *Fallopia baldschuanica*. The grey area indicates the standard deviation of the given mean values.

3.3.3 Transpiration and shading

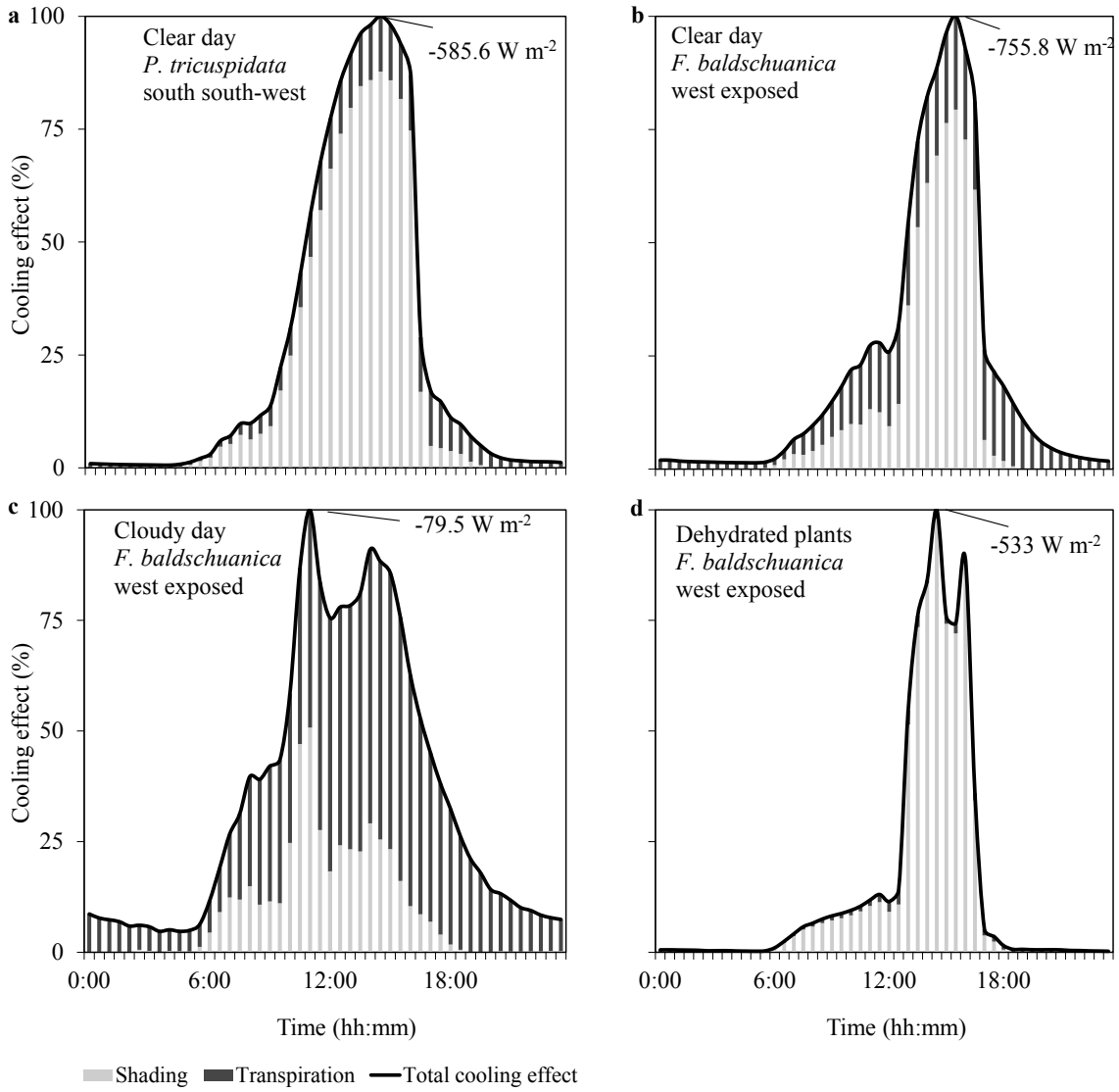

Fig. 3.8 Total cooling effect (transpiration + shading) as well as share of transpiration and shading on this cooling effect, each in relation to the maximum cooling effect of the day, for a) a south south-west exposed facade greened with *Parthenocissus tricuspidata* on a clear summer day (2nd August 2013), b) a west exposed facade greened with *Fallopia baldschuanica* on a clear late summer day (3rd September 2014), c) a cloudy day (*F. baldschuanica*) (12th September 2014) and d) plants under drought-stress (*F. baldschuanica*) (18th September 2014).

Figures 3.8 a and b show the total cooling effect as well as the differentiation between shading and transpiration for *P. tricuspidata* and *F. baldschuanica* on clear summer days. During the night, cooling only depended on transpiration, which was relatively low for *P. tricuspidata*, with values between -1.5 and -5.5 W m^{-2} and a bit higher for the well-irrigated *F. baldschuanica*, with values between -9.7 and -60.6 W m^{-2}. With the first detectable solar radiation, shading became effective.

The total cooling effect of *P. tricuspidata*, was highest from 12:00 to 16:00 with a peak of -585.6 W m^{-2} at 14:00 for a hot summer day (2nd August 2013) with high solar radiation. In

this period, shading accounts for 87 % of the total cooling. For the whole day, shading accounts for only 81.5 % of the total cooling. We found the same proportions for a cold summer day with less radiation during daytime (14th of August 2013, data not shown). The greening of *P. tricuspidata* retained or reflected 75.3 % of the incoming short-wave radiation (transmissivity = 0.25). IP et al. (2010) found leaf solar transmissivities for *P. tricuspidata* between 0.12 and 0.45, depending on the number of leaf layers. Furthermore, the shading effect changed throughout the year due to leaf-growing and leaf-shedding with maximum shading performance in August and September (IP et al. 2010).

For *F. baldschuanica*, at the 3rd September 2014 the peak cooling of -755.8 W m^{-2} occurred at 15:30, thus later as at site A due to the west exposition. It depended on shading to 79.4 % and on transpiration to 21.6 %. For the whole day, transpiration had a higher contribution of 39.9 %. For a 13 days measuring period (3rd to 15th September 2014) with nice late summer weather conditions (average air temperature = 19.2 °C, average daily cumulative incoming short-wave radiation = 5,149,086 J m^{-2}), transpiration contributed to almost the same extent as shading (transpiration = 47.5 %). For a cloudy day (12th September 2014), the proportion of transpiration was even 73 % on a daily basis (Fig. 3.8 c). However, the total cooling effect for this day was relatively low with a peak of only -79.5 W m^{-2}. During the dehydration experiment, the contribution of transpiration on the total cooling effect decreased to only 6.1 % due to water stress (Fig. 3.8 d). For *F. baldschuanica* the transmissivity was only 0.09 as measured in September 2014.

Whether the differences in contributions of shading and transpiration for *P. tricuspidata* and *F. baldschuanica* on the total cooling effect are only plant specific or also due to the irrigation status or the meteorological conditions could not be completely assessed in this study. However, we could show that these factors influence the proportioning of the total cooling effect to a large extent.

3.3.4 Transpiration rates and water demand

The daily transpiration rates per unit LA were similar for the three investigated climber species with an average of 0.5 L d^{-1} m^{-2} (Tab. 3.1). However, in preliminary indoor studies, *F. baldschuanica* was the species with the highest daily transpiration rate of 2.7 L d^{-1} m^{-2} (LA) (HOELSCHER 2013). The lower rates in this outdoor experiment can be explained by the measurements done in September and not in August like for the other plant species (due to technical reasons). Consequently, incoming global radiation and air temperatures were lower during those measurements.

The daily transpiration rates per unit WA were lowest for *P. tricuspidata* due to the lower WLAI. On the 2nd August (hot day), with 1.3 L d^{-1} m^{-2} (WA) we measured the highest daily transpiration rate for this species. The lowest daily transpiration rate was measured on the 14th August (coldest day) with only 0.7 L d^{-1} m^{-2} per unit WA. This corresponds to an average energy conversion between 19.9 and 35.4 m^{-2} (WA). Estimated exemplary for the whole greened facade of 36 m^2 at site A, a water amount of 25.2 to 45.0 L d^{-1} is needed in summer. However, for typical urban sites - sealed, compacted and providing only limited rooting volumes - the availability of such high water amounts can be critical on hot summer days.

This corresponds to the authors' observation that autumnal colouring of *P. tricuspidata* occurs earlier in the city centre than in the outskirts. In contrast, we observed premature senescence and fall of leaves for a north oriented *F. baldschuanica* in beginning in October 2014, while the irrigated one at site C showed autumn foliage beginning only at the 20th November 2014 (derived from daily photos).

Tab. 3.1 Mean, maximum and minimum daily sap flow rates of *Parthenocissus tricuspidata* (2nd to 15th August 2013), *Hedera helix* (1st to 6th August 2014) and *Fallopia baldschuanica* (2nd to 15th September 2014) based on leaf area (LA) and wall area (WA).

	Per LA ($L\ d^{-1}\ m^{-2}$)	Per WA ($L\ d^{-1}\ m^{-2}$)	Per WA ($W\ m^{-2}$)
Parthenocissus tricuspidata (n = 14, wall leaf area index (WLAI) = 1.9)			
Daily sap flow			
mean	0.5	0.9	26.6
maximum	0.7	1.3	35.4
minimum	0.4	0.7	19.9
Hedera helix (n = 6, WLAI = 3.0)			
Daily sap flow			
mean	0.5	1.6	45.6
maximum	0.6	1.7	49.5
minimum	0.4	1.2	32.8
Fallopia baldschuanica (n = 14, WLAI = 3.0)			
Daily sap flow			
mean	0.5	1.4	39.3
maximum	0.8	2.3	65.6
minimum	0.2	0.7	19.6

In preliminary studies on climbers, it was confirmed that their cooling effects can turn into the opposite, namely leaf surfaces warmer than ambient air temperatures when they were not sufficiently irrigated. Furthermore, a drought-stressed plant showed up to 2.5 °C higher leaf temperatures than a well-watered plant (HOELSCHER 2013).

For *H. helix* at site B, the daily transpiration rates varied from 1.2 to 1.7 $L\ d^{-1}\ m^{-2}$ (WA) which corresponds to an energy equivalent between 32.8 and 49.5 $W\ m^{-2}$. In contrast, for *F. baldschuanica* the daily transpiration rates per WA were 0.7 to 2.3 $L\ d^{-1}\ m^{-2}$ which results to an energy conversion of up to 65.6 $W\ m^{-2}$. As a consequence for hot summer days, the provided water amount for *F. baldschuanica* must be at least 1.3 times that for *H. helix* and twice as high as for *P. tricuspidata*.

Please note that these irrigation demands are derived from sap flow measurements. Although the applied calibration method for the sap flow data is widely accepted and in use, there are hints that the derived transpiration rates are underestimated (e.g. LEUZINGER et al. 2011). Obviously, this also leads to some uncertainties in the statements on the contribution of shading and transpiration on the total cooling effect. Finally, the above stated water demands can only be rough estimates. However, they strongly indicate the need to irrigate facade greenings, if they should contribute to building cooling and urban climatic effects. This is another argument to consider facade greening as a form of artificial urban green with a high maintenance demand not only in pruning and service but also in irrigation.

3.4 Conclusions

Our study demonstrated cooling effects of facade greening through transpiration and shading. While the surface temperatures of the exterior and interior building walls were clearly decreased by the greening, no clear differences in ambient air temperature were measurable. Based on interior wall temperatures, we could show that facade greening is most effective during nighttime, which is very relevant for the reduction of nocturnal indoor heat stress. However, we also demonstrated possible disadvantages through its insulation effect during the night. Therefore, we could show that the design of the facade greening has major impacts on cooling effects towards the street canyon and the building. Depending on the climatic aim of the facade greening, direct or indirect facade greenings are to favour.

The provided cooling effects on hot summer days mainly depended on shading, whereas a lower proportion was due to transpiration. Whether these differences in contributions of shading and transpiration for *P. tricuspidata* and *F. baldschuanica* on the total cooling effects were only plant specific or also due to the irrigation status or the meteorological conditions could not be completely assessed in this study and should therefore be further investigated. Facade greenings must be sufficiently irrigated with up to 2.5 L d^{-1} m^{-2} (WA) in order to be able to provide their cooling performance.

Acknowledgments

NIKOLA SCHWARZER, JOACHIM BUCHHOLZ, BJÖRN KLUGE and STEFFEN TRINKS from the Chair of Soil Conservation and FRED MEYER from the Chair of Climatology are thanked for their help and great support during the measurement campaign. We also thank COLIN JAMES SANDERS for his English corrections and language expertise.

This work was financed by the Deutsche Forschungsgemeinschaft (DFG) Research Unit FOR 1736 “urban climate and heat stress in mid-latitude cities in view of climate change (UCaHS)” (www.UCaHS.org).

4 A new consistent sap flow baseline-correction approach for the stem heat balance method using nocturnal water vapour pressure deficits and its application in the measurements of urban climbing plant transpiration[3]

MARIE-THERESE HOELSCHER[a,*], MARTIN ANDREAS KERN[b], GERD WESSOLEK[a] and THOMAS NEHLS[a]

[a] Department of Ecology, Soil Conservation, Technische Universität Berlin

[b] Department of Ecology, Soil Science, Technische Universität Berlin

*corresponding author; e-mail address: marie-therese.hoelscher@tu-berlin.de

Abstract

The stem heat balance (SHB) method is a widely used sap flow technique to determine the transpiration and the water demands of herbaceous and woody plants, especially those with small diameters (e.g. climbers). The accuracy of the sap flow derived by this method (Q_S) depends on correction of the total measured heat input (Q_t) by subtracting unintended heat losses; these heat losses are referred to as "fictitious flow" (Q_{fic}) ($Q_S = Q_t - Q_{fic}$).

We developed a physically consistent baseline-correction approach using minimum nocturnal water vapour pressure deficits (*VPD*). This *VPD* approach was compared to the so-called "night value subtraction" (NVS) approach and direct gravimetric determination for potted climbing plants and an outdoor climbing plant stand. In addition, performance tests were also conducted on artificial model stems and cut plant stems.

In the tests with the outdoor climbing plant stand, sap flow corrected by the NVS approach underestimated daily transpiration by up to 33 % compared to direct gravimetric determination. In contrast, the newly developed *VPD* approach underestimated or overestimated transpiration by only 5 % to 10 %. The *VPD* approach makes use of the direct dependence of sap flow on *VPD* during zero-radiation conditions (night). This means, Q_{fic} is the constant of the linear regression of the *VPD* and the lowest recorded Q_t at night. Therefore, the correction is based on all recorded sap flow data from the measurement period itself, which in turn accounts for all factors influencing Q_{fic}, including *RH* and T_{air}; these latter parameters are often recorded in any case. This also means that this method can be subsequently applied to currently available data sets in order to improve their quality.

[3]Published: HOELSCHER, M.-T., M.A. KERN, G. WESSOLEK and T. NEHLS. A new consistent sap flow baseline-correction approach for the stem heat balance method using nocturnal water vapour pressure deficits and its application in the measurements of urban climbing plant transpiration. *Agricultural and Forest Meteorology* 248: 169-176.

Our results suggest that when the raw data are corrected appropriately, the SHB method is practicable when attempting to determine transpiration rates of climbing plants. This is especially true for urban areas, with their illumination, typically high *VPD*s and increased T_{air} at night.

Keywords

Sap flow, baseline-correction, night-time transpiration, water vapour pressure deficit, climbing plants, stem heat balance method

4.1 Introduction

Sap flow measurements are often used to determine water demand and transpiration of plants and plant stands in ecology, forestry, agriculture and horticulture (e.g. PERTIERRA et al. 2002, MATYSSEK et al. 2009, RODRIGUEZ-DOMINGUEZ et al. 2012). They can be installed without great effort and automated easily with continuous recording and high temporal resolution (SMITH and ALLEN 1996). They function as indirect methods, using heat as a tracer for sap movement in the xylem of intact plant stems. However, the operating principles are basically different according to the various techniques (SMITH and ALLEN 1996, VANDEGEHUCHTE and STEPPE 2013).

One widely used technique, applicable for rather small diameters of herbaceous and woody plant stems, is the stem heat balance (SHB) method. Two needle thermocouples are inserted into a stem and the section around the upper one is heated electrically. While the temperature difference between both thermocouples is kept constant, the amount of heat introduced is directly proportional to the amount of water passing through the stem (LINDROTH et al. 1995, ČERMÁK et al. 2004). In order to calculate water transport from the recorded heat input, it is necessary to apply a baseline-correction for unintended heat losses, which would otherwise be interpreted as water flow and ultimately transpiration. These unintended heat losses are caused by conduction through (i) the plant tissue which consists of solid cell material and variable amounts of water (and air), (ii) the sensor material and (iii) the insulation material around the thermocouples, no matter how good it is. These conduction losses occur in radial and vertical directions and cause the detection of a sap flow which does not actually occur; it is referred to as "fictitious flow" (Q_{fic}) (GRIME and SINCLAIR 1999, TRCALA and ČERMÁK 2012). These losses and their dependencies on boundary conditions such as ambient air temperature have only been studied to a limited degree (GRIME and SINCLAIR 1999). Instead, Q_{fic} is often determined when water flow in the plant is assumed to be zero or negligible. Numerous studies have chosen the lowest measured heat input (Q_t) from measurement periods at night before sunrise as Q_{fic} (e.g. DUGAS et al. 1994, LINDROTH et al. 1995, LANGENSIEPEN et al. 2014). This night value subtraction (NVS) assumes that plants close their stomata in the dark and that no transpiration occurs in these periods. However, this

assumption has been investigated and hotly debated for a long time (RAWSON and CLARKE 1988, DAWSON et al. 2007, FISHER et al. 2007). Ultimately, it must be assumed that most plant species do not completely close their stomata and consequently transpire at night. Moreover, it is well known that transpiration through the cuticle is very limited for some plant species, but cannot be ruled out altogether. FORSTER (2014) concluded that night-time transpiration is common across a wide range of species from all biomes and seasons, making up an average of 12 % of the total daily transpiration. Nevertheless, the NVS approach is still used and manufacturers even suggest this procedure in their manuals (e.g. EMS BRNO 2010) or sap flow logger software calculates it automatically (e.g. DYNAMAX INC. 2007).

Other studies assumed zero-flow conditions after a heavy rainfall with high air humidity and intercepted water on the surfaces of leaves (ALLEN and GRIME 1995). However, CIENCIALA et al. (1992) revealed that even after rain fall events, sap flow of *Picea abies* still remained significant. Consequently, such assumptions of zero-flow conditions (e.g. at night or after rainfall events) should be applied with caution because they probably result in an underestimation of water fluxes and thus water demands.

Q_{fic} can also be measured after cutting the stem at the end of an investigation period to stop sap flow (e.g. URBAN et al. 2012). This approach promises to be "the most accurate way" to determine zero flow, according to DAWSON et al. (2007), but it is somewhat destructive. Furthermore, Q_{fic} may vary from sensor to sensor and from stem to stem. Thus, the results are not transferable to other experiments.

Alternatively, researchers have attempted to approximate Q_{fic} with the help of other instruments, e.g. by measuring the stomata conductance with a porometer or a gas exchange system (e.g. LEUZINGER et al. 2011) or by gravimetric measurements in lysimeters (e.g. CASPARI et al. 1993). However, these instruments are not able to directly quantify Q_{fic} and these comparisons would rather introduce inter-methodical uncertainties. TRCALA and ČERMÁK (2012) improved the trunk segment heat balance method by improving the sensor geometry. Such sensors, however, are not applicable to small diameter stems of herbaceous and woody plants.

For this reason, a better method for the determination of Q_{fic} is needed, taking into account the site specific, plant specific and sensor specific influences.

4.1.1 Facade greening in urban settings as an application example for sap flow measurements

Facade greening with climbing plants has frequently been discussed as a promising countermeasure to mitigate heat stress in cities (BUCHIN et al. 2015). Shading and transpiration are the most important cooling mechanisms, with the latter directly depending on water availability (HOELSCHER et al. 2015). Therefore, the water demand of climbers is of great practical interest. So far, only limited data are available (e.g. LEUZINGER et al. 2011, HOELSCHER et al. 2015), but could be easily obtained from sap flow measurements. However, site conditions in urban areas are very different from natural ecosystems, which make the applicability of the NVS approach questionable. Due to higher water vapour

pressure deficits (*VPD*) of the ambient air, urban climbers are hypothesised to exhibit redistribution and transpiration during warm summer nights. Not only transpiration through the stomata is probably high for plants with a high leaf area index (LAI) and thin and smooth leaves, such as *Fallopia baldschuanica* (HOELSCHER et al. 2015), but also transpiration through the cuticle. Additionally, artificial light has been detected as global radiation at night (JÄNICKE et al. 2015). Sap flow measurements could be useful for studying climbing plants in urban areas, provided that they are calibrated correctly.

4.1.2 Aims

For applied flow rates, we (i) determined Q_{fic} and its detection limits as well as Q_{fic} depending on air temperatures. We then (ii) developed a new practicable calibration method for deriving transpiration data from sap flow measurements that uses data from the measurement campaign itself as well as data on air temperature (T_{air}) and relative air humidity (*RH*). Finally, we (iii) assessed the applicability of the common NVS approach and the newly developed *VPD* approach based on simultaneous weight measurements to derive transpiration rates of climbing plants. Thereby, we tested the influence of wind and drought stress on the results.

4.2 Materials and methods

4.2.1 Sap flow measurements

Sap flow measurements were conducted using EMS 62 sap flow sensors (EMS Brno, Czech Republic) based on the SHB method, with external heating and internal temperature sensing, described in detail by LINDROTH et al. (1995) and ČERMÁK et al. (2004). Two needle thermocouples were installed for stem diameters 8 to 12 mm and 10 to 20 mm, respectively. Both parts were wrapped with insulation foam and an additional shield was installed around each sensor to protect against direct solar radiation and precipitation.

While the temperature difference ΔT between both thermocouples was constant at 4 K, the input power was continually recorded at 1 and 10 minute intervals, respectively. Sap flow Q_S (L h^{-1}) expressed on a volume basis, assuming a water density of 1 g cm^{-3}, was calculated as follows (LINDROTH et al. 1995):

$$Q_S = Q_t - Q_{fic} = \frac{P}{\Delta T\, c_w} - Q_{fic}, \qquad \text{(eq. 4.1)}$$

where Q_t is the total measured heat input, P (J h^{-1}) is the power input to the heater, ΔT (K) is the temperature difference between the two thermocouples, c_w (J L^{-1} K^{-1}) is the specific heat of water and Q_{fic} (L h^{-1}) is the fictitious water flux.

4.2.2 Variation of Q_{fic} for different flow rates and T_{air} levels

We determined the dependence of Q_{fic} on flow rates and air temperatures in the laboratory and climatic chamber experiments, respectively (Tab. 4.1).

Tab. 4.1 Overview of the different experiments.

Experiment (no.)	Scientific aim	Site	Object	Sensor and stem position
	Variation of Q_{fic} for different…			
1	… flow rates	Laboratory	Model stem	Vertical (reversed)
2	… T_{air}	Climatic chamber	Model stem Cut stems	Horizontal Horizontal
3	Testing different baseline-correction approaches	Indoor (laboratory)	Potted climbing plants	Vertical
4	Testing different baseline-correction approaches	Outdoor (facade)	Climbing plant stand	Vertical

Experiment 1: variation of Q_{fic} for different flow rates

We performed a continuous flow through a model stem in a laboratory experiment (T_{air} from 24.1 to 26.3 °C and *RH* from 33.7 to 46.9 %) to determine Q_{fic}. For the model stem, we took a PVC hose with an inner and outer diameter of 6 and 10 mm, which was filled with water. This simplified model stem can be reproduced easily and enabled us to get very reproducible results that are not possible for real plant stems. We used a syringe pump (Perfusor 8878, B. Braun Melsungen AG, Germany) and applied flow rates between 0.01 and 0.06 L h^{-1} (3 repetitions in each case). To minimise heat loss by BROWNIAN motion of heated water in an upward flow direction, we reversed the measuring construction, so that the water flowed downwards. Measurements were recorded at 1 minute intervals. The detected Q_t slightly increased with time t during the measurement period (e.g. $Q_t = 0.0067 \ln t + 0.11$, for flow rate = 0.06 L h^{-1}). Therefore, mean values were calculated for the different flow rates. These mean values were then used in the later further analysis.

Experiment 2: variation of Q_{fic} for different levels of T_{air}

The effect of the ambient air temperature (T_{air}) on Q_{fic} was studied in a climatic chamber (HGC 1014, serial no. 58566187660040, Weiss Technik UK Ltd., United Kingdom). The same sap flow sensor (for stem diameters of 8 to 12 mm) was mounted to a PVC hose in which carboxymethyl cellulose paste (3 g per 0.1 L water; Metylan normal, Henkel AG & Co. KGaA, Germany) was added in order to reduce the movement of free water, similar to water in plant stems. The sensor was subsequently employed on two cut stems of *F. baldschuanica*. One of the plant stems was freshly cut (stem diameter 11.52 mm ± 0.19);

the other one has been previously saturated with water (11.51 mm ± 0.41). The cut areas were sealed with medium-viscosity vacuum grease (Baysilone-Paste, GE Bayer Silicones, Germany) and covered with adjusted rubber nipples to minimise water losses. The measurement took place under constant *RH* of 70 % while the T_{air} was adjusted within the range of 10 to 35 °C (linear T_{air} change of 5 °C in 30 min, 3 h constant T_{air}). The experiment recorded Q_t at 1 minute intervals under zero-flow conditions.

4.2.3 Methods of comparing different approaches to sap flow correction

The next step of the experiment was to test different baseline-correction approaches for potted climbers indoors and for an actual climbing plant stand outdoors.

Experiment 3: indoor setup

Two individuals of single stem *Parthenocissus tricuspidata* were placed on the window sill of a south-west facing facade centrally located in Berlin, Germany (lat. 52°51'N, long. 13°32'E). The plants, approx. 1 m in height, originated from a tree nursery and were planted in six-litre pots with peat substrate. Sap flow was recorded over a period of two weeks from 18th to 29th August 2012. Simultaneously with the sap flow measurements (see above), the entire plant pots were placed on a balance (Kern 572, Kern & Sohn GmbH, Germany) and their mass was recorded at 10 minute intervals. The pots were covered to prevent substrate evaporation, meaning that mass changes are regarded as directly measured transpiration. In addition, we used an EMS 33 sensor (EMS Brno, Czech Republic) to measure T_{air} and *RH* as well as an EMS 11 to measure incoming short-wave radiation at 10 minute intervals. Afterwards, all data measured were aggregated in 30 minute groups. Table 4.2 shows mean, maximum and minimum values over the time period.

Experiment 4: outdoor setup

The outdoor experiment took place on a west exposed climbing plant stand in the city centre of Berlin, Germany (lat. 52°51'N, long. 13°32'E) and was conducted between 2nd and 22th September 2014. Table 4.2 compares the meteorological conditions during the experiment to the conditions over the entire vegetation period. The investigated facade greening consisted of six plants of *F. baldschuanica* with 32 stems in total (diameters ranging from 6 to 13 mm). Five stems (diameters 8 to 13 mm) were chosen for the sap flow measurements mainly for their appropriateness for the sensors and to represent the centre part of the 2 m wide facade greening.

The plants grew in covered containers filled with humic coarse sand. The rooting zone had a depth of about 0.6 m and was supplied with nutrient solution from below at a constant water level. This level was replenished from a reservoir standing on a balance (Sartorius Signum1, Sartorius Weighing Technology GmbH, Germany) with its mass recorded continuously at 1 minute intervals (Fig. 4.1). Evaporation losses from the covered containers were at most 0.013 L h^{-1} (SCHWARZER 2015) and consequently negligible in relation to measured stand transpiration rates, which ranged from 0.4 to 2 L h^{-1} (see Fig. 4.5). In

addition, T_{air} and *RH* (HC2-S3, Rotronic Messgeräte, Germany), wind speed (Ultrasonic anemometer 3D, Adolf Thies GmbH & Co. KG, Germany) and incoming short-wave radiation (LP02-05, Hukseflux Thermal Sensors B.V., the Netherlands) were measured at a height of about 3 m at 5 minute intervals (Tab. 4.2). All values were aggregated into 30 minute groups.

Tab. 4.2 Means, maxima and minima of air temperature, relative air humidity, incoming short-wave radiation, wind speed and nocturnal *VPD* for the indoor and the outdoor experiment.

	Air temperature	Relative humidity	Incoming short-wave radiation	Wind speed	VPD_{night}
	(°C)	(%)	(W m^{-2})	(m s^{-1})	(hPa)
Indoor experiment (18th - 29th August 2012)					
mean	29.0	39.3	43.2	-	21.3
max	40.4	59.2	310.4	-	33.6
min	21.8	20.8	0.0	-	16.0
Outdoor experiment (2nd - 22th September 2014)					
mean	17.4	77.1	57.2	0.4	4.8
max	23.8	95.7	663.5	1.0	13.9
min	12.4	51.6	0.0	0.1	0.8
Outdoor experiment (entire vegetation period, 1st March - 31th October 2014)					
mean	11.4	74.1	59.6	0.4	3.7
max	29.8	99.0	860.2	1.2	25.5
min	1.4	31.9	0.0	0.1	0.1

4.2.4 Sap flow correction approaches

We assessed the applicability of the commonly used NVS approach and the newly developed *VPD* approach by making a comparison using gravimetric determinations. Additionally, we tested the influence of wind and drought stress on the results. The following provides an explanation of the approaches:

The new approach - estimating Q_{fic} for VPD = 0 (Q_{fic}^{VPD})

Evapotranspiration depends on the radiation and the water vapour pressure deficit of the air, *VPD* (hPa) $= e_s(T)$-e which is the difference between the saturation vapour pressure $e_s = f(T)$ and the vapour pressure e. It is obvious that evapotranspiration also occurs at night (with no radiation) as long as the *VPD* is higher than zero. The PENMAN-MONTEITH equation, a physically based, widely used and broadly accepted approach, describes the actual evapotranspiration ET_a accordingly (ALLEN et al. 1998). For zero-radiation conditions (night), ET_a, and thus sap flow Q_S are proportional to the *VPD* of the ambient air:

$$Q_S = ET_a = \frac{1}{a} VPD\,, \qquad \text{(eq. 4.2)}$$

with a incorporating all other constants given in the PENMAN-MONTEITH equation. Assuming that redistribution flows are quantifiable (via a dendrometer) or negligible, it is possible to quantify Q_{fic} from the total measured nocturnal heat transport Q_t (see Fig. 4.7 a and b). With $VPD = 0$, the axis intercept of the linear relationship between VPD and the lowest of the measured Q_t at night corresponds to Q_{fic} (L h^{-1}), designated Q_{fic}^{VPD}.

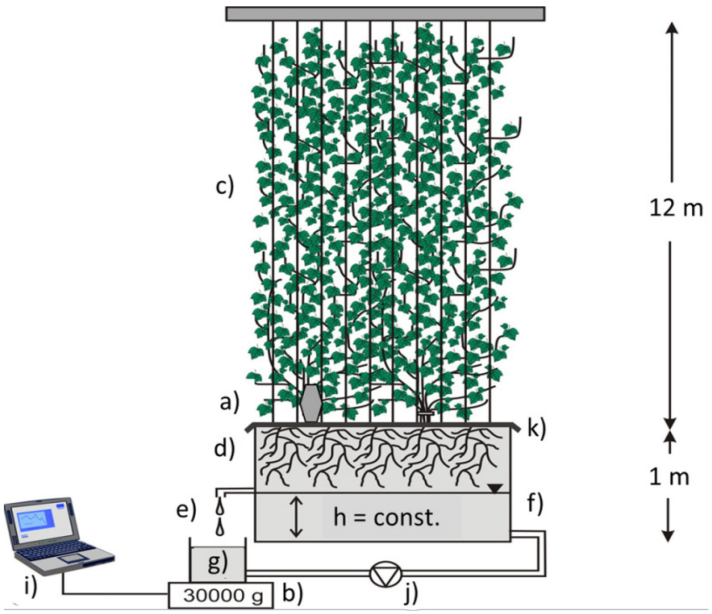

Fig. 4.1 Design for the outdoor experiment: transpiration measured by sap flow sensors and balance: a) sap flow sensor with radiation shield (for 5 plant stems in total), b) balance measuring the water uptake for all 32 stems, c) climbing plants (*Fallopia baldschuanica*), d) rooting zone in the hydroponic system, e) free outflow, f) intake, g) water reservoir refilled automatically, h) constant water level, i) data logger, j) pump, k) cover.

Night value subtraction (NVS)

For testing the commonly used NVS approach, it was necessary to determine Q_{fic}^{NVS} (L h^{-1}), which was usually the lowest measured sap flow value during the measurement period; this occurred at night, just before sunrise. In our case, we measured the same lowest value on two different nights (T_{air} 12.8 and 16.9 °C and RH 93.0 and 96.2 %). For these conditions, Q_S is assumed to be zero and thus:

$$Q_{fic}^{NVS} = \frac{P}{\Delta T\, c_w}. \qquad \text{(eq. 4.3)}$$

Both approaches were also tested under calm conditions by choosing only data for wind speeds $< 0.3\ m\ s^{-1}$, which corresponds to 0 on the BEAUFORT Scale. These values were accordingly named $Q_{fic}^{VPD\_calm}$ and $Q_{fic}^{NVS\_calm}$ ($L\ h^{-1}$).

In order to reduce Q_S at night, a drought experiment was conducted from 16th to 20th September 2014 at the outdoor facade greening. At this time, the water within the containers was drained and the automatic refill was stopped, so that only the water stored in the substrate was left for the plants. The water capacity of the coarse sand is $0.06\ m^3\ m^{-3}$, which results in a maximum of 40 L available water from the root zone. The plants showed initial phenological and irreversible damages after about 3 days, when the plants emptied the water stored in the pore system of the humic sand. The lowest measured sap flow during the drought period was defined as $Q_{fic}^{NVS\_drought}$ ($L\ h^{-1}$), similar to that of Q_{fic}^{NVS} (T_{air} 15.1 °C and RH 94.5 %). The corresponding Q_{fic} for the *VPD* approach was designated $Q_{fic}^{VPD\_drought}$ ($L\ h^{-1}$).

4.3 Results and discussion

4.3.1 Variation of Q_{fic} for different flow rates and T_{air} levels

Experiment 1: variation of Q_{fic} for different flow rates

Q_t values show a clear linear relationship to the adjusted flow rates f ($Q_t = 1.022\,f + 0.019$), at least in the range between 0.02 and $0.06\ L\ h^{-1}$ (Fig. 4.2). In this range, only small variations of the three repetitions were observed and $Q_{fic} = 0.019\ L\ h^{-1}$ was derived from the linear regression (Fig. 4.2). In contrast, for flow rates between 0.01 and $0.015\ L\ h^{-1}$, the three repetitions show major variation and do not follow the linear relationship given above. This means that flow rates $\leq 0.015\ L\ h^{-1}$ cannot be detected with the sap flow sensor used, but represent the limit of detection of this sensor for the PVC hose model stems.

GRIME and SINCLAIR (1999) have shown that the proportions of conductive and convective heat fluxes change with the sap flow rate. According to them, radial and vertical heat losses by conduction were highest at low sap flow rates. Therefore, the estimation of sap flow can become very inaccurate - not only for the tested model stems but for real stems as well. We hypothesise that calibration methods measuring Q_{fic} under zero-flow conditions, e.g. by cutting the stems after measurements, can underestimate sap flow.

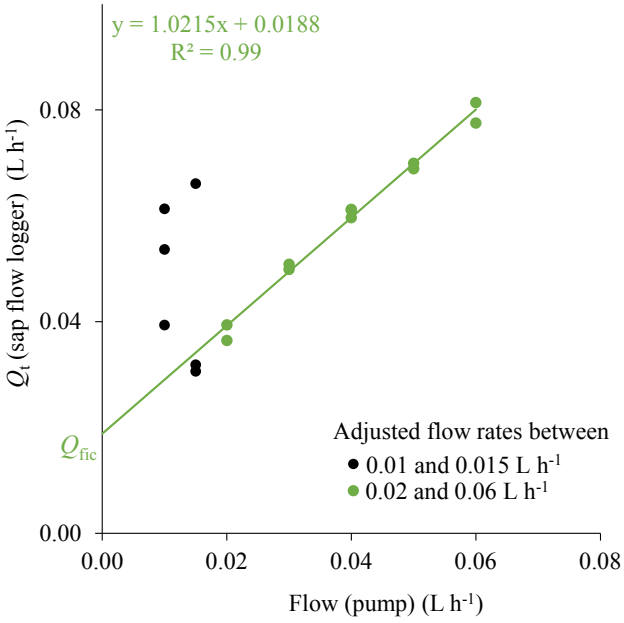

Fig. 4.2 Adjusted flow rates (syringe pump) and related measured heat input (Q_t) recorded by the sap flow logger. Points indicate mean values over the measurement period for a PVC hose filled with water.

Experiment 2: variation of Q_{fic} for different T_{air}

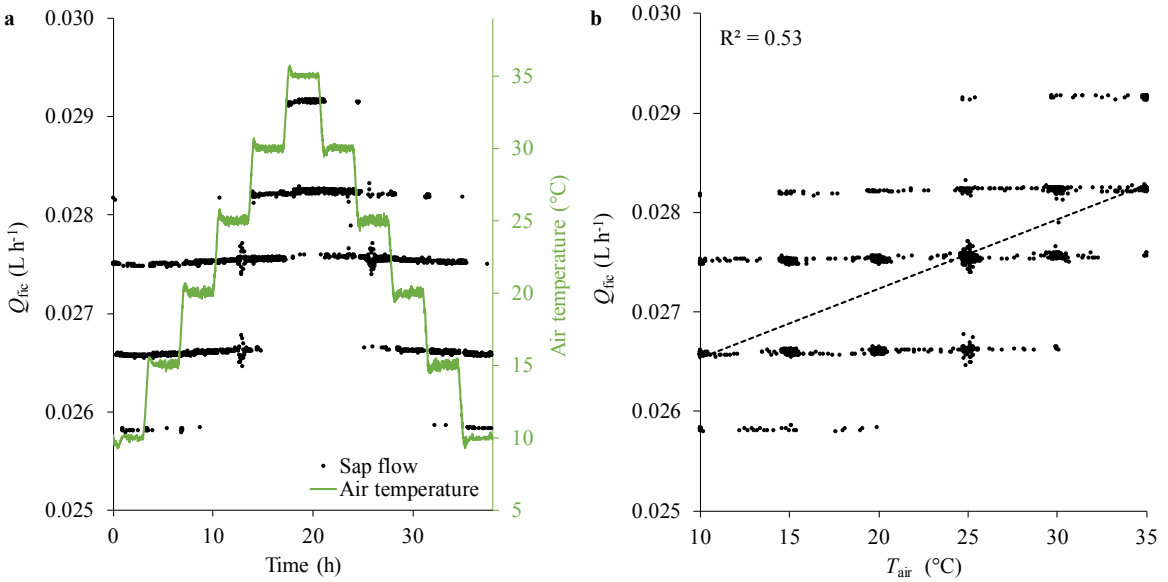

Fig. 4.3 a) Course of the fictitious water flux (Q_{fic}) for dynamic changes of the ambient air temperature (T_{air}), b) Q_{fic} dependent on T_{air}. Measurements under zero-flow conditions with a horizontally placed freshly harvested stem of *Fallopia baldschuanica*, $RH = 70$ %. The horizontal lines in the figures are caused by the limited resolution of the sap flow sensor.

The influence of the ambient air temperature on Q_{fic} was detectable for all investigated stems; the freshly harvested plant stem serves as an example (Fig. 4.3 a and b). The higher T_{air} is, the higher the mean of Q_{fic} becomes. For the stems under study and the fore-mentioned conditions, the relationship is represented by the equation:

$Q_{fic} = 7 \times 10^{-5}\ T_{air} + 0.0258$, $R^2 = 0.53$. As such, the relationship is not very robust. The dependence of Q_{fic} on T_{air} is caused by the dependence of the thermal conductivity of the stem and the resulting heat loss from the heated stem to the ambient air ($\Delta T = 4$ K).

However, the variation in Q_{fic} is in the same order of magnitude as the resolution of the sap flow sensor, indicated by the horizontal lines in figures 4.3 a and b. The overall influence of T_{air} is much lower than that of the flow rate. We conclude that the temperature effect is only applicable for ecosystems with extreme temperature differences in the diurnal cycle, e.g. high mountain regions. There, the correction could be applied using a diurnal cycle of Q_{fic} instead of constant Q_{fic} values. In mid latitudes, T_{air} differences between day and night usually account for less than 25 K. Therefore, we conclude that the relevance of temperature for Q_{fic} should not be overstated.

Obviously, higher temperature differences may also occur due to seasonal changes. However, since data for calibration are derived from the individual measuring campaigns, the *VPD* approach already incorporates seasonal changes of Q_{fic}^{VPD}. As measuring campaigns are limited in time as a general rule (14 days is the typical limit), seasonal changes would not significantly interfere with the results of the campaigns.

4.3.2 Comparing different sap flow baseline-correction approaches (experiment 3 and 4)

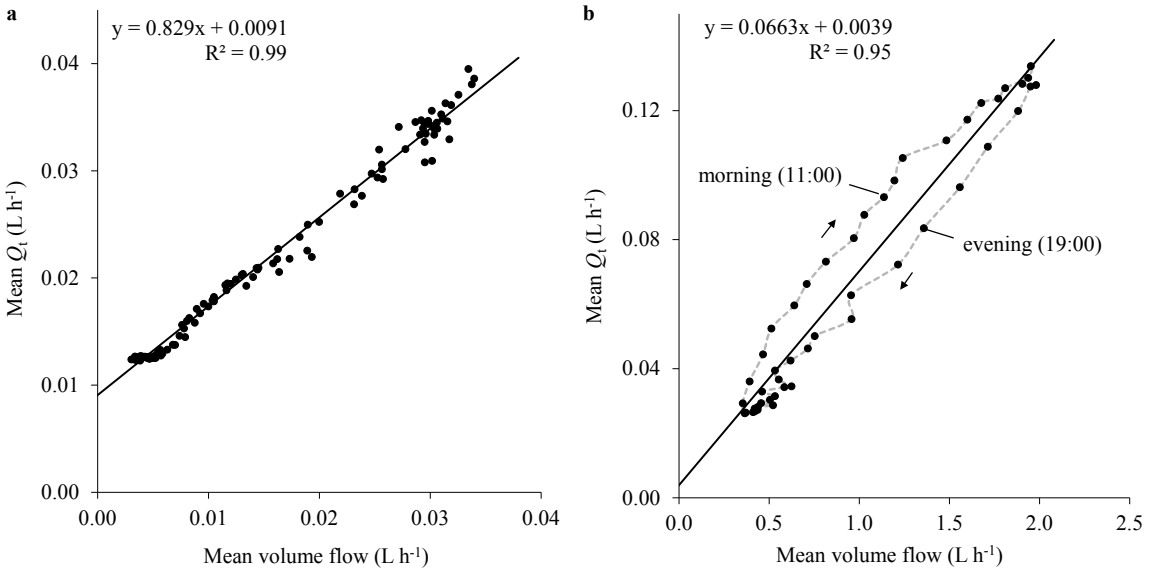

Fig. 4.4 Calibration of the measured heat input (Q_t) by adaptation to weighed volume flow; a) for a single potted plant stem, measured under indoor conditions. Points indicate mean values from 18th to 29th August 2012 for *Parthenossisus tricuspidata*; b) for a real climbing plant stand outdoors. For weighing data, values for the total greening (32 stems) are shown and for Q_t, mean values of the five instrumented stems are shown. Points indicate mean values from 2nd to 16th and from 21th to 22th September 2014 for *Fallopia baldschuanica*.

In order to assess the different baseline-correction approaches for sap flow data, we compared the corresponding Q_S data with the simultaneously measured mass losses for

i the single *P. tricuspidata* plant in a pot on a balance and ii for the entire stand of six *F. baldschuanica* plants in the lysimeter. In both cases, sap flow data have been scaled to the gravimetric measurements by linear regression. The axis intercepts of the linear relationship between sap flow and gravimetric measured transpiration corresponds to Q_{fic}^{grav}, which was 0.0091 L h^{-1} for the single stem of *P. tricuspidata* under indoor conditions and 0.0039 L h^{-1} for the *F. baldschuanica* real stand under outdoor conditions (Fig. 4.4 a and b. Note, that the coefficients of indoor and outdoor calibration curves are very different. There is broad consensus that sap flow must be scaled according to the whole xylem cross sectional area (JIMÉNEZ et al. 2000. However, in the outdoor experiment, stems (with the same diameters differed in leaf area, light conditions (shading, streetlamps, wind and temperature (thermal radiation from the rear wall, which influenced sap flow. Therefore, we applied linear regression instead of xylem area scaling.

On closer inspection of the data, a hysteresis is noticeable in sap flow measurements: at night, sap flow was higher than gravimetrically determined transpiration; during the day, it was reverse (Fig. 4.4 b). This could be due to the fact that during hot days in particular, plants transpire water at a higher rate than they can extract it from soil. At night, they compensate for these water losses with an uptake that is higher than transpiration. This behaviour leads to shrinking and swelling of stems during their diurnal cycles (TATARINOV and ČERMÁK 1999). This means, transpiration measured by sap flow might be overestimated at night and underestimated at daytime. However, with the 1 m tall, young *P. tricuspidata* in the indoor experiment, this phenomenon was barely detectable (Fig. 4.4 a), while it was more pronounced for the 12 m tall *F. baldschuanica* stand outdoors, even though the investigated stems were similar in diameter. Even if climbers have relatively small stem diameters and even if they exhibit only minor swelling and shrinking, this phenomenon can nevertheless be highly relevant for established facade greenings in light of their long stems and high LAI. Note that climbers (e.g. *F. baldschuanica*) wind around supporting structures and thus have much longer stem lengths than the plant height would suggest.

Transpiration measured by the balance never reached zero at any point during the measurement period and was relatively high at night (Fig. 4.5, in contrast to the NVS approach, which forces the baseline to zero. Consequently, there were great differences between Q_S^{NVS} and Q_S, calibrated using Q_{fic}^{grav}, as results from 7th September 2014 (Fig. 4.6 a show as an example. On a daily basis, the NVS-corrected sap flow data were between 13.9 and 33.4 % lower than weighing data. During the measurement period, *VPD* was always higher than zero (Tab. 4.2. The NVS approach leads to high uncertainties and an underestimation of transpiration, especially when the *VPD* remains high at night, e.g. on hot and dry summer nights in cities.

We also tested the NVS approach for drought conditions to derive $Q_{fic}^{NVS\_drought}$. Drought experiments reduced the level of day-time transpiration considerably (Fig. 4.5. However, night-time sap flow appeared to be unchanged and no reduction was observed. In fact, estimated night-time sap flow was higher than for well-watered conditions (Fig. 4.6 a. Drought stress probably led to a stronger nocturnal rehydration of depleted xylem water reserves. According to GRIME and SINCLAIR (1999, heat losses by conduction are more

difficult to determine and become more important in the heat balance under drought stress conditions. Consequently, the NVS approach is rather uncertain for calibrating sap flow under drought conditions. In contrast, $Q_{fic}^{VPD\_drought}$ is not influenced by drought conditions (data not shown).

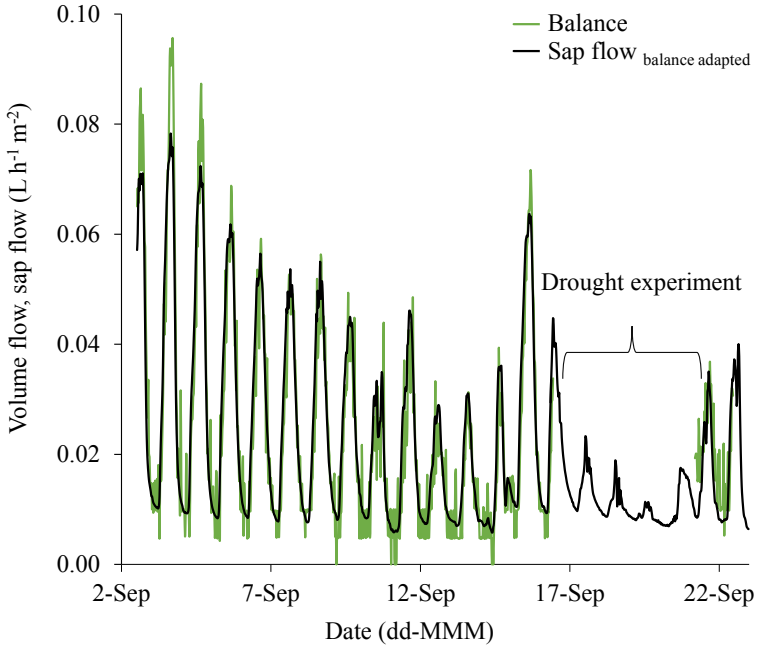

Fig. 4.5 Diurnal cycles of transpiration per m^2 leaf area (*Fallopia baldschuanica*) from 2nd to 22th September 2014 estimated by sap flow measurements (mean values of the five sensors, calibrated using a balance) and estimated by the use of a balance.

Concerning the applicability of Q_{fic}^{VPD}, our results show that sap flow depends on *VPD*, shown for outdoor conditions (Fig. 4.7 a). At first glance, it looks as though this relationship is not linear. Due to the cooling of distinctive air parcels at night, only certain values for *VPD* occurred. Separate curves, shown for two nights, demonstrate that *VPD* and sap flow were high at the beginning of these nights and then decreased. As we measured for 20 days, several values for Q_t appeared for the same *VPD*s. This might be due to the influence of wind on transpiration, but it might also be due to the fact that the climbers were 12 m high and probably experienced different *VPD*s at different heights. However, we were only able to calculate *VPD* at the height of 3 m. The axis intercept of the linear relationship between *VPD* and the lowest corresponding Q_t values returned $Q_{fic}^{VPD} = 0.0079\ L\ h^{-1}$. Compared to direct weighing, the sap flow values calibrated using Q_{fic}^{VPD} were up to 5.5 % higher and 10.6 % lower on a daily basis, as data from the 7th September shows as an example (Fig. 4.6 b).

We applied the *VPD*-based approach for indoor measurements as well. In these experiments, *VPD* was relatively high at night (> 16 hPa) which is why the dependence of sap flow on *VPD* was not as pronounced as for outdoor conditions.

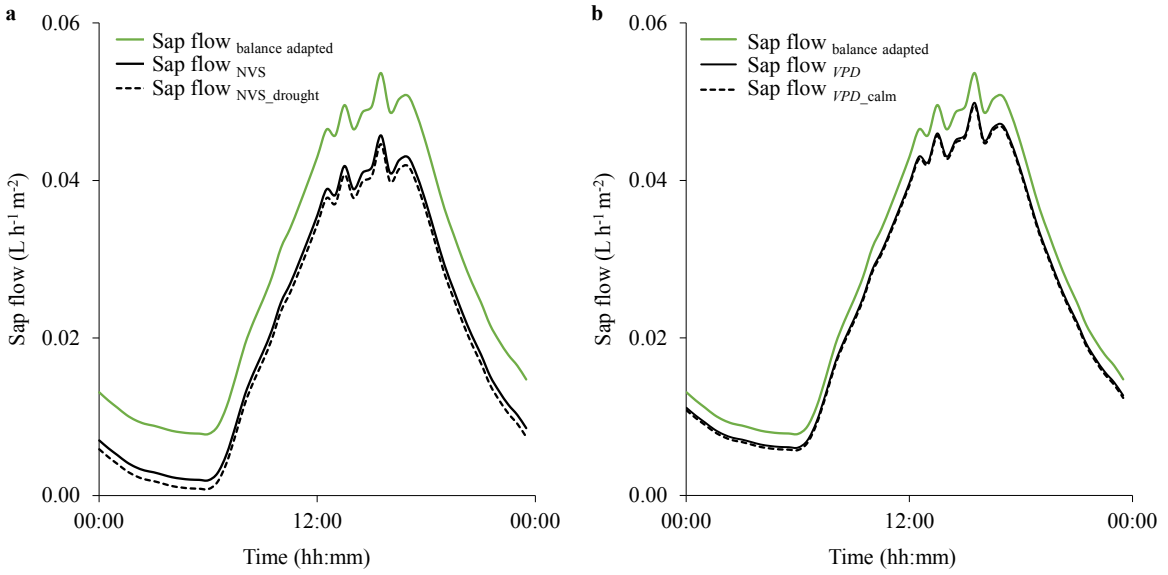

Fig. 4.6 Diurnal cycle of transpiration per m^2 leaf area (*Fallopia baldschuanica*), using data from the 7th September 2014 as an example; calibration approaches: baseline-correction by a) night value subtraction (NVS), night value subtraction for drought experiment (NVS_drought); b) vapour pressure deficit (*VPD*) and vapour pressure deficit under calm conditions (*VPD*_calm). All measurements are for outdoor conditions.

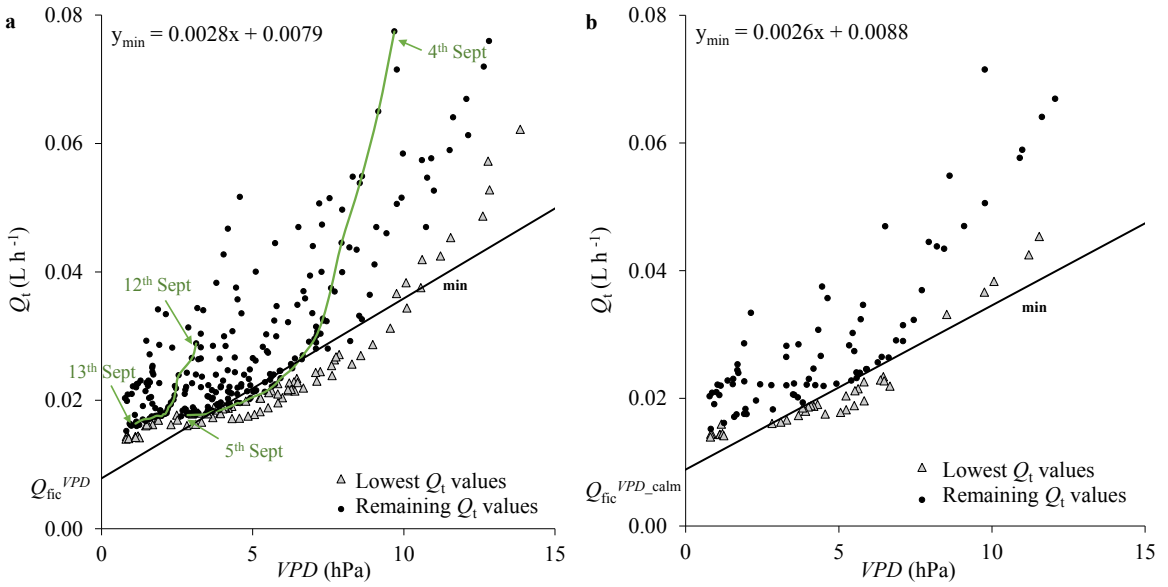

Fig. 4.7 Vapour pressure deficit (*VPD*) of the ambient air and related recorded heat input (Q_t) from 2rd to 22th September 2014. Quantification of the fictitious water flux (Q_{fic}) is indicated by the axis intercept of the linear relationship between *VPD* and the lowest of the measured Q_t values (triangles). a) *VPD*: without detectable radiation; the green lines indicate two chosen nights and b) *VPD*_calm: without detectable radiation and under calm conditions (according to BEAUFORT Scale = 0).

In order to eliminate the previously discussed influence of wind on the variability of *VPD* vs. Q_t, we calculated Q_{fic} for calm conditions: $Q_{fic}^{VPD\_calm} = 0.0088\ L\ h^{-1}$ (Fig. 4.7 b). This was only slightly higher than Q_{fic}^{VPD} and resulted in transpiration rate differences of less than

3 %. Therefore, it may not be necessary to measure wind for a good calibration of Q_t using the *VPD*-based approach.

4.4 Conclusions

Heat losses from SHB sap flow sensors result in a fictitious flow (Q_{fic}). For this reason, in order to calculate transpiration rates from SHB sap flow measurements, they must be calibrated. In our study, we developed a consistent correction approach which quantifies Q_{fic} taking advantage of the *VPD* of the ambient air. This approach takes site-specific, plant-specific and sensor-specific influences into consideration as it derives Q_{fic} from the measured data itself and from *VPD*. The *VPD* approach returns much better results than the frequently applied NVS approach and is comparable to the (usually infeasible) direct gravimetric determination. Once sap flow is calibrated correctly, our results suggest that the SHB method is practicable for determining transpiration rates of climbing plants in a city on a daily basis, which can be as high as 0.8 L d^{-1} m^{-2} per leaf area for *F. baldschuanica* in late summer.

A particularly welcome aspect of this development is that, *VPD* correction can be retrospectively applied to improve the accuracy and reliability of previously measured data, as T_{air} and *RH* are available in most cases in any case.

Acknowledgments

HANS-PETER KLÄRING, INGO HAUSCHILD, THOMAS RUNGE and the Leibniz-Institut für Gemüse- und Zierpflanzenbau (IGZ) in Großbeeren, Germany are thanked for their great support and for providing the climatic chamber. JIŘÍ KUČERA and GERHARD KAST are thanked for providing the sap flow sensors and their personal introduction into the methodology.

This work was funded by the Deutsche Forschungsgemeinschaft (DFG), Research Unit FOR 1736 “urban climate and heat stress in mid-latitude cities in view of climate change (UCaHS)” (www.UCaHS.org).

5 Evaluation of the health-risk reduction potential of countermeasures to urban heat islands[4]

OLIVER BUCHIN[a,*], MARIE-THERESE HOELSCHER[b], FRED MEIER[c], THOMAS NEHLS[b] and FELIX ZIEGLER[a]

[a] Department of Energy Engineering, Energy Conversion Technologies, Technische Universität Berlin

[b] Department of Ecology, Soil Conservation, Technische Universität Berlin

[c] Department of Ecology, Climatology, Technische Universität Berlin

*corresponding author; e-mail address: oliver.buchin@tu-berlin.de

Abstract

Traditional assessment of heat-related health risks neglects the influence of the building physics as outdoor conditions are used as predictor variables. Data on heat-related mortality from Berlin, Germany and from the US are evaluated with a risk concept which differentiates between outdoor and indoor hazards. Such, the influence of non-linear building physics on heat-related risks can be considered and the impact of adaptation strategies can be examined.

The number of heat-related deaths in the age-group 65+ for Berlin is expected to double with each 1 K increase in ambient temperature. It can be reduced by 50 % with a mean ambient air temperature reduction of 0.8 K. Countermeasures to urban heat islands are evaluated according to their reduction potential on hazards, both indoors and outdoors. The analysis shows that classic UHI countermeasures, which are effective in reducing air temperatures outdoors, do not necessarily reduce the indoor hazard. Regarding indoor heat-related hazards, trees, facade and roof greening, cool roofs and cool pavements have a low impact only. Measures at the building level, namely cool roofs and facade greening perform best, however, passive cooling and air-conditioning are most effective. To reduce the number of excess deaths in a changing climate, combined measures are necessary.

[4]Published: BUCHIN, O., M.-T. HOELSCHER, F. MEIER, T. NEHLS and F. ZIEGLER (2015). Evaluation of the health-risk reduction potential of countermeasures to urban heat islands. *Energy and Buildings* 114 (2016): 27-37.

Keywords

Risk analysis, heat wave, heat-related risks, heat stress, cool roof, cool pavement, urban green, passive building design, air-conditioning

5.1 Introduction

The urban heat island (UHI) effect is a localised anthropogenic climate modification in the canopy layer of the urban atmosphere where almost all daily human activities take place (OKE 1982, GIANNAROS et al. 2014). At the individual level, increased temperatures promote the inability to balance the heat flows from the human body by the thermoregulation system. This leads to health risks ranging from heat rash and heat cramps, through heat exhaustion, heat stroke, to death. Furthermore, pre-existing medical conditions, such as heart or lung diseases, may be exacerbated. Thus, especially elderly people are at risk (BASU and SAMET 2002, STAFOGGIA et al. 2008).

A significant increase in heat-related health risks (mortality and morbidity) is projected for many mid-latitude cities if no adaptation and mitigation strategies are implemented (LI et al. 2013, JENKINS et al. 2014, WU et al. 2014). The amplification of the occurrence of extreme temperatures, due to the UHI effect or climate change, will lead to elevated heat-related risks, especially in urban areas. The relevance will increase even without the external driving factors, due to demographic change in many mid-latitude cities. Obviously, mitigation strategies to reduce absorption of radiation and storage of heat (e.g. cool roofs and cool pavements) or to increase evaporation, transpiration and biomass production (green roofs, urban green) on a region or city-wide implementation, which are referenced to as countermeasures to UHI, seem to impose a reduction potential for health risks. However, even a qualitative assessment or estimate of the risk reduction potential of the countermeasures is missing, as necessary knowledge and data is distributed across several disciplines (climatology, epidemiology, social sciences, building physics, horticulture and engineering).

Statistical evaluation in the form of risk assessment at population level has been established within the climate change adaptation community (IPCC 2012). Heat-related risks in cities were addressed by various studies in recent years (see reviews of KOVATS and HAJAT 2008, GOSLING et al. 2009, SCHERER and ENDLICHER 2013), with heat-related mortality being one of the most researched heat-stress related risks due to its drastic impact and availability of reliable time-series data. However, there is disagreement concerning epidemiological studies on heat-related risks and appropriate concepts and methods for quantifying heat-stress related hazards, vulnerabilities and risks are still under development and discussion. Disagreement in heat-related mortality data is due to the methods to define days or episodes of heat stress, the use of different types of mortality data, methods to account for displaced deaths or the methods to estimate base mortality rates (SCHERER and ENDLICHER 2013).

Furthermore, risks vary substantially between and within cities, since both hazard and vulnerability display strong spatial and temporal patterns (O'NEILL et al. 2003, HARLAN et al. 2006, CARDIL et al. 2014, ROSENTHAL et al. 2014, SCHUSTER et al. 2014).

On a spatial scale, climate variability between different building types is often higher than the one originating from the outdoor climate on the mesoscale (OIKONOMOU et al. 2012). However, due to the heterogeneity of the building stock (and the missing involvement of the building experts), heat-related risk assessment is often based on outdoor climate only.

On the contrary, it is well known that the living conditions, especially building structure and air-conditioning, have a significant effect on the risk. Many studies have documented statistically significant higher mortality rates of residents in top-floor apartments or in buildings with poor insulation or high glazing fraction (SEMENZA et al. 1996, VANDENTORREN et al. 2006). Reduced risk is documented for people with access to air-conditioning (SEMENZA et al. 1996, KILBOURNE 1997, DAVIS et al. 2003, O'NEILL et al. 2005). A statistically sound explanation of heat-related mortality, with elevated indoor temperatures calculated with a building model, was presented for Frankfurt, Germany (BRANDT 2006) and for Berlin, Germany (BUCHIN et al. 2016).

Despite the qualitative and quantitative evidence of the influence of the building parameters and air-conditioning on the heat-related risks, these are not yet covered systematically in traditional risk analysis and thus are not implemented in respective projections. A concise evaluation of risk reduction potentials has to differentiate between the actual risk and the underlying hazard, both indoors and outdoors. Outdoor health risks are often due to direct exposure to sun, such as sunburn or heat stroke, whilst heat-related mortality and exacerbated diseases are associated with elevated indoor temperatures and reduced recreation due to elevated night-time indoor temperatures. BUCHIN et al. (2016) have shown that it is very suitable to evaluate heat-related mortality with indoor hazards as vulnerable groups are mainly subjected to indoor conditions and the lag in risk development during heat events can be explained with the thermal inertia of the building stock. The objective of this study is the qualitative evaluation of the risk reduction potential of several countermeasures to urban heat islands, applying a risk concept with differentiated indoor and outdoor hazards developed by BUCHIN et al. (2016). The concept was developed within the DFG Research Unit 1736 "urban climate and heat stress in mid-latitude cities in view of climate change (UCaHS)". It considers building physics and indoor climate conditions. Countermeasures to UHI are compared to passive and active adaptation measures on the building level.

The paper first explains the risk concept and analyses the validity of the main influential parameters. The validity for the indoor hazard on indoor risk is tested with data on mortality of Berlin. Different countermeasures to UHI are analysed concerning their potential of hazard and risk reduction and are compared on a qualitative basis with further adaptive measures. Suggestions for concrete measures and further research conclude the paper.

5.2 Methods and data

5.2.1 Heat-related risk concept

The detailed description of the heat-related risk concept in this subsection is based on a previous work of the research group (BUCHIN et al. 2016). The risk r of a specific effect during a hazardous process, e.g. heat-related excess mortality at a day during a heat wave, can be described by the product of a hazard value h representing a hazardous process and the vulnerability v to this effect.

$$r = h * v \,. \qquad \text{(eq. 5.1)}$$

The advantage of a risk concept like this is that it is differentiated between external driving factors and a hazard-independent vulnerability. In general, all variables are specific for one system, which is defined by its elements (e.g. a sub-group of inhabitants) and its spatial distribution (e.g. an urban district). For instance, $r_{\text{mortalityheat-stress, 65+Berlin}}$ represents the excess mortality related to heat stress for the group of inhabitants in the age of 65 years and older in Berlin.

Nonetheless, it is useful to differentiate the total number of persons at risk N_{tot} according to their exposure into three groups. There is one group N_{out}, which is predominantly exposed to outdoor conditions, whilst the others are exposed to the indoors, either in unconditioned ($N_{\text{in, uc}}$) or air-conditioned ($N_{\text{in, ac}}$) climates. A plausible implementation is additive as follows:

$$r = \frac{N_{\text{out}}}{N_{\text{tot}}} h_{\text{out}} v + \frac{N_{\text{in, uc}}}{N_{\text{tot}}} h_{\text{in, uc}} v + \frac{N_{\text{in, ac}}}{N_{\text{tot}}} h_{\text{in, ac}} v \,. \qquad \text{(eq. 5.2)}$$

In equation 5.2 the vulnerability v in the different environments is assumed to be equal, although there are hints that people with pre-existing health issues tend to be more restricted to indoor climates.

Two new parameters are defined: a is an air-conditioning ratio which describes the fraction of inhabitants in air conditioned environments to the total number of individuals indoors ($a = N_{\text{in, ac}} / N_{\text{in}}$); e is an exposure-parameter describing the mean exposure of the group at risk towards the outdoor hazard ($e = N_{\text{out}} / N_{\text{tot}}$). With this equation 5.2 reads:

$$r = e h_{\text{out}} + (1 - e)(a h_{\text{in, ac}} + (1 - a) h_{\text{in, uc}}))v \,. \qquad \text{(eq. 5.3)}$$

The exposure e varies between 0 and 1 with $e = 1$, meaning that the system group is exposed to the outdoor hazard only, whilst $e = 0$ describes the full exposure to the indoor hazard. The

indoor hazard $h_{\text{in, uc}}$ in equation 5.3 is considered to be valid for the building stock without air-conditioning. It is assumed that the climate of the air-conditioned space generally fulfils comfort criteria and does not promote heat-related risks. Thus, it can be neglected ($h_{\text{in, ac}} = 0$) and equation 5.3 is reduced to:

$$r = ((1-e)(1-a)h_{\text{in, uc}} + eh_{\text{out}})v\,. \qquad \text{(eq. 5.4)}$$

Furthermore, it can be assumed that most people in mid-latitude cities are subjected to indoor conditions during more than 80 % of their time, even during the summer season (KRAUSE and SCHULZ 1998) and e can be approximated to be negligible ($e = 0$). Equation 5.4 then reads:

$$r = (1-a)h_{\text{in, uc}}v\,. \qquad \text{(eq. 5.5)}$$

5.2.2 Hazard calculation

The hazard intensity h has to be based on variables that are available to measure. To simplify the analysis, we use a hazard definition based on excess-temperature:

$$h = T - T_{\text{th}} \quad \text{if} \quad T - T_{\text{th}} > 0\,,\ h = 0 \quad \text{otherwise.} \qquad \text{(eq. 5.6)}$$

The hazard intensity has to be representative for the spatial and temporal resolution of the risk data, which is often coarse due to data collection or data privacy protection. Therefore, indoor hazards can be calculated with a simplified building model. A building model with two parameters τ and λ is used to calculate a time-series of a representative indoor temperature T_{in} from a time-series of outdoor air temperature T_{out} and global horizontal irradiance I. The following equation is derived by BUCHIN et al. (2016):

$$T_{\text{in}}(t + \Delta t) = \max\left[\hat{T}_{\text{out}} + \lambda \hat{I} + (T_{\text{in}}(t) - \hat{T}_{\text{out}} - \lambda \hat{I})e^{-\Delta t/\tau};\, T_{\text{heat}}\right]. \qquad \text{(eq. 5.7)}$$

τ is a time constant which is a measure for the thermal inertia of the building, λ covers the temperature elevation due to solar gains. For the cold season, it can be assumed that the indoor temperature does not fall below a minimum temperature T_{heat}, which is set by the heating system. For the warm season, it can be assumed that internal heat sources are negligible compared to the solar heat flux into the zone. $T_{\text{in}}(t)$ is the initial indoor temperature for the time interval Δt. The time-series of T_{in} is calculated in a forward scheme with an initial starting value for T_{in} ($t = 0$) and arithmetic mean values for the ambient climate data (e.g. $\hat{T}_{\text{out}} = 0.5 \times T_{\text{out}}(t) + 0.5 \times T_{\text{out}}(t + \Delta t)$). The temporal resolution of the

climate data determining the time step Δt has to be set high enough, so that the outdoor climate conditions can be assumed constant during this time step. Of course, the building model parametrisation has to be representative for the building stock in the region for which risk data are available.

5.2.3 Vulnerability calculation

The influence of rising temperatures on the risk can be modelled to be linear above the threshold temperature T_{th} used in the hazard definition. If vulnerability is assumed to be constant, it can be calculated as slope of the regression curve:

$$v = \frac{\mathrm{d}r}{\mathrm{d}h} = \frac{\mathrm{d}r}{\mathrm{d}T} \qquad \text{for} \qquad T - T_{th} > 0\,. \qquad \text{(eq. 5.8)}$$

Finally, it can be stated that the risk is dependent on three variables (v, T_{out}, I) and four parameters (a, T_{th}, τ and λ). Section 5.3 will elaborate on the plausibility of the parameters and on their influence on the regression analysis. The analysis will be based on the exemplary data described in the following subsection.

5.2.4 Data

Climate data

A time-series of outdoor air temperature from Berlin-Tempelhof during the period from 1st January 2001 to 31th December 2010 in hourly resolution (DWD 2014) is used for the hazard calculation (see Fig. 5.1 (top)). Furthermore, hourly data of global horizontal irradiation from the urban climate observation network operated by Technische Universität Berlin (FENNER et al. 2014) is used for the application of the simplified building model. The daily sums of global horizontal irradiation observed at site Rothenburgstraße in Berlin-Steglitz are shown in figure 5.1 (bottom).

Risk data

The database is the age-classified number of deaths in Berlin in daily resolution and the half-yearly population data interpolated to daily resolution. Both data sets are valid for the group of people in the age of 65 years and older and for the period 1st January 2001 to 31th December 2010 (SOBB 2013). The data are presented in figure 5.2. Obviously, death rates are elevated during the winter season, but also during summer. The heat waves of 2006 and 2010 can easily be detected in the time-series data with 2010 exceeding even the maximum winter season death-rates.

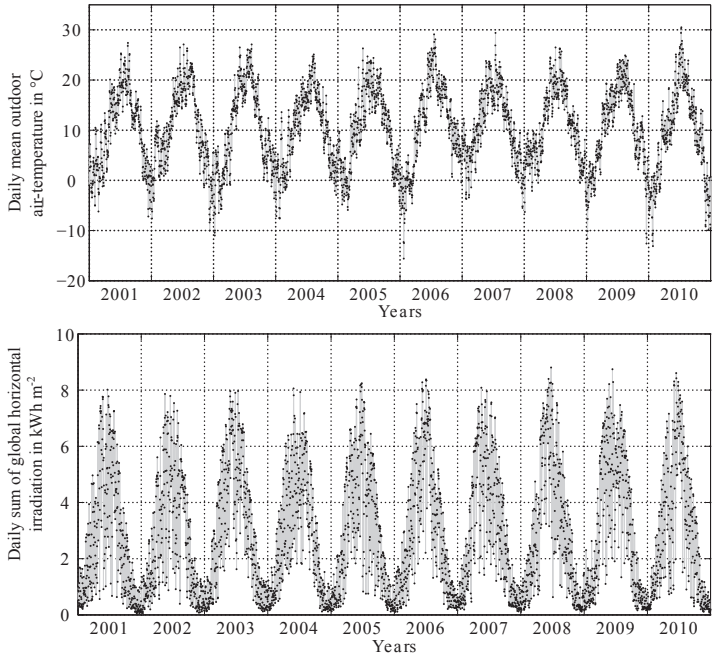

Fig. 5.1 Top: daily mean air temperature at Berlin-Tempelhof from 1st January 2001 to 31th December 2010. Bottom: daily sums of global horizontal irradiation at a weather station in Berlin-Steglitz from 1st January 2001 to 31th December 2010.

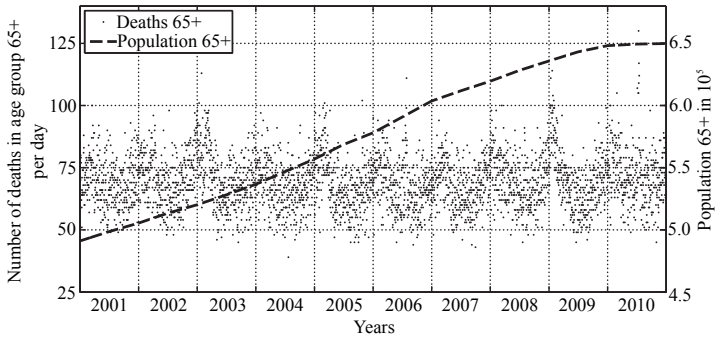

Fig. 5.2 Number of deaths and population for the group of people in the age of 65 years and older in Berlin from 1st January 2001 to 31th December 2010.

All-cause mortality rates are calculated as risk data:

$$r_{\text{mortality, }65+} = \frac{\text{no. of deaths }_{65+}}{\text{population }_{65+}}. \qquad \text{(eq. 5.9)}$$

The heat-related excess mortality r is calculated from the risk data by subtracting the base mortality rate r_0. It is the mean mortality rate at temperatures below the threshold temperature which cannot be associated to the heat. To withdraw the effect of the elevated mortality during the winter season only risk data associated to daily mean outdoor temperatures above 15 °C and to daily mean indoor temperatures above 22 °C are evaluated (see also Section 5.3).

5.3 Analysis

5.3.1 Parametrisation of the building model and threshold temperature

The system group is assumed to be fully exposed to the indoor climate ($e = 0$) without air-conditioning ($a = 0$) which is a good approximation for the Berlin region where air-conditioning is only prevalent in some offices and in automobiles.

The climate data are available in hourly resolution and are transformed to indoor temperatures with the simplified building model. The minimum temperature T_{heat} and T_{in} ($t = 0$) is set to 20 °C. The building model was parametrised with $\tau = 100$ h and $\lambda = 0.0175$ K W^{-1} m^2 according to its calibration using simulation results for a typical residential building for the Berlin region done with a detailed EnergyPlus building model (for details see BUCHIN et al. 2016).

The relation between the risk and daily mean of the outdoor air temperature and the modelled indoor air temperature is depicted in figure 5.3. Boxplot diagrams are prepared in 1 K intervals and show the median, 25th and 75th percentiles (boxes) and range (whiskers) of the mortality data. Outliers are defined as being outside of 1.5 times the interquartile range above or below the quartiles.

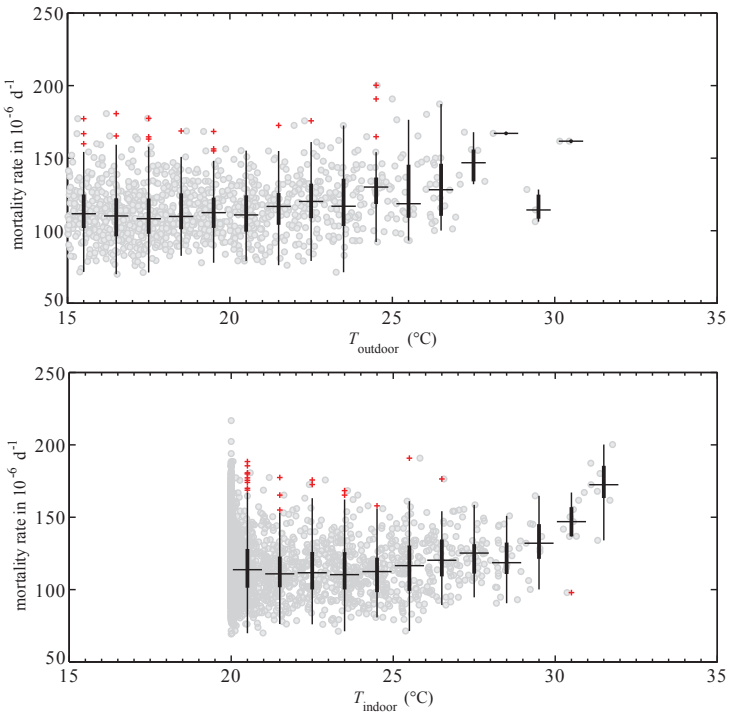

Fig. 5.3 Mortality rates for the age-group 65+ in Berlin in relation to outdoor (top) and indoor (bottom) temperatures as predictor variables and boxplots for 1 K intervals with median, 25th and 75th percentiles (boxes), range (whiskers) and outliers (orange crosses).

The median mortality and the lower and upper quartiles, increase for outdoor temperatures above 20 °C. At outdoor temperatures exceeding 27 °C no clear trend can be detected. The

median mortality and the quartiles, increase as well for high indoor temperatures (> 28 °C). Obviously the high mortality rates correspond better to indoor than to outdoor temperatures.

The breakpoint in the underlying data can be detected by a comparative regression analysis with changing threshold temperatures. Higher threshold temperatures yield higher coefficients of determination R^2 as long as data before the breakpoint are influencing the regression. When the threshold temperature exceeds the breakpoint, R^2 remains at a constant level as the rising trend is covered and uncertainty σ is increasing as the number of data points is reduced. The coefficient of determination R^2 can be interpreted as explained variance in the given data. Note that deviating from a standard segmented regression analysis only the sloped part of the regression curve above the threshold temperature is used to determine R^2 and σ as it is essential to describe the extreme risk data with high accuracy. The slope of the regression curve yields the vulnerability *v*.

For instance, a threshold temperature of 26 °C yields a vulnerability of 7.3×1^{-6} d^{-1} K^{-1} at a base mortality rate of 1.15×10^{-4} d^{-1} with $R^2 = 0.23$ and $\sigma = 0.097$. A threshold temperature of 29 °C yields a vulnerability of 2.4×10^{-5} d^{-1} K^{-1} at a base mortality rate of 1.15×10^{-4} d^{-1} with $R^2 = 0.49$ and $\sigma = 0.12$. Obviously, the choice of an appropriate threshold temperature significantly influences the vulnerability whilst the base rate is not significantly affected. The regression curves of the two examples are depicted in figure 5.4. The estimation of the breakpoint from the given data is described in the following section.

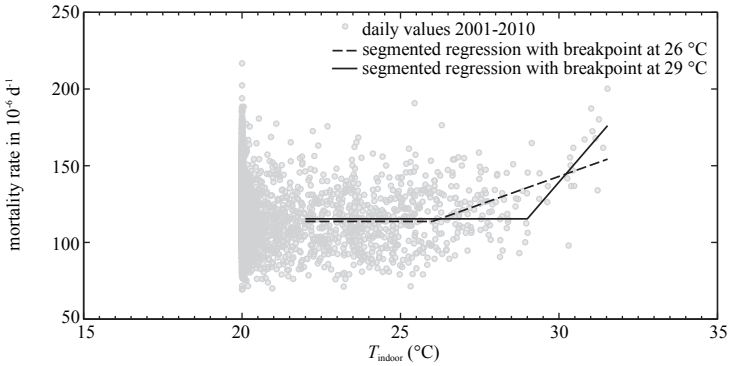

Fig. 5.4 Mortality rates for the age-group 65+ in Berlin in relation to indoor air temperatures and segmented regression curves for threshold temperatures of 26 °C and 29 °C.

The regression performance is not only dependent on the threshold temperatures but also on the representativeness of the underlying building which is characterised by the two parameters τ and λ. The accuracy of the chosen parametrisation and the sensitivity of the regression on the model parameters is evaluated for the given risk data. The dependence of the coefficient of determination R^2 and the uncertainty σ for changes in τ is presented in figure 5.5 (top).

It can be seen that for the reference model ($\tau = 100$ h, $\lambda = 0.0175$ K W^{-1} m^2) and threshold temperatures above 22 °C, the explained variability in the data is steadily rising until it flattens at values of about 0.5 at temperatures of 28 to 29 °C. The uncertainty remains at a level of about 0.1. The flattening behaviour can be associated with excessing of the breakpoint in the data. For higher temperatures, the behaviour is unsteady and uncertainty is

increasing at temperatures above 30 °C, as data are removed from the segment. For lower and higher values of τ (50 h and 150 h), the flattening region indicating the breakpoint is in a similar temperature range, however, with a lower coefficient of determination. So, τ = 100 h is a good choice with a breakpoint of about 28 to 29 °C at λ = 0.0175 K W^{-1} m^2.

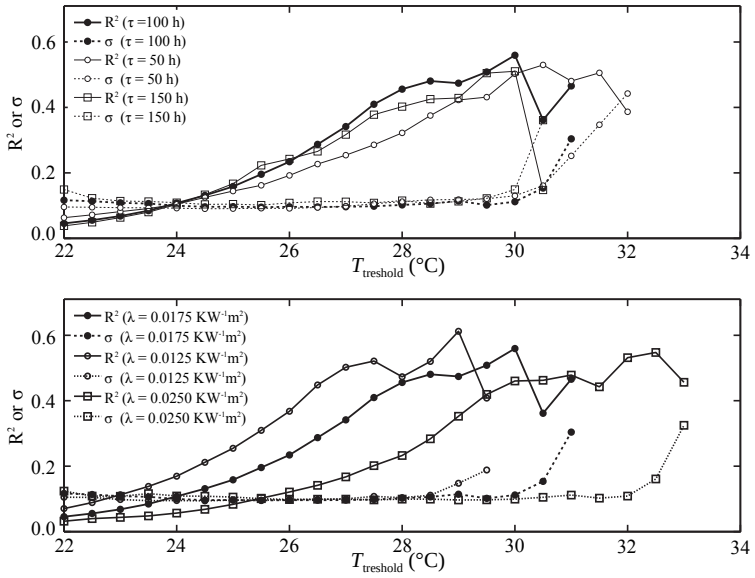

Fig. 5.5 Sensitivity of R^2 and σ in a regression analysis with mortality rates of age-group 65+ in Berlin and indoor air temperatures in dependence of threshold temperatures and different values of τ (top) and λ (bottom).

Figure 5.5 (bottom) shows the influence of λ on the regression performance. This parameter covers the temperature elevation due to solar gains. For λ = 0.0125 K W^{-1} m^2 the range in which the curve of R^2 flattens is starting at about 26 °C, whilst at λ = 0.025 K W^{-1} m^2 this region is shifted to 30 °C. The coefficient of determination R^2 in these regions is comparable for all three curves with values of approximately 0.5.

This temperature offset in the regression curves can be explained with the effect of λ in equation 5.7:

$$T_{in} = T_0 e^{-\Delta t/\tau} + T_{out}(1 - e^{-\Delta t/\tau}) + \underbrace{\lambda I(1 - e^{-\Delta t/\tau})}_{\approx constant}. \qquad \text{(eq. 5.10)}$$

At elevated indoor air temperatures, shifted thresholds can be explained if the daily mean radiation is at a constant level. In this case λ just scales a temperature offset. Especially during heat event days, at clear sky conditions during the summer months, the mean daily irradiation rate is on a comparable level.

From the analysis we learn, firstly, that the time constant τ is significant for the regression performance and the values which do explain the data best are consistent to the ones obtained

from the reference building and its underlying detailed building simulation. Secondly, for a given representative model, the accuracy of the threshold temperature obtained from the regression analysis is influenced by the accuracy of the solar gain parameter (λ) of the simple building model. Finally, we see that countermeasures aiming at the reduction of solar gains will be of high importance, as these directly influence the general temperature level within the zone.

The regression curve for a threshold temperature of 29 °C and a building model with the reference parametrisation of $\tau = 100$ h and $\lambda = 0.0175$ K W^{-1} m^2 is used in the subsequent section (see Fig. 5.4). This regression curve yields $R^2 = 0.49$, $\sigma = 0.12$, a vulnerability of 2.4×10^{-5} d^{-1} K^{-1} at a base mortality rate of 1.15×10^{-4} d^{-1}.

5.3.2 Mortality in regions with prevalent air-conditioning

If the above assumptions of equation 5.5 hold true, data on the development of risks at changing fractions of air conditioned buildings during the years should fulfil equation 5.5 and relative risks $r / (h_{\mathrm{in,\,UC}}\, v)$ have to show a linear dependence with respect to a.

The assumptions are exemplarily applied to data of heat-related excess mortality from different decades extracted from (DAVIS et al. 2003, Fig. 5.4). These data were collected for 28 cities in the United States and grouped in eight regional clusters for the decades 1980 and 1990. For these clusters, the percentage of homes with air-conditioning was available which can be interpreted as air-conditioning fraction a. To allow for comparison of the trends within the different clusters, relative annual excess mortality rates r_{rel} are defined:

$$r_{\mathrm{rel}} = \frac{r}{r_{\mathrm{un}}} = \frac{r(1 - \hat{a})}{\hat{r}}. \qquad \text{(eq. 5.11)}$$

r_{un} represents the expected risk for the persons exposed to a fully unconditioned building stock ($a = 0$). Assuming that mean vulnerability and mean hazards were constant during the decades, r_{un} can be estimated for each cluster from the mean mortality rate $\hat{r} = 0.5\,(r_{1980} + r_{1990})$ and the mean air-conditioning fraction $\hat{a} = 0.5(a_{1980} + a_{1990})$: $r_{\mathrm{un}} = r / (1-\hat{a})$.

Figure 5.6 shows the proportional decrease of the risk with an increase in air-conditioning coverage according to equation 5.11. For $a = 1$, no relative risk is expected, whilst at $a = 0$ it is 1. As can be seen, this general behaviour is in accordance to the risk data of (DAVIS et al. 2003, Fig. 5.4). Of course, deviations from the expected slope exist and are possibly due to a decadal change in hazards and vulnerabilities, which are influenced by e.g. migration, demographic change or changes in medical care. Unfortunately, it is not possible to extract these influences from the underlying data. Note, that one cluster (MT) with the cities of Phoenix and Denver shows an increasing trend. However, the data on the excess mortality rate for these hot climates are at a very low level, between 4 and 10×10^{-6} d^{-1}

(DAVIS et al. 2003) and the underlying data for this cluster are not in accordance with further data in the same publication.

From figure 5.6 it is obvious that the heat-related risk is highly influenced by the indoor conditions, otherwise the impact of air-conditioning on mortality rates could not be explained. Thus, for evaluation of the risk reduction potential of countermeasures to UHI the specific influence on the indoor conditions has to be considered.

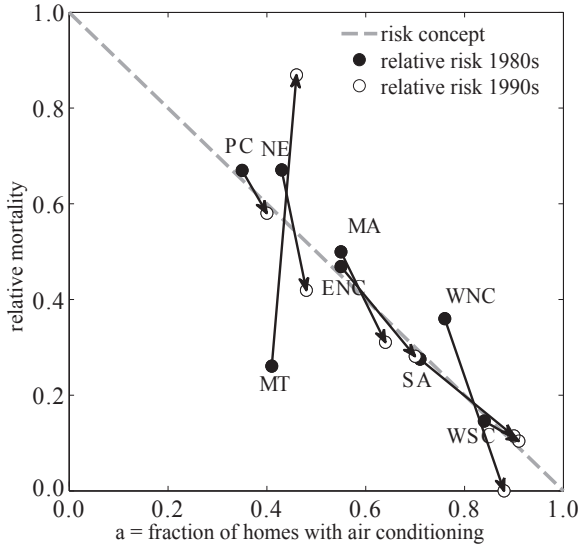

Fig. 5.6 Decadal change in relative heat-related excess mortality rates for different regions in the US (calculated with data from DAVIS et al. (2003)). Abbreviations: ENC - East North Central; MA - Mid Atlantic; MT - Mountain; NE - Northeast; PC - Pacific; SA - South Atlantic; WCS - West South Central; WNC - West North Central.

5.3.3 Countermeasures to UHI and hazard reduction

Countermeasures to UHI change the urban atmosphere and thus the heat-stress related hazard, both outdoors and indoors. Many quantitative studies on countermeasures document the influence on energetic fluxes, temperatures or bioclimatic indices in the outdoors. However, the influence of countermeasures on the indoor climate is often not addressed or research is focussed on a specific region, climate time-series or building type. To allow, despite the missing data, for a general conclusion on the health risk reduction potentials, the following evaluation considers the physical processes of sensible heat transfer, short-wave and long-wave radiation and latent fluxes in a qualitative manner. The qualitative evaluation of the UHI countermeasure in terms of a hazard reduction primarily concerns their effect on outdoor and indoor air temperature.

A qualitative scaling is applied to differentiate the measures. It comprises three levels for positive impacts on the hazard, a neutral level and one negative level (+++, ++, +, 0, −). The highest positive scale (+++) is used for measures which always provide comfort, whilst the negative scale (-) is used for measures which increase the hazard. Furthermore, heat wave resilience is classified, describing the potential indoor hazard reduction potential during

long-term adverse climate conditions. Finally, resource demand (water, electricity and heat) is considered for a concise discussion.

The following short review on the specific countermeasures is clustered into the spatial scale of implementation (mesoscale, building scale, room scale) and it is summarised in table 5.1. The objective of this summary is to visualise a general trend of the hazard reduction potential of countermeasures to UHI effect. The given classification might change in dependence on regional influences, the existing building stock and pre-existing implementations of countermeasures.

Tab. 5.1 Classification of countermeasures to UHI, levels: (+) small, (++) medium, (+++) high, (0) no and (−) negative effectiveness. Abbreviations: (AC) air-conditioning, (HW) during heat wave, (e) electric energy, (h) heat, (w) water.

Measures	Hazard reduction potential		Resources
	Outdoors	Indoors (HW)	
City scale (pavement and urban green)			
Cool pavements	+	+	
Trees	++	+	w
Grass	+	0	w
Building scale (roof and facade)			
Cool roof	+	+	w
Green roof	+	+(0)	w
Green facade	+	+	
Room scale (passive and active cooling)			
Overhangs and shutters	0	++	
Curtains	0	+	
Night ventilation	0	++(+)	
Vapour compression AC	−	+++	e
Absorption based AC	−	+++	h
Evaporative cooling	0	++	w

Cool pavements

Materials that have high solar reflectance (spectrum 0.3 to 2.5 µm) and high thermal emittance (spectrum 4 to 80 µm) maintain low surface temperatures. These "cool" or "reflective" materials reduce the surface-to-air temperature difference and therefore the sensible heat flux into the urban atmosphere (KUTTLER 2011). These materials reduce also the heat transport from the surface into the ground or wall at direct sun exposure. Thus, the sensible heat flux and heat storage are reduced resulting in a general air temperature reduction if applied on city scale.

A review of measurements and simulation studies was given by SANTAMOURIS (2013) and serves as a basis for classification according to the physical contribution of albedo and emissivity. Whilst the influence of reflectivity on surface temperatures is significant for daytime, emissivity is important for the nocturnal temperature depression. Temperature

differences between black ($a = 0.03$) and white ($a = 0.45$) asphalt surfaces are reported to reach 12 K during daytime (SANTAMOURIS 2013). Even though peak surface-temperature reduction is documented to be high, the general contribution on hazard reduction is limited, as the effect is highest for open spaces exposed to direct radiation. Furthermore, increased reflectivity (albedo) increases the heat input on the nearby individual and dwellings during daytime due to the reflected radiation. Nonetheless, the general temperature reduction reduces the flow into the thermal storage and therefore reduces also night-time temperatures. In addition to the reflective characteristics, the pavers can be constructed to be porous or the pavement geometry can be designed to store water at the surface (NEHLS et al. 2015). Both characteristics would add the cooling effect of evaporation if water is available. This effect can turn into a disadvantage when the evaporation leads to high air humidities in the surface near atmosphere (2 m) where pedestrians regularly suffer from high sultriness after summer rainfall events. Considering these effects, the overall outdoor and indoor hazard reduction potential is considered to be low (+) with its effectiveness depending on water availability in the pavement. The performance of cool pavements can be maintained also during hazardous conditions (+).

Urban green

This countermeasure encompasses high (trees) and low vegetation (lawn, bushes). Urban green modifies the urban atmosphere through evapotranspiration, shading and photosynthetic energy conversion. These processes reduce the energy flux into the build environment. The theoretical maximum of the photosynthetic conversion efficiency is in the order of 4.6 % for C3-photosynthesis at 30 °C and 380 ppm CO_2 (ZHU et al. 2008). Due to the low efficiency of the conversion process, this effect can be considered to be negligible in terms of hazard reduction. Evapotranspiration reduces the surface temperature of leaves (MEIER and SCHERER 2012) and the temperature of surfaces beneath trees. Low moisture availability and predominately impervious surfaces reduce the evapotranspirative effect in areas with high-rise buildings (KOTTHAUS and GRIMMOND 2014) and during heat waves (COUTTS et al. 2013). On average, the cooling effect of parks compared to urban surroundings is about 0.9 K during day and 1.2 K during night as reviewed by BOWLER et al. (2010). However, strength of cooling effects varies largely (SKOULIKA et al. 2014). The simulations for the city of Berlin of SCHUBERT and GROSSMAN-CLARKE (2013) show an air temperature reduction during extreme heat events of up to 0.5 K for an increase of the natural surface fraction by 15 %.

Some studies highlight the relevance of shading rather than evapotranspiration (GROSS 2012, SANEINEJAD et al. 2014). Therefore, it is useful to differentiate the hazard reduction potential for high and low vegetation. The highest hazard reduction potential (++) can be attributed to a reduction of direct short-wave radiation by the shading effect of high vegetation (SHASHUA-BAR et al. 2011). It is considered to be low (+) for the low vegetation as the net energy flux is not significantly reduced. Shading can reduce both indoor (MORAKINYO et al. 2013) and outdoor heat-stress hazards (SHASHUA-BAR et al. 2011, GROSS 2012, BERRY et al. 2013, SANEINEJAD et al. 2014). High vegetation can reduce ventilation and trap long-wave radiation during the night and such curtails its hazard reduction potential. Furthermore, urban green cannot be established everywhere in the city due to a lack of available ground area and

a high use concurrence in inner city quarters, where urban green would be most important. Moreover, evapotranspiration increases atmospheric water vapour and relative humidity, which weakens the cooling effect for the human body, as the thermoregulation via sweat evaporation is reduced. However, epidemiological studies on the effect of humidity on mortality show no clear trend (BRAGA et al. 2002). Water scarcity and drought reduce the evapotranspirative effect of urban green especially during heat waves (COUTTS et al. 2013) and lowers its indoor hazard reduction potential to a low level (+) for high vegetation (trees) and to a negligible level (0) for low vegetation.

Cool roofs

The outdoor hazard reduction potential of cool roofs is comparable to the implementation of cool pavements. However, the influence on the street level can be considered to be negligible for high rise buildings (SANTAMOURIS 2014). In a meta-study of SANTAMOURIS (2014) an ambient temperature reduction in the range of 0.3 K per 0.1 increase in overall albedo is calculated. KRAYENHOFF and VOOGT (2010) modelled the impact of this countermeasure and their review suggests that a 0.10 average increase in urban albedo (equivalent to a 0.40 roof albedo increase for a roof area plan fraction of 0.25) will generate a peak daytime air temperature reduction on the order of 0.5 K for typical clear-sky mid-latitude summer conditions. Overall, the ambient air temperature reduction can be considered to be low (+). However, the application of cool materials at the roof or facade surface also has a direct effect on the indoors: reduced indoor temperatures for non-conditioned buildings or a reduced cooling demand in air-conditioned buildings. Exemplarily, an average decrease in indoor air temperatures of about 8 K for the non-insulated attic of a roof painted with cool colour compared to the blank asphalt roof was reported (BOZONNET et al. 2011). The adjacent top-floor room still benefited by an average 0.7 K decrease in indoor air temperatures. Obviously, the indoor temperature reduction is greatest in the top-floor apartments which impose also the highest hazard potential. However, the effect is reduced for new buildings with improved insulation standards. The adaptive effect is maintained during heat-waves (+).

Green roofs and green facades

The outdoor hazard reduction potential of extensive, meaning not irrigated green roofs and green facades is comparable to the implementation of urban green. The effects of actively managed systems like irrigated green roofs and irrigated facade greening add a higher evapotranspirative cooling to the anyway given shading effect. Obviously, the indoor hazard reduction potential is higher. However, for green roofs a separate discussion of the contribution of insulation, evapotranspiration and shading is often missing in comparative studies and the main effect might often be contributed to a change of insulation (SANTAMOURIS 2014), which is not considered in this evaluation. Comparing green roofs to cool roofs, the former can often not compensate the reflective advantage of cool roofs by latent heat rejection (SANTAMOURIS 2014). Furthermore, the cooling effect of evaporation on green roofs can also be obtained within a non-vegetated drainage layer and its performance is limited during hazardous conditions if irrigation is a problem or if the

drainage layer is dry (SAVI et al. 2013). Therefore, the hazard reduction potential is considered to be low (+), indoors and outdoors. The effect of the greened roof on the street level is negligible in areas with medium and high rise buildings (CHEN et al. 2009).

Observations of mean radiant temperature in front of a building facade in Berlin reveal that facade greening contributes only slightly to a reduction of heat-stress hazards outdoors (JÄNICKE et al. 2015). HOELSCHER et al. (2015) separated cooling effects of vertical facade greening through transpiration and shading in an experimental study. Surface temperatures of the building walls were decreased by the greening up to 15.5 K for the exterior side and up to 1.7 K for interior side. The measurements have shown that facade greening is effective on indoor temperatures during nighttime, which can be predominantly attributed to the shading effect during the day. Only a lower proportion was due to transpiration. However, the actual effectiveness is highly dependent on the thermal design of and thermal retardation in the adjacent walls. The nightly heat loss by long-wave emittance and convective heat flux from the walls may be reduced by an insulating effect of the leaf layer, which depends on the vegetation density and greening design (HOELSCHER et al. 2015). Thus, the overall potential to reduce the hazard indoors and outdoors is low (+).

Passive cooling

Passive cooling covers all processes of heat control and dissipation without or only with minor usage of energy (GIVONI 1994). Following this general definition, all countermeasures to UHI which focus on the microclimate can be considered as passive cooling strategies. However, within this section only measures which can be influenced by the user on the room scale are addressed, namely solar control and night ventilation. The effect of these measures on the outdoor climate can be considered to be neutral (0), as the energy fluxes remain within the urban microclimate. Insulation, solar control and ventilation techniques were evaluated in a simulation study for typical end and mid terrace houses in Greater London, UK for different occupancy profiles (PORRITT et al. 2012). In general, preventive techniques are much more efficient than dissipation of the heat into the microclimate. The reduction of solar gains is most important and can be realised with overhangs, shutters, blinds or curtains. Shading elements at the external side of the room, such as shutters, are more effective (++) than internal shading elements (+), such as curtains, as the absorbed heat is partially released at the shading element. However, orientation of the room and occupant behaviour are often more influential (MAVROGIANNI et al. 2012, PORRITT et al. 2012). Night ventilation is documented to have a high potential for temperature reduction (++) (SANTAMOURIS et al. 2010, PORRITT et al. 2012). However, during hazardous conditions its effectiveness is limited (+), as the diurnal driving potentials (wind, temperature difference) are often not pronounced.

Active cooling

Active cooling measures, namely all types of air-conditioning, are effective, as these provide a comfortable indoor climate (+++), albeit at the cost of electrical or thermal energy. In most cases electrically driven vapour compression systems are installed either in centralised or decentralised form. Thermally driven systems are predominantly used in centralised systems and if (low-grade) heat is available. While all these systems improve the indoor climate, the heat rejection increases outdoor ambient temperatures (−). The systems are dependent on energy, either electricity or heat, which is a possible means for reduced effectiveness during heat waves, as the system efficiency is reduced and power shortages are more probable. However, the stability of the underlying electricity network is not under consideration in this study and the effectiveness of the cooling systems is considered to be maintained also during heat waves (+++).

Evaporative cooling has a positive cooling effect, especially at dry outdoor conditions, however, its effectiveness is highly dependent on the outdoor climate. Therefore, its indoor hazard reduction potential is considered to be at a medium level (++). Despite the released humidity, its effect on the outdoor hazard is considered to be neutral (0). Effectiveness is reduced at humid outdoor conditions and might be effected by water shortages during heat waves. However, the spatially confined use of water can be seen as being superior to the use of the same amount of water in the outdoor environment for urban green, keeping the hazard reduction potential at a medium level (++).

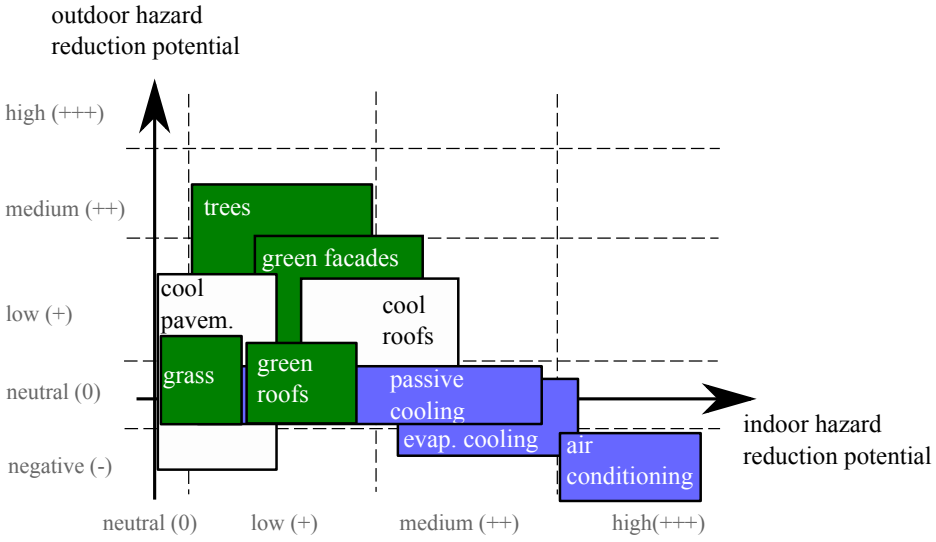

Fig. 5.7 Hazard reduction potential of countermeasures to UHI and active and passive cooling measures on the room scale.

Comparison

The qualitative contribution of the different countermeasures on the hazard reduction is represented in figure 5.7. The classification levels for outdoor hazard reduction potential and indoor hazard reduction during heat waves of table 5.1 is used. Further positioning between the measures is based on the above qualitative evaluation.

It can be seen that measures focussing on attenuation or reflection of short-wave radiation perform best outdoors. Trees thus impose the highest hazard (and risk) reduction potential outdoors. If they are placed in vicinity of the buildings, it can also have a significant effect on the indoors. However, the effect of measures at the building scale, facade greening and cool roofs, is higher. Air-conditioning has the best hazard reduction potential indoors, however, at the cost of deteriorated outdoor conditions. Passive cooling and evaporative cooling also has a significant hazard reduction potential indoors, without deteriorated outdoor conditions.

5.3.4 Risk reduction potential

The effect of the hazard reduction potential of the adaptation measures on mortality is evaluated for the group of persons aged 66 and older in Berlin. The functional interrelation of hazard and risk and the parametrised building model as derived in Section 5.3 are used. The analysis is restricted to the influence of air temperature as this can be considered to be the most influential climate variable. The influence is modelled with a general offset of ΔT on the given time-series of ambient air temperature for the years 2001 to 2010. This temperature difference can be interpreted as being determined by either climate change or by implemented countermeasures.

Rising ambient air temperature has a progressive influence on mortality. The influence on the relative change in the heat-related number of deaths (age group 65+) is calculated for a risk function as determined from the risk data (threshold temperature 29 °C). The heat-related number of deaths is calculated from the risk data with the modified time-series of the weather and the population at the end of 2010 as presented in the above sections. It is related to the heat-related number of deaths calculated with the original weather and the population at the end of 2010 (45.7 ± 5.3 deaths / year). Results are presented in figure 5.8. Additionally, several development paths of countermeasures A to E are given.

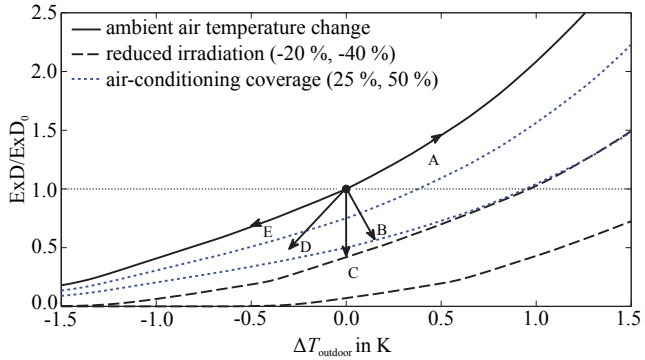

Fig. 5.8 Relative change in number of heat-related excess deaths (ExD) for changing outdoor temperatures for the age group 65+ in Berlin, Germany with ExD 0 calculated for the decade 2001 to 2010. Exemplary, qualitative development paths for (A) increasing ambient air temperature, (B) increasing fraction of air-conditioning, (C) increasing fraction of passive cooling measures on the room level, (D) increasing share of vertical green in the vicinity of buildings and (E) decreasing ambient air temperatures.

Several studies have projected a climate-change induces increase in ambient air temperatures. The ENSEMBLES-project reported on a shifting probability density function with a mean off- set of about 1 K for the summer months for the projection period 2021 to 2050 compared to the reference period 1961 to 1990 for the Berlin region (DÉQUÉ 2009). A 1.8 to 2.3 K increase in mean annual temperatures for scenarios A1B and B1 (IPCC) calculated with a regional downscaling model (WETTREG) was reported for Germany for the projection period 2071 to 2100 (WERNER and GERSTENGARBE 2007). The analysis yields that an increase by 0.5 K in ambient temperatures increases the number of heat-related deaths by 46 % (development A), whilst at 1 K it is doubled, at 1.5 K it is tripled and at 2.0 K it is quadrupled. This progressive behaviour is driven by more days exceeding the threshold temperature and by the linearly increasing risk magnitude above the threshold temperature (see Fig. 5.4). Given these findings it is obvious that rising temperatures, either by increasing UHI effect or climate change will result in rising risks and adaptation and mitigation strategies have to be evaluated in scope of increasing regional temperatures.

Considering the countermeasures, a 50 % fraction of buildings with air-conditioning or a reduction of effective irradiation by 20 % will stabilise the number of excess deaths at the same level even at a 1 K increase in ambient air temperatures. If air-conditioning coverage is increasing to 50 % of the buildings this will result in a slight increase in outdoor temperatures indicated by development path B. The projected change in relative excess deaths for this path accounts to a decrease by 44 %. Applying passive cooling on the building scale (development path C) has a neutral impact on the ambient climate. A reduction of the effective irradiation by 20 % is projected to reduce the number of excess deaths by 58 %. The risk development with measures that additionally have an impact on the outdoor climate, such as trees or cool roofs, is depicted with path D with a risk reduction of 52 %. Heat-related mortality reduction by 32 % is possible if the ambient temperature is lowered by 0.5 K only (development path E). This might be accomplished by measures which only affect outdoor air temperatures, such as cool pavements or urban green. It is noteworthy that measures reducing the effective radiation on the buildings by about 40 % allow for a quasi-elimination of the heat-related mortality under present conditions. This is equivalent to the effect of a mean ambient air temperature reduction of 2 K.

5.4 Discussion

5.4.1 Countermeasures to UHI and risk reduction

Following the risk concept of this paper, the highest hazard (and risk) reduction potential for urgent heat-risks, such as mortality, lies in the indoor environment. Classical UHI countermeasures focussing on the urban scale often do only have a marginal direct effect on the indoor climate. Of course, the outdoor environment is an important driver with outdoor temperatures being the most discussed climate variable in UHI research. However, the actual risk reduction potential of measures which predominantly influence the outdoor air

temperature (cool pavements, grass areas, etc.) can be considered to be small as the cooling effect is spatially confined (BOWLER et al. 2010). This study suggests that measures on the building level, cool roofs, green facades or nearby trees have the highest potential on the indoor environment. However, direct measures on the room scale, either passive or active, have a larger effect and are favourable if decisions on measures have to be exclusive. The indoor based risk concept estimates a lower hazard reduction potential to urban green, as the indoor climate is not directly affected and evapotranspiration is limited during hazardous conditions. Only if directly installed in the vicinity of dwellings (facade greening or trees) a risk reduction for the inhabitants can be maintained by shading effects.

The absolute risk reduction potential has to be discussed in relation to the fraction of air-conditioning. It was shown that the approximation of the linear influence of the fraction of air-conditioned buildings can explain the risk reduction in the given data. However, reliable data on the distribution of air-conditioning are often not available. Furthermore, the linear approach neglects the underlying adaptive behaviour driving air-conditioning installations. At low levels of a the installation of air-conditioning equipment is directly focussed on the temperature reduction in overheated rooms, whilst at highly saturated levels, accessibility to air-conditioning is determined by the socio-economic status (O'NEILL et al. 2005). Therefore, the overall risk-magnitude will possibly decrease with larger slope at small fractions of air-conditioning and with flattening slope at saturated regions. In many U.S. cities, the fraction of air-conditioning is already very high and absolute heat-related risks are low (DAVIS et al. 2003). Under such conditions, mitigation strategies have to directly address the remaining groups at risk, often homeless or socially poor classes which cannot afford air-conditioning (HARLAN et al. 2006). In these cases, special focus has to be put on the education of these groups. Furthermore, it is necessary to identify the buildings with the most hazardous indoor climates by research on the spatial indoor climate distribution within a city (SMARGIASSI et al. 2008).

Personal adaptation, both physically and psychologically, is evidently an important factor and has to be considered. Physical adaptation covers variation of clothing, changes in activity levels and choice of exposure to specific environments. Psychological adaptation is documented to depend on recent experience, expectations and degree of freedom to expose oneself to a certain climate condition (BRAGER and DE DEAR 1998, NIKOLOPOULOU and LYKOUDIS 2006). The adaptation potential is higher outdoors as there normally exist many possibilities to change between spaces of different climate conditions. Indoors, the physical and psychological adaptation potential is limited and highly dependent on the thermal quality of the building and possibilities to influence overheating. Thus, the evaluation of specific countermeasures on the outdoor climate has to focus on the activity and adaptation patterns of the persons at risk. For instance, cool pavements might increase the overall heat flux to the human body during sunny days due to the reflected short-wave radiation which promotes heat-stress despite decreased surface temperatures. But such places can be avoided during daytime and impose reduced hazards during the evening hours due to the lower surface temperatures and less stored energy. Due to the reduced net heat flux into the city, an additional positive net effect on the indoors can be expected.

SCHUSTER and LAKES (2014) investigated the perception of heat in the urban population in a cross-sectional household survey. Individual physical constitution, mainly determined by health status and physical fitness, was identified as major determinant of individual vulnerability and the authors identified active mobility concepts (walking, cycling) as highly effective adaptation (and mitigation) strategies. As the metabolic rate is higher e.g. for cyclists and attractiveness of the transport routes is essential for transition from passive vehicle based mobility to sustainable mobility (BANISTER 2008), it is necessary to focus on the climate conditions along main transportation routes. Shading by trees or canopies along with greened areas have a hazard reducing effect and can additionally encourage shifting from passive to active mobility by increased climatic attractiveness.

Combined adaptation on all scales, on the building scale with passive building design and on the micro-climate scale, might be a useful alternative to adaptation by air-conditioning. However, the effective potential is dependent on the actual climate and existing building design. At the city level, the increase in outdoor air temperature due to air conditioning might be in the same order of magnitude as the reduction potential of UHI countermeasures. Therefore, to reduce heat-related risks efficiently it is essential to support UHI countermeasures and passive cooling especially in regions where air-conditioning is not yet common practice. A combined mitigation strategy implementing outdoor measures and supporting passive cooling might maintain indoor temperatures below hazardous thresholds.

The design of urban spaces on the basis of microclimate studies with bioclimatic evaluation of comfort is intended to foster the social interaction and life during normal summer conditions and extreme conditions are often out of focus. Obviously, at extreme conditions people can easily adapt outdoors by avoiding these places. However, it is necessary to quantify the effect of the countermeasures on the indoors also at extreme condition to implement efficient strategies.

Finally, it has to be mentioned that additional positive and negative feedback has to be weighted before implementation. In many mid-latitude cities the cold-related number of deaths often exceeds the heat-related number (LI et al. 2013, GASPARRINI et al. 2015). Thus, a thorough analysis has to address the impact on the winter-season risks also. Obviously, the application of the indoor risk concept with indoor temperatures will fail under these conditions, as the elevated winter mortality cannot be explained with the constant indoor temperatures. For heat-related mortality, direct effects on the respiratory system are probably more important, while for cold-related mortality, analysis yielded evidence of indirect effects involving increased incidence of influenza and other respiratory infections (KUNST et al. 1993). Furthermore, implications on water run-off management, energy consumption or urban biodiversity as well as cost effectiveness have to be balanced in a sound management process (O'NEILL et al. 2003).

5.4.2 Further research topics

The qualitative analysis has shown that the physical interpretation of the energy fluxes is important to evaluate and compare different measures. However, research on specific measures often only documents the resulting effect: temperature reduction. A differentiation in the energetic fluxes (irradiation, radiative emission, evapotranspiration, storage) is essential to quantify their impact on micro- and building scale and foster comparability of the measurements.

The analysis has shown that it is important to include the exposure and adaptation patterns of the persons at risk and the design of urban microclimate has to address the underlying activity patterns. Projections on the development of heat-related health risks in a changing climate often exclude the adaptation of the individuals. To make projections more reliable, research has to address the underlying decision making on the individual level and quantify climatic thresholds which trigger adaptive measures, e.g. the installation of air-conditioning.

The paper has focussed on indoor air temperature as predictive hazard variable. It is well known that temperature is the predominant variable to describe heat-stress indoors, however, bioclimatic indices which are based on the thermoregulation and adaptation of the human body possibly increase the quality of the risk concept. Considering that the reference ambient temperature is measured at Tempelhof weather station, at the former airport area, which does not necessarily include the UHI effect (SCHERER et al. 2014) the effective threshold temperatures might be even shifted by the mean UHI island intensity. To allow for a concise implementation of bioclimatic indices, their applicability on the indoor climate and their validity for the groups under consideration has to be assured.

5.5 Conclusions

This study presents a risk concept, which differentiates between heat-stress hazards within indoor and outdoor environments. It is shown that a separate focus on indoor and outdoor hazards is necessary to discuss efficient mitigation strategies and evaluate risk reduction potentials.

Indoor hazards can be calculated from the outdoor climate with a simple building model. The analysis has shown that it is important to parametrise the building with a representative time constant τ. Uncertainties in the parameter λ, which covers the temperature elevation due to solar irradiation, can be compensated with a change in the threshold temperature of the risk assessment. Mortality data from Berlin, Germany for the age group 65+ were evaluated with calculated indoor temperatures from the building model. The analysis has shown that the relative risk increases progressively with rising temperatures and doubles approximately with each 1 K increase in ambient temperature. Considering the reduction potential indoors, it is necessary to focus on the air-conditioning coverage. For cities in which air-conditioning coverage is saturated, the risk reduction potential by UHI countermeasures is negligible. For cities in which air-conditioning coverage is low, classic

UHI countermeasures and passive cooling measures on the building level are more effective. Especially shading measures and cool roofs, might be sufficient to reduce overheating and an associated increase in indoor based risks.

A future diffusion of air-conditioning will decrease risks. At the same time additional energy consumption should be avoided. So, also air-conditioning should be avoided or based on regenerative sources if possible. Therefore, the implementation of passive measures on the room level should be a major focus of urban planning and policy. Possibly only a combination of a rigorous passively cooled building design and countermeasures on the urban scale will keep indoor temperatures below critical thresholds.

Acknowledgments

This study is funded by Deutsche Forschungsgemeinschaft (German Research Foundation) with research grant: DFG 1736 “urban climate and heat stress in mid-latitude cities in view of climate change (UCaHS)” (www.UCaHS.org) under codes SCHE 750/8-1, SCHE 750/9-1, WE1125/30-1 and ZI 524/9-1. We thank the members of the research group for enriching discussions.

6 Outlook: modelling evapotranspiration of urban facade greening

6.1 Introduction

Evapotranspiration (*ET*) or rather transpiration measurements (e.g. by lysimeters or sap flow techniques) are usually laborious and associated with high purchase and installation costs. In addition, the prediction of water demand and the transferability to other locations is limited due to the complexity of individual ecosystems and the different meteorological conditions. Processed-based prediction models such as PENMAN-MONTEITH are often applied for conventional plant stands such as agricultural crops or forests. Their suitability for the description of urban facade greenings' evapotranspiration not discussed so far.

The grass reference evapotranspiration of the FAO (Food and Agriculture Organization of the United Nations) is recommended as an international, uniform standard and can be easily calculated from meteorological data (global radiation, *RH*, T_{air} and wind speed). It is derived from the process-based PENMAN-MONTEITH equation but is independent of water resources and crop. The equation describes the potential evapotranspiration (ET_0) of a defined reference surface covered with grass (ALLEN et al. 1998). It is often applied using correction factors (= crop coefficients, K_c) for other plant species with their special water consumption (ASCE-EWRI 2005). Thus, the grass reference evapotranspiration could be also useful for a process-based modelling on the transpiration of facade greenings.

In this outlook, (i) *ET* of a typical urban facade greening with *Fallopia baldschuanica* is determined by lysimeter measurements and compared with results, calculated by the grass reference evapotranspiration. Furthermore, (ii) first simple relationships (like K_c) are derived.

6.2 Materials and methods

6.2.1 Site and plant species

In order to determine transpiration rates of urban facade greenings, measurements were carried out during the vegetation period 2014 (March until October) at a west exposed building wall, centrally located in Berlin, Germany (lat. 52°51' N, long. 13°32' E). The investigated facade was greened with *F. baldschuanica* (for further details see 3.2.2 (c) and 4.2.3).

Transpiration rates were calculated based on wall area (WA). Seasonal variations of the wall surface coverage were determined by photographs.

6.2.2 Measuring *ET* and meteorological parameters

In order to measure *ET* of the climbing plants, a new and modified lysimeter system was developed (SCHWARZER 2015). Thereby, maximum evaporation rate from the substrate was 0.013 L h^{-1} (SCHWARZER 2015) and negligible in relation to transpiration rates of the climbing plants. A briefly description of the measurement setup is given in the general introduction (see 1.4.2 and Fig. 1.4) and in chapter 4 (see 4.2.3).

Meteorological measuring stations were installed in front of the greened facade in a height of about 3 m. Thereby, the measuring height differs slightly from the requirements of the grass reference equation. T_{air}, *RH*, incoming short-wave radiation reaching the facade, wind speed (see 4.2.3) as well as incoming and outgoing long-wave radiation (RA01 radiometer, Hukseflux Thermal Sensors B.V., the Netherlands) were measured in 5 min intervals.

6.2.3 Calculation of the grass reference evapotranspiration

The grass reference evapotranspiration was calculated using the standardised equation proposed by the ASCE (American Society of Civil Engineers) which allows calculations for varying time steps (see C_n and C_d) (ASCE-EWRI 2005):

$$ET_0 = \frac{0.408 * \Delta * (R_n - G) + \gamma \frac{C_n}{T_{air} + 273} * u_2 (e_s - e_a)}{\Delta + \gamma * (1 + C_d * u_2)}, \qquad \text{(eq. 6.1)}$$

where:

ET_0 is the standardised reference crop evapotranspiration for short surfaces in daily (mm d^{-1}) or hourly (mm h^{-1}) time steps,

R_n is the mean daily or hourly net radiation at crop surface (MJ m^{-2} d^{-1}) or (MJ m^{-2} h^{-1}),

G is the soil heat flux density (MJ m^{-2} d^{-1}) or (MJ m^{-2} h^{-1}),

T_{air} is the mean daily or hourly air temperature at 1.5 to 2.5 m height (°C),

u_2 is the mean daily or hourly wind speed at 2 m height (m s^{-1}),

e_s is the mean saturation vapour pressure at 1.5 to 2.5 m height (kPa),

e_a is the mean actual vapour pressure at 1.5 to 2.5 m height (kPa),

Δ is the mean slope of saturation vapour pressure-temperature curve (kPa K^{-1}),

γ is the psychrometric constant (kPa K^{-1}),

C_n is a numerator constant that considers time step and aerodynamic roughness of the surface; it was 900 for daily (K mm s^3 Mg^{-1} d^{-1}) and 37 for hourly (K mm s^3 Mg^{-1} h^{-1}) time steps,

C_d is a denominator constant that considers time step, bulk surface resistance and aerodynamic resistance (s m^{-1}); it was 0.34 for daily and 0.24 (daytime, $R_n > 0$) or 0.96 (nighttime) for hourly time steps and

408 is a conversion factor to get equivalent evapotranspiration from energy fluxes (m^2 mm MJ^{-1}).

The reference crop corresponds to an adequately watered grass surface with a height of 0.12 m, an albedo of 0.23, an aerodynamic resistance of 208 u_2^{-1} and a minimal surface resistance of 70 s m^{-1} (ALLEN et al. 1998). In this case, it refers to one square meter WA.

For the calculation of ET_0, half-hourly and daily resolutions were used. According to FANK (2007), short time steps of up to 10 minutes are useful to compare lysimeter data with calculations by the ASCE equation.

Due to the small magnitude of the daily soil heat flux beneath a vegetated grass surface, G is ignored in daily calculations (ALLEN et al. 1998). For shorter time periods, however, G correlates well with R_n and can be calculated as a fraction of it (ALLEN et al. 1998, ASCE-EWRI 2005):

$$G_{day} = 0.1 * R_n \quad \text{for day-time and} \quad \text{(eq. 6.2)}$$

$$G_{night} = 0.5 * R_n \quad \text{for night-time periods.} \quad \text{(eq. 6.3)}$$

6.3 Results and discussion

6.3.1 Diurnal variation

Mean meteorological conditions in front of the greened facade are exemplarily shown for July, the hottest month in the year 2014 with mean T_{air} of 22.8 °C (Fig. 6.1 a). This month had 28 summer days ($T_{max} \geq 25$ °C), including 21 hot days ($T_{max} \geq 30$ °C). Highest T_{air} in front of the greened wall of 39.5 °C was measured.

The diurnal cycle of the measured *ET* (lysimeters) was greatly influenced by the meteorological conditions (Fig. 6.1 a and b). It was highest with up to 4.5 L d^{-1} m^{-2} per WA in the afternoon between 15:00 and 15:30. At that time, also incoming short-wave radiation (433.4 W m^{-2}), outgoing long-wave radiation (453.0 W m^{-2}), T_{air} (29.3 °C) and wind speed (0.6 m s^{-1}) were highest, while *RH* was lowest (42.4 %). Evapotranspiration also took place during the whole night (average 0.7 L d^{-1} m^{-2} per WA) when no short-wave radiation reached the facade, but *VPD* of the ambient air is still high (≥ 3.8 hPa). Evapotranspiration during nighttime also occurred during all other months (data not shown).

Moreover, fluctuations in the diurnal cycle of *ET* are visible that cannot be explained by meteorological factors. They were caused by the performance of the pump, which irrigated the plants. The pump performance depends on the fill level of the water reservoir (SCHWARZER 2015). The fluctuations were higher in periods with high evapotranspiration. It was not possible to eliminate them completely with a filter and they restricted the temporal resolution of *ET*.

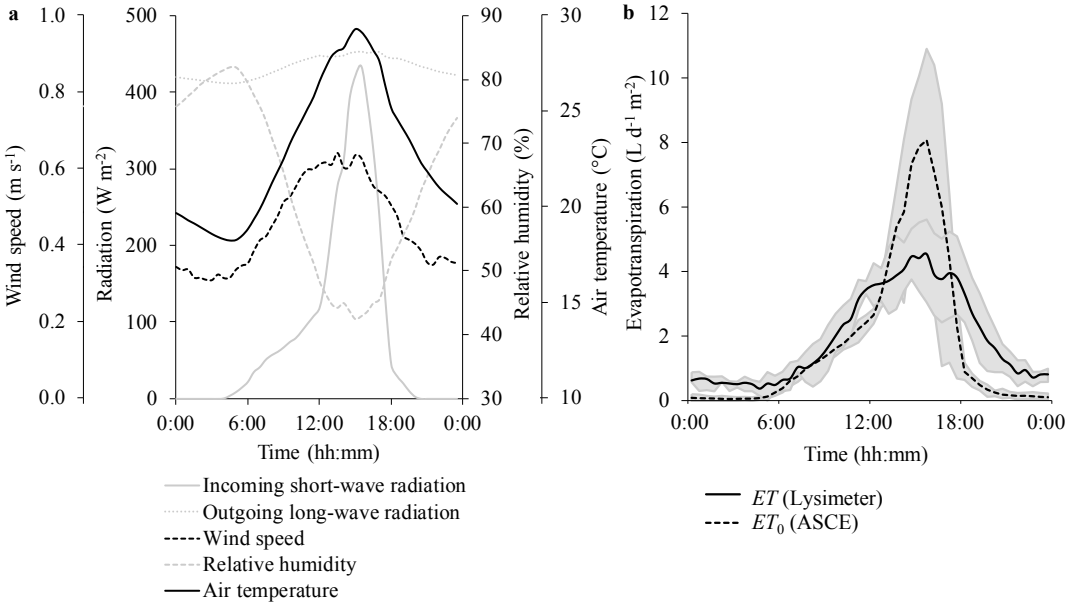

Fig. 6.1 a) Mean meteorological conditions in front of a greened wall in July 2014. b) Mean diurnal evapotranspiration per m^2 wall area in July 2014 determined by lysimetry (*ET*) (*Fallopia baldschuanica*) and calculated by the ASCE grass reference evapotranspiration (ET_0). The grey area indicates the range between the 25th and 75th percentiles. All results are for a west exposed facade in Berlin, Germany.

Furthermore, figure 6.1 b shows the diurnal cycle of ET_0, calculated by the ASCE grass reference equation which differs from the lysimeters measurements. It was mainly influenced by the incoming short-wave radiation and also highest in the afternoon, but clearly overestimated the measured transpiration by up to 80 % at that time (8.1 L d^{-1} m^{-2} per WA). The LAI of both plants were very similar and probable not the reason for these differences: 3.0 for *Fallopia* (calculated at the end of September, see 3.2.2) and 2.9 for grass (24 x h, h = 0.12 = height in m, according to ALLEN et al. 1998). An alternative explanation is that leaf water stress increases with the vegetation height due to gravitation and path length resistance (= hydraulic limitation hypothesis, HLH) (RYAN and YODER 1997). That would mean that higher parts of the facade greening actually evapotranspirate less than theoretically calculated by the grass reference equation. The HLH is mainly investigated for high trees (RYAN et al. 2006), but less for other plant groups (e.g. CAO et al. 2012 for grasses).

Best correspondences between measurements and calculation were in the morning between 6:30 and 12:30. In the late afternoon, when the incoming short-wave radiation strongly decreased, also ET_0 strongly decreased while *ET* measured with the lysimeter is still considerable. One reason could be the varying lighting situation at the building facade during

that time. Whereas the lower parts of the facade greening and also the meteorological measuring instruments are already shaded by a facing building, the upper parts of the greenery are still directly illuminated (Fig. 6.2 a-c).

During the night, calculated ET_0 is about zero and therefore the actual evapotranspiration is underestimated. The impact of the outgoing long-wave radiation from the wall is maybe higher than calculated in the grass reference formula.

a

b

c

Fig. 6.2 Lighting situation at the west exposed building facade on the 15th July 2014 at about a) 17:40, b) 18:10 and c) 18:40. Lower parts of the wall are shaded by a facing building while the upper parts are still directly illuminated.

Altogether, on a daily basis, measurements in July were slightly higher (2.0 L d^{-1} m^{-2} per WA) than the calculated values (1.8 L d^{-1} m^{-2} per WA). Calculations consequently underestimate the evapotranspiration by about 8.4 %.

6.3.2 Daily values

Measured *ET* in August was 2.0 L d^{-1} m^{-2} per WA on average which results in an overall water consumption of approximately 50 L m^{-2} for the 25 evaluated days (Fig. 6.3). However, calculations with the help of the grass reference equation are clearly lower and therefore underestimate the actual evapotranspiration. Summation curve of ET_0, calculated with daily values, results in only 30.8 L m^{-2} which is 38.0 % less than the measurements. Calculations with a half hourly resolution are more precise (34.4 %).

Interestingly, while the measurements of *ET* were on average the same for July and August (about 2.0 L d^{-1} m^{-2} per WA), calculations of ET_0 were very different (1.8 and 1.2 L d^{-1} m^{-2}). The reasons are the different meteorological conditions (mainly radiation) in both months which are included in the calculations. On average, incoming short-wave radiation in August was 22.5 % (1,749,825 J d^{-1} m^{-2}) less than in July. This indicates that the maximum water conductivity of *F. baldschuanica* was probably reached in hot times of the day and is a further explanation for the overestimation of calculated ET_0 in the afternoons.

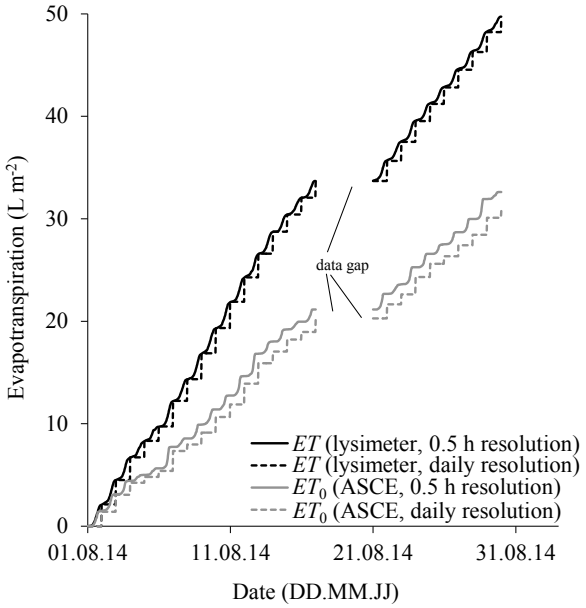

Fig. 6.3 Cumulative evapotranspiration per m^2 wall area in August 2014 determined by lysimetry (*Fallopia baldschuanica*) and calculated by the ASCE grass reference evapotranspiration (ET_0). All results are for a west exposed facade in Berlin, Germany.

Calculated evapotranspiration is plotted against measured evapotranspiration from lysimeter data (Fig. 6.4). With a linear regression of both data sets, a first calibration function has been derived. It resulted in a calibration factor ("K_c") of around 1.25 or a mean underestimation in the calculations of 25 %, respectively. With the help of this factor, it is possible to calculate and assess *ET* for other urban facades greened with *F. baldschuanica*. For the first time, results can be transferred to other locations and climatic conditions. However, the uncertainty of the linear regression is very great ($R^2 = 0.51$) and therefore, further research (e.g. more precise presentation of diurnal cycles of *ET*, see above) is necessary in order to underpin these results.

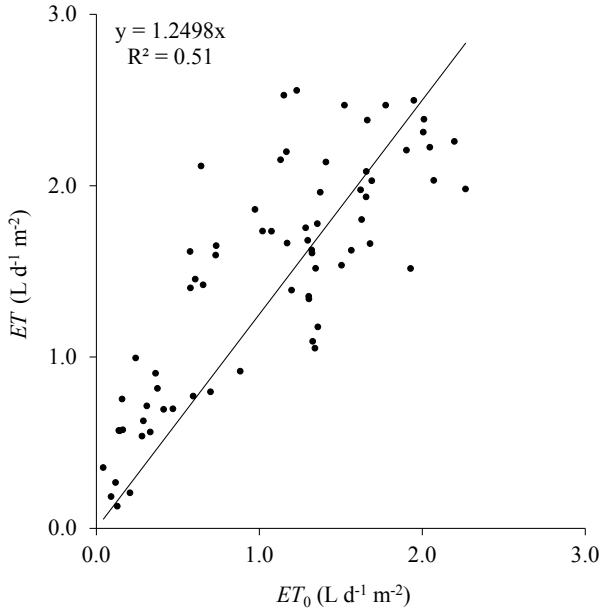

Fig. 6.4 Calibration of the calculated ASCE grass reference evapotranspiration (ET_0) by adaptation to lysimeters measurements with *Fallopia baldschuanica* (*ET*). Points indicate mean daily values per m^2 wall area in the period from June until October 2014 for a west exposed facade in Berlin, Germany (for further details see Tab.A1 in the appendix).

6.4 Conclusions

This outlook demonstrates a first approach towards process-based modelling on evapotranspiration of urban facade greenings. For this purpose, the standardised grass reference evapotranspiration of the ASCE was used and compared with lysimeter measurements.

Diurnal variation of evapotranspiration (*ET*) can be represented with the reference calculation, but with a great uncertainty. Best correspondence to lysimeter data were in the morning while during nighttime and in the afternoon *ET* was clearly underestimated or overestimated, respectively. Altogether, on a daily basis, *ET* is underestimated with the ASCE equation by about 25 %, resulting in a correction factor of 1.25.

For an improved adaptation, further research is needed. A derivation of the lighting situation for the whole facade with a 3D city model (e.g. ecotect), height-dependent *ET* performance as well as different plant species and expositions should be integrated in prediction models for facade greenings.

7 Synthesis

7.1 Transpiration rates and water demand - revisited

Sap flow measurements were applied to determine water demand and transpiration rates of urban climbing plants. Practical applications, however, showed that with the commonly recommended and applied calibration method (night value subtraction, NVS), daily transpiration is underestimated by up to 33 %. Thus, a new calibration approach was developed, which quantifies the calibration baseline with the help of the minimum nocturnal vapour pressure deficits (*VPD*) during the measurement campaign.

A further advantage of the *VPD*-based approach is that it can be retrospectively applied to previously measured data if T_{air} and *RH* were also recorded. Therefore, sap flow data of chapter 3 (see 3.3.4) were newly calibrated with the *VPD* approach (Tab. 7.1).

Tab. 7.1 Mean, maximum and minimum daily transpiration rates of *Parthenocissus tricuspidata* (2nd to 15th August 2013), *Hedera helix* (1st to 6th August 2014) and *Fallopia baldschuanica* (2nd to 15th September 2014) based on leaf area (LA) and wall area (WA). Transpiration rates were derived from sap flow measurements and calibrated with the NVS and the *VPD* approach, respectively; n.a. = not available.

	Per LA ($L\ d^{-1}\ m^{-2}$)		Per WA ($L\ d^{-1}\ m^{-2}$)	
	NVS	*VPD*	NVS	*VPD*
Parthenocissus tricuspidata (n = 14, wall leaf area index (WLAI) = 1.9)				
Daily sap flow				
mean	0.5	0.5	0.9	1.0
maximum	0.7	0.7	1.3	1.3
minimum	0.4	0.4	0.7	0.7
Hedera helix (n = 6, WLAI = 3.0)				
Daily sap flow				
mean	0.5	n.a.	1.6	n.a.
maximum	0.6	n.a.	1.7	n.a.
minimum	0.4	n.a.	1.2	n.a.
Fallopia baldschuanica (n = 14, WLAI = 3.0)				
Daily sap flow				
mean	0.5	0.6	1.4	1.7
maximum	0.8	1.0	2.3	3.0
minimum	0.2	0.3	0.7	0.9

Transpiration was highest for *F. baldschuanica*. Under late summer conditions in September, mean daily transpiration rate was $0.6\ L\ d^{-1}\ m^{-2}$ per unit leaf area (LA) and $1.7\ L\ d^{-1}\ m^{-2}$ per wall area (WA). The lysimeter studies showed that the transpiration rates were even higher in July and August with an average of about $2.0\ L\ d^{-1}\ m^{-2}$ per WA. In contrast for *P. tricuspidata*, the mean transpiration rate in August was only $0.5\ L\ d^{-1}\ m^{-2}$ per

LA. Due to the lower WLAI of *P. tricuspidata*, the differences became still larger per WA: just 1.0 L d^{-1} m^{-2} was consumed. Unfortunately, the *VPD* approach could not be applied for *H. helix* because data base of T_{air} and *RH* was insufficient. However, at least a water amount between 1.2 and 1.7 L d^{-1} m^{-2} per WA is needed on hot days (estimated with the NVS approach). In conclusion, the provided water amount for *F. baldschuanica* must be at least 1.3 times higher as that for *H. helix* and twice as high as for *P. tricuspidata*.

With an assumed facade area of 36 m^2, even for *P. tricuspidata* a water amount of 25.2 to 45.0 L d^{-1} is needed in summer. However, these high amounts of water can be critical on hot days. For instance in summer 2014, it only rained an average of 1.7 L d^{-1} m^{-2} in Berlin (Tempelhof) (DWD 2014). Limited root space, often occurring in urban areas, additionally restricts the water availability.

Water deficits considerably reduced the transpiration during daytime and the cooling effect can even turn into the opposite. Preliminary studies show that a drought-stressed plant had higher leaf temperatures than the ambient air and up to 2.5 °C higher leaf temperatures than a well-watered plant (HOELSCHER 2013). That strongly indicates the need of elaborated water management and irrigation concepts (e.g. usage of rainwater runoff from roofs) for facade greenings to contribute to building cooling and outdoor climate effects.

7.2 Cooling effects of urban facade greenings

7.2.1 Transpiration and shading - revisited

The energy balance given in the introduction was exemplarily calculated for *F. baldschuanica* on a clear late summer day (Fig. 7.1, see also 1.3.2). On this day, about 89 % of the daily incoming short-wave radiation could be retained or reflected by the greening (transmissivity = 0.11). This shading effect depended on the WLAI and changed with the seasons due to leaf-growing and leaf-shedding with a maximum performance from May to October (86 to 89 %). Due to the lower WLAI, it was only 75.3 % for *P. tricuspidata* on a clear hot summer day (2nd August 2013). Furthermore, *F. baldschuanica* cooled the surrounding air through transpiration by -65.6 W m^{-2} (evaporation was negligible), which resulted in less sensible heat. Due to the lower transpiration rates, it was lower for *P. tricuspidata* (-30.0 W m^{-2}).

The newly calibrated transpiration rates of table 7.1 were retrospectively applied to revise the initial statements on the contribution of shading and transpiration on the total cooling effect (see 3.3.3). Figures 7.2 a and b display the initial results as well as the new ones, which are exemplarily shown for *F. baldschuanica* on the previously mentioned clear day and on a cloudy day. Differences to the initially data, indicated by the green colour, were overall small. Highest differences were found for the cloudy day.

The proportion of shading and transpiration on the total cooling effect varied over the course of the day. At night, cooling only depended on transpiration, though it was relatively low. Shading became effective with the first incoming solar radiation and

was highest when also the solar radiation was highest. During that time the total cooling effect accounted for up to 87 % on shading.

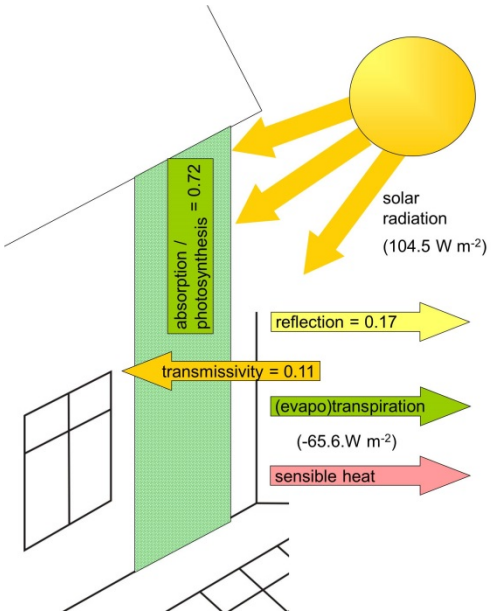

Fig. 7.1 Individual components of the energy balance, exemplarily calculated for a west exposed facade greened with *Fallopia baldschuanica* on a clear late summer day (3rd September 2014).

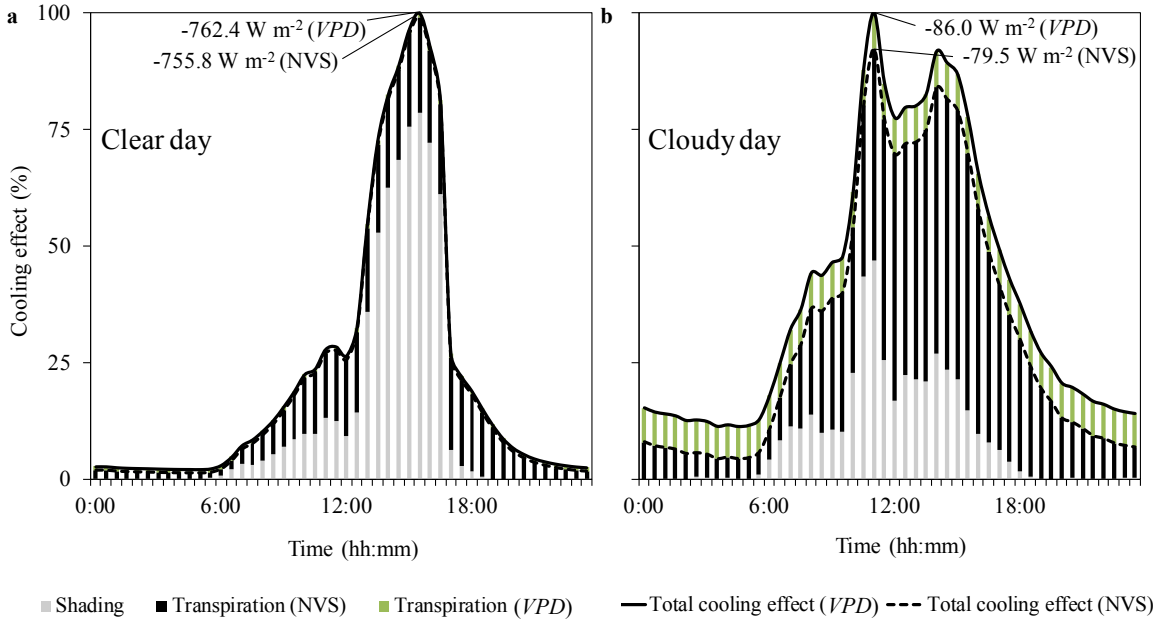

Fig. 7.2 Total cooling effect (transpiration + shading) as well as share of transpiration and shading on this cooling effect for a west exposed facade greened with *Fallopia baldschuanica* on a) a clear late summer day (3rd September 2014) and b) a cloudy day (12th September 2014). Transpiration was estimated by sap flow measurements and calibrated with the NVS approach and the new *VPD* approach, respectively. Values are presented in relation to the maximum cooling effect of the day, estimated with the *VPD* approach.

For the whole day, the provided cooling effect of *P. tricuspidata* also mainly depended on shading, whereas a lower contribution was due to transpiration. The proportions were about 4:1 for hot as well as for colder summer days. For *F. baldschuanica*, transpiration had a clearly higher contribution, which was 42.1 % on a clear day (Fig. 7.1 a), and the same extent as shading for the entire measurement period (3rd to 15th September 2014). The proportion of transpiration was even 78.0 % on a cloudy day, but the total cooling effect was relatively low then with a peak of only -86 W m^{-2} (Fig. 7.1 b). For comparison, a peak cooling effect of -762.4 W m^{-2} was calculated for the clear day.

Whether these differences in the proportions of transpiration and shading were only plant specific or also due to the different irrigation status and meteorological conditions, could not be completely assessed in this dissertation and should be further investigated.

7.2.2 Effect of facade greening on outdoor and indoor climate

Facade greening showed only minor effects on outdoor climate and thus on outdoor heat-stress hazards. No clear differences in the ambient T_{air} were detectable, which was probably caused by density differences of air parcels and consequently mixing air in front of the walls. The effect on the T_{mrt} was weakly pronounced with a reduction of 2 K compared to a bare wall. Although the emitted long-wave radiation was clearly reduced, the impact of a greened facade on T_{mrt} accounts for only 22 % if just one wall of a street canyon or yard is greened. With a facade greening attached to more than one wall or to a whole street canyon, the effect on the outdoor climate would be enlarged.

However, a higher outdoor hazard reduction can be achieved by trees with regard to their additional shading effect by reducing direct short-wave radiation (Fig. 5.7). The assessment of the possibility and the conditions at which trees could serve as a barrier for turbulent exchange should be done. Following the results of the used risk concept, the highest hazard reduction potential for urgent heat stress (e.g. mortality) lies in the indoor environment.

While the observations revealed only slight effects for outdoor heat-stress hazards, the effect for the building was clearly detectable. Surface temperatures of the exterior and the interior side of the building walls were decreased by up to 15.5 K and 1.7 K, respectively. Even though the reduction of the interior wall temperature was not extraordinary high, the results of the risk analysis show that already a mean T_{air} reduction of 0.8 K can reduce the number of heat-related deaths.

Furthermore, facade greening was most effective on indoor temperatures during night-time, which is very relevant for the reduction of nocturnal indoor heat stress. However, the results also show possible disadvantages as nightly heat loss by long-wave emissions and convective heat flux from the greened walls were reduced. This insulation effect was highest for direct green facades with a high WLAI and made up differences of up to 1.6 K compared to the bare exterior wall. It was not detectable for the well ventilated double-skin green facade with an air cavity behind the greening systems and free lateral access.

New, flexible greening designs which could be oriented in parallel during the day and perpendicular to the wall during the night would further support nightly heat losses. The actual effectiveness also depended on the thermal retardation in the adjacent walls. It has to be figured out if it is less or not pronounced for isolated old and new building walls.

Classical countermeasures to UHI focussing on the urban scale (e.g. cool pavements, grass, trees) often have a marginal direct effect on the indoor climate as the cooling effect is spatially limited (BOWLER et al. 2010, Fig. 5.7). The effect of measures on the building level, directly installed in the vicinity of the dwellings, is higher. Thus, facade greening is generally more effective than any other urban vegetation and has up to medium potential to reduce indoor heat-stress hazards. In addition, it is also more effective than the best architectonical practice for a bare wall (light and glossy surfaces with high solar reflectance). Cool roofs, however, revealed a similar reduction potential as facade greenings. They could be a good possibility to combine as they mainly affect the top-floor apartments which usually have the highest hazard potential. Direct countermeasures on the room scale, either passive or active cooling, generally revealed the largest effect on the indoor climate. However, it has to be expected that the heat rejection by active cooling measures (air-conditioning) further increases the outdoor T_{air}. Furthermore, the cooling effect of passive cooling measures, such as shutters or curtains, only depends on shading during daytime. Facade greening additionally reduces sensible heat by transpiration cooling, thus it can be also effective during the night, when the windows are open.

7.3 Outlook and further research: modelling transpiration

The grass reference equation of the FAO was used in this dissertation for a first processed-based modelling on urban facade greenings' transpiration. Diurnal variation of transpiration could be represented with this equation. A calibration with lysimeter data resulted in a correction factor ("crop factor") of 1.25, but these results are subjected to a great uncertainty. Therefore, further research is needed in order to improve the adaptation of such prediction models. This research should include a derivation of the lighting situation for an entire facade with a 3D city model, height-dependent transpiration performance as well as different plant species and expositions.

After an improved adaptation of such prediction models to the situation of urban facade greenings, they should be implemented in simulation tools such as Envi-met, SOLWEIG or RayMan (see chapter 2). Envi-met is the only one of these three simulation tools, which is generally able to simulate transpiration, however, it could not reproduced the actual cooling effect of the investigated facade greening.

7.4 Overall conclusions

This dissertation quantified water demand and cooling effects of facade greenings for the building and the urban street canyon. Facade greenings were compared with other countermeasures and their potential for reducing heat stress hazards was assessed. The following conclusions were derived from the experiments:

- A *new calibration approach for sap flow measurements* was developed, which is comparable to the usually infeasible direct gravimetric determination. After a suitable calibration, sap flow measurements are practicable to determine transpiration rates of urban climbing plants at least on a daily basis.
- Facade greening must be *sufficiently irrigated* in order to realise its maximum cooling performance. Transpiration rates and water demand depend on plant species and climatic conditions. The highest transpiration performance can be achieved by *F. baldschuanica* with up to 3.0 L d^{-1} m^{-2} per WA on hot summer days.
- Cooling effects on summer days *mainly depend on shading, whereas a lower contribution is due to transpiration*. However, the proportion of transpiration can get considerably higher, depending on plant species, water supply and meteorological conditions.
- Facade greening showed only *minor effects on outdoor heat-stress hazards*, but the effect can be enlarged if more than one wall is greened. In contrast, the cooling effects for the exterior and interior building walls were clearly detectable. Highest effect on indoor temperatures occurred at night, which is relevant for the reduction of nocturnal heat stress. Facade greening has *up to medium potential to reduce indoor heat-stress hazards* and is generally more effective than any other type of urban vegetation.
- However, facade greening can also *insulate building walls* as nightly heat emission was reduced in certain cases. Thereby, the greening design has a great impact on the effects towards the street canyon and the building. Depending on the climatic aim, direct green facades or double-skin green facades are to favour.
- Transpiration of facade greenings can be calculated with the grass reference equation of the FAO. A calibration resulted in a correction factor of 1.25 but is subjected to a great uncertainty so far.

In sum, this study determined positive climatic effects for reducing indoor and outdoor heat stress hazards. Furthermore, facade greening offers a wide range of environmental co-benefits services, which were not considered here (e.g. noise reduction, filtering pollutants) However, facade greening is simultaneously associated with high installation costs and high maintenance demand in pruning, service and irrigation. It has to be evaluated if facade greening is profitable on a case-by-case basis.

8 References

ALEXANDRI, E. and P. JONES (2004). The thermal effects of green roofs and green façades on an urban canyon. *Plea conference on passive and low energy architecture*. Eindhoven, the Netherlands: 19-22.

ALI-TOUDERT, F. (2005). *Dependence of outdoor thermal comfort on street design in hot and dry climate*. Dissertation Universität Freiburg, Germany.

ALLEN, R.G., L.S. PEREIRA, D. RAES and M. SMITH (1998). Crop evapotranspiration. Guidelines for computing crop water requirements. *FAO Irrigation and drainage paper* 56: 300 pp.

ALLEN, S.J. and V.L. GRIME (1995). Measurements of transpiration from savannah shrubs using sap flow gauges. *Agricultural and Forest Meteorology* 75 (1-3): 23-41.

ARNFIELD, A.J. (2010). Two decades of urban climate research: a review of turbulence, exchanges of energy and water, and the urban heat island. *International Journal of Climatology* 23: 1-26.

ASCE-EWRI (Environmental and Water Resource Institute of the American Society of Civil Engineers) (Ed.) (2005). *The ASCE standardized reference evapotranspiration equation. ASCE-EWRI Task Committee on Standardization of Reference Evapotranspiration.* Final report: 59 pp.

BANISTER, D. (2008). The sustainable mobility paradigm. *Transport Policy* 15 (2): 73-80.

BARTFELDER, F. and M. KÖHLER (1987). *Experimentelle Untersuchungen zur Funktion von Fassadenbegrünungen*. Dissertation Freie Universität Berlin, Germany.

BASU, R. and J.M. SAMET (2002). Relation between elevated ambient temperature and mortality: a review of the epidemiologic evidence. *Epidemiologic Reviews* 24 (2): 190-202.

BERKOVIC, S., A. YEZIORO and A. BITAN (2012). Study of thermal comfort in courtyards in a hot arid climate. *Solar Energy* 86 (5): 1173-1186.

BERRY, R., S.J. LIVESLEY and L. AYE (2013). Tree canopy shade impacts on solar irradiance received by building walls and their surface temperature. *Building and Environment* 69: 91-100.

BOWLER, D.E., L. BUYUNG-ALI, T.M. KNIGHT and A.S. PULLIN (2010). Urban greening to cool town and cities: a systematic review of empirical evidence. *Landscape and Urban Planning* 97 (3): 147-155.

BOZONNET, E., M. DOYA and F. ALLARD (2011). Cool roofs impact on building thermal response: A French case study. *Energy and Buildings* 43 (11): 3006-3012.

BRAGA, A.L.F., A. ZANOBETTI and J. SCHWARTZ (2002). The effect of weather on respiratory and cardiovascular deaths in 12 US cities. *Environmental Health Perspectives* 110 (9): 859-863.

BRAGER, G.S. and R.J. DE DEAR (1998). Thermal adaptation in the built environment: a literature review. *Energy and Buildings* 27 (1): 83-96.

BRANDT, K. (2006). Heatwave forecasting with a coupled air-building model. *Proceedings of 6th International Conference on Urban Climate (ICUC)*. University of Gothenburg, Sweden.

BRUSE, M. and H. FLEER (1998). Simulating surface-plant-air interactions inside urban environments with a three dimensional numerical model. *Environmental Modelling and Software* 13 (3-4): 373-384.

BRUSE, M. (1999). *Die Auswirkungen kleinskaliger Umweltgestaltung auf das Mikroklima*. Dissertation Universität Bochum, Germany.

BUCHIN, O., M.-T. HOELSCHER, F. MEIER, T. NEHLS and F. ZIEGLER (2015). Evaluation of the health-risk reduction potential of countermeasures to urban heat islands. *Energy and Buildings* 114 (2016): 27-37.

BUCHIN, O., B. JÄNICKE, F. MEIER, D. SCHERER and F. ZIEGLER (2016). The role of building models in the evaluation of heat-related risks. *Natural Hazards and Earth System Sciences* 16: 963-976.

BUYANTUYEV, A. and J. WU (2010). Urban heat islands and landscape heterogeneity: Linking spatiotemporal variations in surface temperatures to land-cover and socioeconomic patterns. *Landscape Ecology* 25 (1): 17-33.

CAMERON, R.W.F., J.E. TAYLOR and M.R. EMMETT (2014). What's 'cool' in the world of green façades? How plant choice influences the cooling properties of green walls. *Building and Environment* 73: 198-207.

CARDIL, A., D.M. MOLINA and L.N. KOBZIAR (2014). Extreme temperature days and their potential impacts on southern Europe. *Natural Hazards and Earth System Sciences*. 14: 3005-3014.

CAO, K.-F., S.-J. YANG, Y.-J. ZHANG and T.J. BRODRIBB (2012). The maximum height of grasses is determined by roots. *Ecology letters* 2012: 7 pp.

CASPARI, H.W., S.R. GREEN and W.R.N. EDWARDS (1993). Transpiration of well-watered and water-stressed Asian pear trees as determined by lysimetry, heat-pulse, and estimated by a Penman-Monteith model. *Agricultural and Forest Meteorology* 67 (1-2): 13-27.

ČERMÁK, J., J. KUČERA and N. NADEZHDINA (2004). Sap flow measurements with some thermodynamic methods, flow integration within trees and scaling up from sample trees to entire forest stands. *Trees* 18 (5): 529-546.

CHEN, H., R. OOKA, H. HUANG and T. TSUCHIYA (2009). Study on mitigation measures for outdoor thermal environment on present urban blocks in Tokyo using coupled simulation. *Building and Environment* 44 (11): 2290-2299.

CHEN, Y.-C., T.-P. LIN and A. MATZARAKIS (2014). Comparison of mean radiant temperature from field experiment and modelling: a case study in Freiburg, Germany. *Theoretical and Applied Climatology* 118 (3): 535-551.

CHOW, W.T.L., R.L. POPE, C.A. MARTIN and A.J. BRAZEL (2011). Observing and modeling the nocturnal park cool island of an arid city: horizontal and vertical impacts. *Theoretical and Applied Climatology* 103 (1-2): 197-211.

CHOW, W.T.L. and A.J. BRAZEL (2012). Assessing xeriscaping as a sustainable heat island mitigation approach for a desert city. *Building and Environment* 47 (1): 170-181.

CIENCIALA, E., A. LINDROTH, J. ČERMÁK, J.-E. HÄLLGREN and J. KUČERA (1992). Assessment of transpiration estimates for *Picea abies* trees during a growing season. *Trees* 6 (3): 121-127.

COUTTS, A.M., E. DALY, J. BERINGER and N.J. TAPPER (2013). Assessing practical measures to reduce urban heat: green and cool roofs. *Building and Environment* 70: 266-276.

DAVIS, R.E., P.C. KNAPPENBERGER, P.J. MICHAELS and W.M. NOVICOFF (2003). Changing heat-related mortality in the United States. *Environmental Health Perspectives* 111 (4): 1712-1718.

DAWSON, T.E., S.S.O. BURGESS, K.P. TU, R.S. OLIVEIRA, L.S. SANTIAGO, J.B. FISHER, K.A. SIMONIN and A.R. AMBROSE (2007). Nighttime transpiration in woody plants from contrasting ecosystems. *Tree Physiology* 27 (4): 561-575.

DEBUS, U. (2009). *Vertikale Flächenpotentiale zur Biomasseproduktion im urbanen Raum. Beispiel Berlin.* Diploma thesis Technische Universität Berlin, Germany.

DÉQUÉ, M. (2009). *ENSEMBLES Technical Report No. 5. Temperature and precipitation probability density functions in ENSEMBLES Regional Scenarios*. 63 pp.

DJEDJIG, J., E. BOZONNET and R. BELARBI (2013). Experimental study of the urban microclimate mitigation potential of green roofs and green walls in street canyons. *International Journal of Low-Carbon Technologies* 2013: 1-11.

DONNER, J., J.M. MÜLLER and J. KÖPPEL (2015): Urban heat: towards adapted German cities? *Journal of Environmental Assessment Policy and Management* 17 (2): 17 pp.

DUGAS, W.A., M.L. HEUER, D. HUNSAKER, B.A. KIMBALL, K.F. LEWIN, J. NAGY and M. JOHNSON (1994). Sap flow measurements of transpiration from cotton grown under ambient and enriched CO_2 concentrations. *Agricultural and Forest Meteorology* 70 (1-4): 231-245.

DUGORD, P., S. LAUF, C. SCHUSTER and B. KLEINSCHMIT (2014): Land use patterns, temperature distribution, and potential heat stress risk - The case study Berlin, Germany. Computers, *Environment and Urban Systems* 48: 86-98.

DWD (Deutscher Wetterdienst) (Ed.) (2014). *Time series data of air temperature from 2001 to 2011, Tempelhof, Germany*. http://werdis.dwd.de

DYNAMAX INC. (Ed.) (2007). *User manual for the Flow32-1K sap flow system with CR1000 data logger*. 80 pp. ftp://ftp.dynamax.com/manuals/Flow32/Flow32-1K_08062007.pdf

EMMANUEL, R. and H.J.S. FERNANDO (2007): Urban heat islands in humid and arid climates: role of urban form and thermal properties in Colombo, Sri Lanka and Phoenix, USA. *Climate Research* 34 (3): 241-251.

EMS (Environmental Measuring Systems) BRNO (Ed.) (2010). *EMS 62, EMS 62A Sap flow system for small stems or branches. Instruction manual.* 11 pp. http://www.emsbrno.cz/r.axd/pdf_v_EMS62__userman_u_pdf.jpg?ver=

ENEV (Verordnung über energiesparenden Wärmeschutz und energiesparende Anlagentechnik bei Gebäuden - Energieeinsparverordnung) in its 24th October 2015 version, BGBl. I S. 1789.

ESCALONA, J.M., S. FUENTES, M. TOMÁS, S. MARTORELL, J. FLEXAS and H. MEDRANO (2013). Responses of leaf night transpiration to drought stress in *Vitis venifera* L. *Agricultural Water Management* 118 (2013): 50-58.

EUMORFOPOULOU, E.A. and K.J. KONTOLEON (2009). Experimental approach to the contribution of plant-covered walls to the thermal behaviour of building envelopes. *Building and Environment* 44 (5): 1024-1038.

FANK, J. (2007). Die Gras-Referenzverdunstung: Berechnungsergebnisse in Abhängigkeit von Messgeräten und Messintervall. *12. Gumpensteiner Lysimetertagung*. Irdning, Germany: 53-56.

FENNER, D., F. MEIER, D. SCHERER and A. POLZE (2014). Spatial and temporal air temperature variability in Berlin, Germany, during the years 2001-2010. *Urban Climate* 10 (2) (ICUC8: The 8th International Conference on Urban Climate and the 10th Symposium on the Urban Environment): 308-331.

FISHER, J.B., D.D. BALDOCCHI, L. MISSON, T.E. DAWSON and A.H. GOLDSTEIN (2007). What the towers don't see at night: nocturnal sap flow in trees and shrubs at two AmeriFlux sites in California. *Tree Physiology* 27 (4): 597-610.

FORSTER, M.A. (2014). How significant is nocturnal sap flow? *Tree Physiology* 34 (10): 757-765.

FRANCK, U., M. KRUGER, N. SCHWARZ, K. GROSSMANN, S RODER and U. SCHLINK (2013). Heat stress in urban areas: Indoor and outdoor temperatures in different urban structure types and subjectively reported well-being during a heat wave in the city of Leipzig. *Meteorologische Zeitschrift* 22 (2): 167-177.

GABRIEL, K.M.A. and W.R. ENDLICHER (2011). Urban and rural mortality rates during heat waves in Berlin and Brandenburg, Germany. *Environmental Pollution* 159: 2044-2050.

GASPARRINI, A., Y. GUO, M. HASHIZUME, E. LAVIGNE, A. ZANOBETTI, J. SCHWARTZ, A. TOBIAS, S. TONG, J. ROCKLÖV, B. FORSBERG, M. LEONE, M.D. SARIO, M.L. BELL, Y.-L.L. GUO, C. WU, H. KAN, S.-M. YI, M. DE SOUSA ZANOTTI STAGLIORIO COELH, P.H.N. SALDIVA, Y. HONDA, H. KIM and B. ARMSTRONG (2015). Mortality risk attributable to high and low ambient temperature: a multicountry observational study. *The Lancet* 386: 369-375.

GEORGESCU, M., P.E. MOREFIELD, B.G. BIERWAGEN and C.P. WEAVER (2014). Urban adaptation can roll back warming of emerging megapolitan regions. *Proceedings of the National Academy of Sciences of the United States of America* 111 (8): 2909-2914.

GIANNAROS, T.M., D. MELAS, I.A. DAGLIS and I. KERAMITSOGLOU (2014). Development of an operational modeling system for urban heat islands: an application to Athens, Greece. *Natural Hazards and Earth System Science* 14: 347-358.

GIVONI, B. (1994). *Passive low energy cooling of buildings*. John Wiley & Sons, New York: 267 pp.

GOSLING, S.N., J.A. LOWE, G.R. MCGREGOR, M. PELLING and B.D. MALAMUD (2009). Associations between elevated atmospheric temperature and human mortality: a critical review of the literature. *Climate Change* 92: 299-341.

GRIME, V. and F. SINCLAIR (1999). Sources of error in stem heat balance sap flow measurements. *Agricultural and Forest Meteorology* 94 (2): 103-121.

GROSS, G. (2012). Effects of different vegetation on temperature in an urban building environment. Micro-scale numerical experiments. *Meteorologische Zeitschrift* 21 (4): 399-412.

HARLAN, S.L., A.J. BRAZEL, L. PRASHAD, W.L. STEFANOV and L. LARSEN (2006). Neighborhood microclimates and vulnerability to heat stress. *Social Science and Medicine* 63 (11): 2847-2863.

HEDQUIST, B.C. and A.J. BRAZEL (2014). Seasonal variability of temperatures and outdoor human comfort in Phoenix, Arizona, U.S.A. *Building and Environment* 72: 377-388.

HEß, D. (2008). *Grundlagen der Physiologie und Biotechnologie der Pflanzen*. 11th ed., Ulmer, Stuttgart: 415 pp.

HOELSCHER, M.-T. (2013). *Greenhouse experiments on transpiration of vertical green*. Master thesis Technische Universität Berlin, Germany.

HOELSCHER, M.-T., T. NEHLS, B. JÄNICKE and G. WESSOLEK (2015). Quantifying cooling effects of facade greening: Shading, transpiration and insulation. *Energy and Buildings* 114 (2016): 283-290.

HSIAO, T. (1973). Plant responses to water stress. *Annual Review of Plant Physiology* 24: 519-570.

HUNTER, A.M., N.S.G. WILLIAMS, J.P. RAYNER, L. AYE, D. HES and S.J. LIVESLEY (2014). Quantifying the thermal performance of green façades: a critical review. *Ecological Engineering Building* 63: 102-113.

HUTTNER, S. (2012). *Further development and application of the 3D microclimate simulation ENVI-met*. Dissertation Johannes Gutenberg-Universität Mainz, Germany.

HWANG, R.-L., T.-P. LIN and A. MATZARAKIS (2011). Seasonal effects of urban street shading on long-term outdoor thermal comfort. *Building and Environment* 46 (4): 863-870.

IMHOFF, M.L., P. ZHANG, R.E. WOLFE and L. BOUNOUA (2010). Remote sensing of the urban heat island effect across biomes in the continental USA. *Remote Sensing of Environment* 114 (2010): 504-513.

IP, K., M. LAM and A. MILLER (2010). Shading performance of a vertical deciduous climbing plant canopy. *Building and Environment* 45 (1): 81-88.

IPCC (Intergovernmental Panel on Climate Change) (Ed.) (2012). *Managing the risks of extreme events and disasters to advance climate change adaptation: Special report of the intergovernmental panel on climate change*. Cambridge University Press, Cambridge: 582 pp.

JÄNICKE, B., F. MEIER, M.-T. HOELSCHER and D. SCHERER (2015). Evaluating the effects of façade greening on human bioclimate in a complex urban environment. *Advances in Meteorology* 2015: 15 pp.

JARVIS, P.G. (1976). The interpretation of the variations in leaf water potential and stomatal conductance found in canopies in the field. *Philosophical Transactions of the Royal Society* 273: 593-610.

JENKINS, K., J. HALL, V. GLENIS, C. KILSBY, M. MCCARTHY, C. GOODESS, D. SMITH, N. MALLESON and M. BIRKIN (2014). Probabilistic spatial risk assessment of heat impacts and adaptations for London. *Climate Change* 124 (1): 105-117.

JIMÉNEZ, M.S., N. NADEZHDINA, J. ČERMÁK and D. MORALES (2000). Radial variation in sap flow in five laurel forest tree species in Tenerife, Canary Islands. *Tree Physiology* 20: 1149-1156.

JONES, H.G. (2000). *Plants and microclimate. A quantitative approach to environmental plant physiology*. 2nd ed., Cambridge University Press, Cambridge: 428 pp.

KÁNTOR, N. and J. UNGER (2010). Benefits and opportunities of adopting GIS in thermal comfort studies in resting places: an urban park as an example. *Landscape and Urban Planning* 98 (1): 36-46.

KILBOURNE, E.M. (1997). *Heat waves and hot environments*. In: NOJI, E.K. (Ed.) (1997). *The public health consequences of disasters*. Oxford University Press, New York: 468 pp.

KLEPEIS, N.E.,W.C. NELSON, W.R. OTT, J.P. ROBINSON, A.M. TSANG, P. SWITZER, J.V. BEHAR, S.C. HERN and W.H. ENGELMANN (1995). *The national human activity pattern survey (NHAPS). A resource for assessing exposure to environmental pollutants.* 38 pp. https://indoor.lbl.gov/sites/all/files/lbnl-47713.pdf

KÖHLER, M. (1993): *Fassaden- und Dachbegrünung*. Ulmer, Stuttgart: 329 pp.

KÖHLER, M. (2008). Green facades - a view back and some visions. *Urban Ecosystems* 11 (4): 423-436.

KOTTHAUS, S. and C. GRIMMOND (2014). Energy exchange in a dense urban environment - Part I. Temporal variability of long-term observations in central London. *Urban Climate* 10 (2) (ICUC8: The 8th International Conference on Urban Climate and the 10th Symposium on the Urban Environment): 261-280.

KOVATS, R.S. and S. HAJAT (2008). Heat stress and public health: a critical review. *Annual Review of Public Health* 29: 41-55.

KOYAMA, T., M. YOSHINAGA, H. HAYASHI, K.-I. MAEDA and A. YAMAUCHI (2013). Identification of key plant traits contributing to the cooling effects of green façades using freestanding walls. *Building and Environment* 66: 96-103.

KOYAMA, T., M. YOSHINAGA, K.-I. MAEDA and A. YAMAUCHI (2015). Transpiration cooling effect of climber greenwall with an air gap on indoor thermal environment. *Ecological Engineering* 83: 343-353.

KRAUSE, C. and C. SCHULZ (1998). Aufenthaltszeiten der Deutschen Bevölkerung im Innenraum, im Freien, im Straßenverkehr. *Umweltmedizin in Forschung und Praxis* 3 (4): 249.

KRAWINA, J. and H. LOIDL (1990). *Vertikale Begrünung von Bauwerken*. Wien, Berlin, 201 pp.

KRAYENHOFF, E.S. and J.A. VOOGT (2010). Impacts of urban albedo increase on local air temperature at daily-annual time scales: model results and synthesis of previous work. *Journal of Applied Meteorology and Climatology* 49: 1634-1648.

KRÜGER, E.L., F.O. MINELLA and A. MATZARAKIS (2013). Comparison of different methods of estimating the mean radiant temperature in outdoor thermal comfort studies. *International Journal of Biometeorology* 58 (8): 1727-1737.

KRUPKA, B.W. (1992): *Dachbegrünung. Pflanzen- und Vegetationsanwendung an Bauwerken.* Ulmer, Stuttgart: 508 pp.

KUNST, A.E., C.W.N. LOOMAN and J.P. MACKENBACH (1993). Outdoor air temperature and mortality in the Netherlands: a time-series analysis. *American Journal of Epidemiology* 137 (3): 331-341.

KUTTLER, W. (2011). Climate change in urban areas: Part 2, Measures. *Environmental Science Europe* 23: 1-15.

LANGENSIEPEN, M., M. KUPISCH, A. GRAF, M. SCHMIDT and F. EWERT (2014). Improving the stem heat balance method for determining sap-flow in wheat. *Agricultural and Forest Meteorology* 186: 34-42.

LEUZINGER, S., A. HARTMANN and C. KÖRNER (2011). Water relations of climbing ivy in a temperate forest. *Planta* 233: 1087-1096.

LI, T., R.M. HORTON and P.L. KINNEY (2013). Projections of seasonal patterns in temperature-related deaths for Manhattan, New York. *Nature Climate Change* 3: 717-721.

LIBERT, J.P., V. BACH, L.C. JOHNSON, J. EHRHART, G. WITTERSHEIM and D. KELLER (1991). Relative and combined effects of heat and noise exposure on sleep in humans. *Sleep* 14 (1): 24-31.

LIN, T.-P., A. MATZARAKIS and R.-L. HWANG (2010). Shading effect on long-term outdoor thermal comfort. *Building and Environment* 45 (1): 213-221.

LINDBERG, F., B. HOLMER and S. THORSSON (2008). SOLWEIG 1.0 - modelling spatial variations of 3D radiant fluxes and mean radiant temperature in complex urban settings. *International Journal of Biometeorology* 52 (7): 697-713.

LINDBERG, F. and C.S.B. GRIMMOND (2011). The influence of vegetation and building morphology on shadow patterns and mean radiant temperatures in urban areas: model development and evaluation. *Theoretical and Applied Climatology* 105 (3-4): 311-323.

LINDROTH, A., J. ČERMÁK, J. KUČERA, E. CIENCIALA and H. ECKERSTEN (1995). Sap flow by the heat balance method applied to small size *Salix*-trees in a short-rotation forest. *Biomass and Bioenergy* 8: 7-15.

LU, J., C. LI, C. YU, M. JIN and S. DONG (2012). Regression analysis of the relationship between urban heat island effect and urban canopy characteristics in a mountainous city, Chongqing. *Indoor and Built Environment* 21 (6): 821-836.

MANKIEWICZ, P.S. (2017). Scaling biogeochemical interfaces to regulate ecosystem development: Vernadsky's framework in SUITMA landscapes. *SUITMA 9* (9th international congress Soils of Urban Industrial Traffic Mining and Military areas). Moscow, Russia: conference presentation.

MATYSSEK, R., G. WIESER, K. PATZNER, H. BLASCHKE and K.-H. HÄBERLE (2009). Transpiration of forest trees and stands at different altitude: consistencies rather than contrasts? *European Journal of Forest Research* 128 (6): 579-596.

MATZARAKIS, A., F. RUTZ and H. MAYER (2007). Modelling radiation fluxes in simple and complex environments - application of the RayMan model. *International Journal of Biometeorology* 51 (4): 323-334.

MATZARAKIS, A., F. RUTZ and H. MAYER (2010). Modelling radiation fluxes in simple and complex environments: basics of the RayMan model. *International Journal of Biometeorology* 54 (2): 131-139.

MAVROGIANNI, A., P. WILKINSON, M. DAVIES, P. BIDDULPH and E. OIKONOMOU (2012). Building characteristics as determinants of propensity to high indoor summer temperatures in London dwellings. *Building and Environment* 55: 117-130.

MAYER H. and P. HÖPPE (1987). Thermal comfort of man in different urban environments. *Theoretical and Applied Climatology* 38 (1): 43-49.

MAZZALI, U., F. PERON, P. ROMAGNONI and R.M. PULSELLI (2013). Experimental investigation on the energy performance of living walls in a temperate climate. *Building and Environment* 64: 57-66.

MEIER, F. and D. SCHERER (2012). Spatial and temporal variability of urban tree canopy temperature during summer 2010 in Berlin, Germany. *Theoretical and Applied Climatology* 110 (3): 373-384.

MIDDEL, A., K. HÄB, A.J. BRAZEL, C.A. MARTIN and S. GUHATHAKURTA (2014). Impact of urban form and design on mid-afternoon microclimate in Phoenix Local Climate Zones. *Landscape and Urban Planning* 122: 16-28.

MONTÁVEZ, J.P., J.F. GONZÁLEZ-ROUCO and F. VALERO (2008). A simple model for estimating the maximum intensity of nocturnal urban heat island. *International Journal of Climatology* 28: 235-242.

MORAKINYO, T.E., A.A. BALOGUN and O.B. ADEGUN (2013). Comparing the effect of trees on thermal conditions of two typical urban buildings. *Urban Climate* 3: 76-93.

MÜLLER, N., W. KUTTLER and A.-B. BARLAG (2014). Counteracting urban climate change: adaptation measures and their effect on thermal comfort. *Theoretical and Applied Climatology* 115 (1-2): 243-257.

NEHLS, T. (2010). *Ungenutztes Flächenpotential für die Fassadenbegrünung am Beispiel Berlins.* Bauwerksbegrünung. Kuberski, Stuttgart: 74-75.

NEHLS, T., M. MENZEL and G. WESSOLEK (2015). Depression storage capacities of different ideal pavements as quantified by a terrestrial laser scanning-based method. *Water Science and Technology* 71: 862-869.

NG, E., L. CHEN, Y. WANG and C. YUAN (2012). A study on the cooling effects of greening in a high-density city: an experience from Hong Kong. *Building and Environment* 47 (1): 256-271.

NIKOLOPOULOU, M. and S. LYKOUDIS (2006). Thermal comfort in outdoor urban spaces: analysis across different European countries. *Building and Environment* 41 (11): 1455-1470.

OIKONOMOU, E., M. DAVIES, A. MAVROGIANNI, P. BIDDULPH, P. WILKINSON and M. KOLOKOTRONI (2012). Modelling the relative importance of the urban heat island and the thermal quality of dwellings for overheating in London. *Building and Environment* 57: 223-238.

OKAMOTO-MIZUNO, K., K. TSUZUKI and K. MIZUNO (2004). Effects of humid heat exposure in later sleep segments on sleep stages and body temperature in humans. *International Journal of Biometeorology* 49 (4): 232-237.

OKE, T.R. (1982). The energetic basis of the urban heat island. *Quarterly Journal of the Royal Meteorological Society* 108: 1-24.

O'NEILL, M.S., A. ZANOBETTI and J. SCHWARTZ (2003). Modifiers of the temperature and mortality association in seven US cities. *American Journal of Epidemiology* 157 (12): 1074-1082.

O'NEILL, M.S., A. ZANOBETTI and J. SCHWARTZ (2005). Disparities by race in heat-related mortality in four US cities: the role of air conditioning prevalence. *Journal of Urban Health: Bulletin of the New York Academy of Medicine* 82 (2): 191-197.

PARLOW, E., R. VOGT and C. FEIGENWINTER (2014). The urban heat island of Basel - seen from different perspectives. *Die Erde. Journal of the Geographical Society of Berlin* 145 (1-2): 96-110.

PENG, L.L.H. and C.Y. JIM (2013). Green-roof effects on neighbourhood microclimate and human thermal sensation. *Energies* 6 (2): 598-618.

PÉREZ, G., L. RINCÓN, A. VILA, J.M. GONZÁLEZ and L.F. CABEZA (2011). Green vertical systems for buildings as passive systems for energy savings. *Applied Energy* 88 (12): 4854-4859.

PERINI, K., M. OTTELÉ, A.L.A FRAAIJ, E.M. HAAS and R. RAITERI (2011). Vertical greening systems and the effect on air flow and temperature on the building envelope. *Building and Environment* 46: 2287-2294.

PERTIERRA, R., J. JARA, J. CELIS and F. REYES (2002). Saftflussmessung an Gewächshaustomaten (*Lycopersicon esculentum* Mill.) unter zwei Bewässerungsvarianten. *Gartenbauwissenschaft* 67 (5): 172-181.

PFOSER, N., N. JENNER, J. HENRICH, J. HEUSINGER and S. WEBER (2013). *Gebäude Begrünung Energie. Potenziale und Wechselwirkungen*. Technische Universität Darmstadt, Darmstadt: 307 pp.

PORRITT, S.M., P.C. CROPPER, L. SHAO and C.I. GOODIER (2012). Ranking of interventions to reduce dwelling overheating during heat waves. *Energy and Buildings* 55: 16-27.

PULSELLI, R.M., F.M. PULSELLI, U. MAZZALI, F. PERON and S. BASTIANONI (2014). Emergy based evaluation of environmental performances of living wall and grass wall systems. *Energy and Buildings* 73: 200-211.

PUTZ, F.E. and H.A. MOONEY (Ed.) (1992). *The biology of vines*. Cambridge University, Cambridge: 544 pp.

RAVEN, P.H., R.F. EVERT and S.E. EICHHORN (2005). *Biology of plants*. 4th ed., W.H. Freeman and Company, New York: 942 pp.

RAWSON, H.M. and J.M. CLARKE (1988). Nocturnal transpiration in wheat. *Australian Journal of Plant Physiology* 15 (3): 397-406.

RIZWAN, A.M., L.Y.C. DENNIS and C. LIU (2008). A review on the generation, determination and mitigation of Urban Heat Island. *Journal of Environmental Sciences* 20 (1): 120-128.

RODRIGUEZ-DOMINGUEZ, C.M., W. EHRENBERGER, C. SANN, S. RÜGER, V. SUKHORUKOV, M.J. MARTÍN-PALOMO, A. DIAZ-ESPEJO, M.V. CUEVAS, J.M. TORRES-RUIZ, A. PEREZ-MARTIN, U. ZIMMERMANN and J.E. FERNÁNDEZ (2012). Concomitant measurements of stem sap flow and leaf turgor pressure in olive trees using the leaf patch clamp pressure probe. *Agricultural Water Management* 114: 50-58.

ROSENTHAL, J.K., P.L. KINNEY and K.B. METZGER (2014). Intra-urban vulnerability to heat-related mortality in New York City, 1997-2006. *Health and Place* 30: 45-60.

RYAN, M.G. and B.J. YODER (1997). Hydraulic limits to tree height and tree growth. What keeps trees from growing beyond a certain height? *BioScience* 47 (4): 235-242.

RYAN, M.G., N. PHILIPPS and B.J. BOND (2006). The hydraulic limitation hypothesis revisited. *Plant, Cell and Environment* 29 (2006): 367-381.

SANEINEJAD, S., P. MOONEN and J. CARMELIET (2014). Comparative assessment of various heat island mitigation measures. *Building and Environment* 73: 162-170.

SANTAMOURIS, M., A. SFAKIANAKI and K. PAVLOU (2010). On the efficiency of night ventilation techniques applied to residential buildings. *Energy and Buildings* 42 (8): 1309-1313.

SANTAMOURIS, M. (2013). Using cool pavements as a mitigation strategy to fight urban heat island - a review of the actual developments. *Renewable and Sustainable Energy Reviews* 26: 224-240.

SANTAMOURIS, M. (2014). Cooling the cities - a review of reflective and green roof mitigation technologies to fight heat island and improve comfort in urban environments. *Solar Energy* 103: 682-703.

SAVI, T., S. ANDRI and A. NARDINI (2013). Impact of different green roof layering on plant water status and drought survival. *Ecological Engineering* 57: 188-196.

SCHERER, D. and W. ENDLICHER (2013). Editorial: Urban climate and heat stress - Part 1. *Die Erde. Journal of the Geographical Society of Berlin* 144: 175-180.

SCHERER, D., U. FEHRENBACH, T. LAKES, S. LAUF, F. MEIER and C. SCHUSTER (2014). Quantification of heat-stress related mortality hazard, vulnerability and risk in Berlin, Germany. *Die Erde. Journal of the Geographical Society of Berlin* 144 (3-4): 238-259.

SCHLÖßER, S.A. (2003). *Zur Akzeptanz von Fassadenbegrünung: Meinungsbilder Kölner Bürger - eine Bevölkerungsbefragung*. Dissertation Universität zu Köln, Germany.

SCHLÜNZEN, K.H. and R.S. SOKHI (2008). Overview of tools and methods for meteorological and air pollution mesoscale model evaluation and user training. *WMO Joint Report COST Action 728 GURME* 2008.

SCHOPFER, P. and A. BRENNICKE (2010). *Pflanzenphysiologie*. 7th ed., Ulmer, Heidelberg: 702 pp.

SCHUBERT, S. and S. GROSSMAN-CLARKE (2013). The influence of green areas and roof albedos on air temperatures during extreme heat events in Berlin, Germany. *Meteorologische Zeitschrift* 22: 131-143.

SCHUSTER, C., K. BURKART and T. LAKES (2014). Heat mortality in Berlin-spatial variability at the neighborhood scale. *Urban Climate* 10 (1): 134-147.

SCHUSTER, C. and T. LAKES (2014). Spatial patterns of heat stress and risk factors in Berlin. *Annual Meeting of the Association of American Geographers (AAG) 2014*. Tampa, USA: Conference presentation.

SCHWARZER, N. (2015). *Ein neuartiges Lysimetersystem zur Transpirationsmessung von vertikaler Begrünung in der Aufwuchsphase*. Diploma thesis Technische Universität Berlin, Germany.

SEMENZA, J.C., C.H. RUBIN, K.H. FALTER, J.D. SELANIKIO, W.D. FLANDERS, H.L. HOWE and J.L. WILHELM (1996). Heat-related deaths during the July 1995 heat wave in Chicago. *The New England Journal of Medicine* 335: 84-90.

SENSTADT (Senate Department for Urban Development and the Environment) (Ed.) (2001). *04.04 Temperature in medium low-exchange nocturnal radiation periods (Edition 2001)*. http://www.stadtentwicklung.berlin.de/umwelt/umweltatlas/e_text/eka404.pdf.

SENSTADT (Senate Department for Urban Development and the Environment) (Ed.) (2011). *Stadtentwicklungsplan Klima. Urbane Lebensqualität im Klimawandel sichern*. Medialis, Berlin: 84 pp.

SHAM, J.F.C., T.Y. LO and S.A. MEMON (2012). Verification and application of continuous surface temperature monitoring technique for investigation of nocturnal sensible heat release characteristics by building fabrics. *Energy and Buildings* 53: 108-116.

SHASHUA-BAR, L., D. PEARLMUTTER and E. ERELL (2011). The influence of trees and grass on outdoor thermal comfort in a hot-arid environment. *International Journal of Climatology* 31 (10): 1498-1506.

SKELHORN, C., S. LINDLEY and G. LEVERMORE (2014). The impact of vegetation types on air and surface temperatures in a temperate city: a fine scale assessment in Manchester, UK. *Landscape and Urban Planning* 121: 129-140.

SKOULIKA, F., M. SANTAMOURIS, D. KOLOKOTSA and N. BOEMI (2014). On the thermal characteristics and the mitigation potential of a medium size urban park in Athens, Greece. *Landscape and Urban Planning* 123: 73-86.

SMARGIASSI, A., M. FOURNIER, C. GRIOT, Y. BAUDOUIN and T. KOSATSKY (2008). Prediction of the indoor temperatures of an urban area with an in-time regression mapping approach. *Journal of Exposure Science and Environmental Epidemiology* 18 (3): 282-288.

SMITH, D.M. and S.J. ALLEN (1996). Measurements of sap in plant stems. *Journal of Experimental Botany* 47 (12): 1833-1844.

SOBB (Statistical Office Berlin Brandenburg) (2013): *Daily age-classified number of deaths and semi-annual population data of Berlin by age groups between 2001 and 2010*. Derived from the register of residents.

SRIVANIT, M. and K. HOKAO (2013). Evaluating the cooling effects of greening for improving the outdoor thermal environment at an institutional campus in the summer. *Building and Environment* 66: 158-172.

STAFOGGIA, M., F. FORASTIERE, D. AGOSTINI, N. CARANCI, F. DE'DONATO, M. DEMARIA, P. MICHELOZZI, R. MIGLIO, M. ROGNONI, A. RUSSO and C.A. PERUCCI (2008). Factors affecting in-hospital heat-related mortality: a multi-city case-crossover analysis. *Journal of Epidemiology Community and Health* 62: 209-215.

STEC, W.J., A.H.C. VAN PAASSEN and A. MAZIARZ (2005). Modelling the double skin façade with plants. *Energy and Buildings* 37: 419-427.

STERNBERG, H., H. VILES and A. CATHERSIDES (2011). Evaluating the role of ivy (*Hedera helix*) in moderating wall surface microclimates and contributing to the bioprotection of historic buildings. *Building and Environment* 46: 293-297.

STEWART I.D. and T.R. OKE (2012). Local climate zones for urban temperature studies. *Bulletin of the American Meteorological Society* 93 (12): 1879-1900.

SUSOROVA, I., M. ANGULO, P. BAHRAMI and B. STEPHENS (2013). A model of vegetated exterior facades for evaluation of wall thermal performance. *Building and Environment* 67: 1-13.

TAKEBAYASHI, H. and M. MORIYAMA (2007). Surface heat budget on green roof and high reflection roof for mitigation of urban heat island. *Building and Environment* 42: 2971-2979.

TAN, C.L., N.H. WONG and S.K. JUSUF (2014). Effects of vertical greenery on mean radiant temperature in the tropical urban environment. *Landscape and Urban Planning* 127: 52-64.

TATARINOV, F. and J. ČERMÁK (1999). Daily and seasonal variation of stem radius in oak. *Annals of Forest Science* 56 (7): 579-590.

THÖNNESSEN (2002). *Elementdynamik in fassadenbegrünendem Wilden Wein (Parthenocissus tricuspidata. Nährelemente, anorganische Schadstoffe, Platin-Gruppen-Elemente, Filterleistung, immissionshistorische Aspekte, methodische Neu- und Weiterentwicklungen.* Dissertation Universität Köln, Germany.

THORSSON, S., F. LINDBERG, I. ELIASSON and B. HOLMER (2007). Different methods for estimating the mean radiant temperature in an outdoor urban setting. *International Journal of Climatology* 27 (14): 1983-1993.

TRCALA, M. and J. ČERMÁK (2012). Improvement of the trunk heat balance method including measurement of zero and reverse sap flows. *Agricultural and Forest Meteorology* 166-167: 120-126.

URBAN, J., KROFTA, K. and J. KUČERA (2012). Calibration of stem heat balance sensors upon a study of water balance of the hop plantation. *Acta horticulturae* 951: 79-86.

VANDEGEHUCHTE, M.W. and K. STEPPE (2013). Sap-flux density measurement methods: working principles and applicability. *Functional Plant Biology* 40 (3): 213-223.

VANDENTORREN, S., P. BRETIN, A. ZEGHNOUN, L. MANDEREAU-BRUNO, A. CROISIER, C. COCHET, J. RIBERON, I. SIBERAN, B. DECLERCQ and M. LEDRANS (2006). August 2003 heat wave in France: risk factors for death of elderly people living at home. *European Journal of Public Health* 16 (6): 583-591.

WANG, L. and H.-Q. XU (2008). Study on the information extraction of evapotranspiration and its relation with the urban heat island and urban expansion in Fuzhou City with its surrounding areas of SE China. *2008 International Workshop on Earth Observation and Remote Sensing Applications (EORSA)*: 6 pp.

WERNER, P.C. and F.W. GERSTENGARBE (2007). *Welche Klimaänderungen sind in Deutschland zu erwarten?* In: ENDLICHER, W. and F.W. GERSTENGARBE (Eds.) (2007). *Der Klimawandel*. Potsdam-Institut für Klimafolgenforschung e.V., Potsdam: 56-59.

WILLMOTT, C.J., S.G. ACKLESON, R.E. DAVIS, J.J. FEDDEMA, K.M. KLINK, D.R. LEGATES, J. O'DONNELL and C.M. ROWE (1985). Statistics for the evaluation and comparison of models. *Journal of Geophysical Research* 90 (5): 8995-9005.

WONG, N.H., A.Y. KWANG TAN, Y. CHEN, K. SEKAR, P.Y. TAN, D. CHAN, K. CHIANG and N.C. WONG (2010). Thermal evaluation of vertical greenery systems for building walls. *Building and Environment* 45 (3): 663-672.

WU, J., Y. ZHOU, Y. GAO, J.S. FU, B.A. JOHNSON, C. HUANG, Y.M. KIM and Y. LIU (2014). Estimation and uncertainty analysis of impacts of future heat waves on mortality in the eastern United States. *Environmental Health Perspectives* 122 (1): 10-16.

YANG, F., S.S.Y. LAU and F. QIAN (2011). Thermal comfort effects of urban design strategies in high-rise urban environments in a sub-tropical climate. *Architectural Science Review* 54 (4): 285-304.

YANG, X., L. ZHAO, M. BRUSE and Q. MENG (2013). Evaluation of a microclimate model for predicting the thermal behavior of different ground surfaces. *Building and Environment* 60: 93-104.

ZHU, X.G., S.P. LONG and D.R. ORT (2008). What is the maximum efficiency with which photosynthesis can convert solar energy into biomass? *Current Opinion in Biotechnology* 19 (2): 153-159.

Appendix

Tab. A.1 Mean daily evapotranspiration per m^2 wall area in the period from June until October 2014 determined by lysimetry and calculated by the ASCE grass reference evapotranspiration as well as mean daily air temperature, relative humidity and incoming short-wave radiation. Evapotranspiration values were the data basis for the calibration in Fig. 6.4.

Date	Lysimeter	Calculation	T_{air}	*RH*	Incoming short-wave radiation
(DD.MM.JJJJ)	(L d^{-1} m^{-2})	L d^{-1} m^{-2})	(°C)	(%)	(W m^{-2})
27.06.2014	1.78	1.36	18.86	61.19	85.22
28.06.2014	1.98	1.62	20.63	61.35	89.72
29.06.2014	1.45	0.61	17.76	78.38	32.60
30.06.2014	1.75	1.29	16.99	73.00	72.83
01.07.2014	1.52	1.93	17.19	60.48	115.54
02.07.2014	1.52	1.35	17.25	60.62	75.54
11.07.2014	2.03	2.07	21.76	66.39	109.13
12.07.2014	1.62	1.57	17.72	73.61	93.52
13.07.2014	1.61	1.32	18.13	75.45	84.49
14.07.2014	1.80	1.63	21.27	73.55	97.51
15.07.2014	1.98	2.27	22.63	62.79	128.33
16.07.2014	2.08	1.66	23.24	57.09	92.30
17.07.2014	2.22	2.05	24.63	53.95	130.14
18.07.2014	2.21	1.90	25.42	53.10	113.75
19.07.2014	2.26	2.20	27.30	46.29	123.80
20.07.2014	2.47	1.78	28.59	46.59	97.51
01.08.2014	2.14	1.41	23.06	57.65	73.83
02.08.2014	2.38	1.66	25.09	63.29	78.95
03.08.2014	2.20	1.17	24.90	70.50	70.22
04.08.2014	1.61	0.58	21.68	74.47	32.78
05.08.2014	1.40	0.58	20.44	78.12	36.25
06.08.2014	2.50	1.95	21.67	60.25	120.25
07.08.2014	2.11	0.64	21.29	66.96	44.61
08.08.2014	2.53	1.15	22.14	65.07	83.76
09.08.2014	2.47	1.52	22.75	63.32	71.99
10.08.2014	2.56	1.23	22.94	66.92	72.86
11.08.2014	2.39	2.01	21.04	61.65	106.08
12.08.2014	2.31	2.01	19.27	55.63	120.15
13.08.2014	2.15	1.13	20.11	57.27	54.69
14.08.2014	1.66	1.17	19.02	69.07	60.43
15.08.2014	1.65	0.74	17.76	71.88	44.09
16.08.2014	1.62	1.32	16.83	73.35	69.47
21.08.2014	1.96	1.38	15.86	60.82	95.13
22.08.2014	1.86	0.97	17.23	50.56	47.29
23.08.2014	2.03	1.69	17.28	58.56	97.85
24.08.2014	1.68	1.30	14.90	65.08	80.00
25.08.2014	1.59	0.73	15.22	61.59	51.17
26.08.2014	1.73	1.08	15.96	64.67	72.30
27.08.2014	1.73	1.02	16.63	61.81	76.44
28.08.2014	1.93	1.66	18.54	53.04	109.58
29.08.2014	1.42	0.66	18.49	66.46	39.18
02.09.2014	1.39	1.20	17.20	72.83	71.24
03.09.2014	1.66	1.68	18.56	61.97	104.51
04.09.2014	1.53	1.51	19.68	63.35	93.49
05.09.2014	1.34	1.31	21.51	63.04	75.07
06.09.2014	1.18	1.36	22.08	59.67	70.66

Appendix

Date	Lysimeter	Calculation	T_{air}	*RH*	Incoming short-wave radiation
(DD.MM.JJJJ)	(L d^{-1} m^{-2})	L d^{-1} m^{-2})	(°C)	(%)	(W m^{-2})
07.09.2014	1.09	1.33	22.68	69.33	84.73
08.09.2014	1.05	1.34	20.99	65.93	90.46
09.09.2014	0.92	0.88	17.42	64.86	52.88
10.09.2014	0.69	0.41	15.47	80.33	25.98
11.09.2014	0.80	0.70	15.07	81.86	45.87
12.09.2014	0.58	0.16	16.78	86.97	7.74
13.09.2014	0.57	0.14	18.04	89.21	10.30
14.09.2014	0.54	0.28	18.33	88.09	19.24
15.09.2014	1.35	1.30	21.56	59.86	73.88
21.09.2014	0.99	0.24	16.65	85.16	22.28
09.10.2014	0.90	0.36	18.71	75.74	20.37
10.10.2014	0.82	0.38	16.64	79.27	28.24
11.10.2014	0.19	0.09	15.08	94.50	5.86
12.10.2014	0.70	0.47	15.19	80.85	37.39
13.10.2014	0.71	0.31	16.48	81.74	19.25
14.10.2014	0.75	0.16	16.07	81.59	21.68
15.10.2014	0.77	0.60	15.60	78.11	44.55
16.10.2014	0.35	0.04	12.92	89.24	8.00
17.10.2014	0.63	0.29	14.58	86.06	29.56
22.10.2014	0.27	0.12	10.10	94.97	4.68
23.10.2014	0.57	0.14	11.40	87.03	6.77
29.10.2014	0.56	0.33	7.82	75.37	29.18
30.10.2014	0.13	0.13	9.68	88.64	6.60
31.10.2014	0.21	0.21	11.82	88.78	18.17

List of publications in this dissertation

Postprint-Version, page 67-89 in this dissertation:

BUCHIN, O., HOELSCHER, M.-T., MEIER, F., NEHLS, T. and F. ZIEGLER (2015). Evaluation of the health-risk reduction potential of countermeasures to urban heat islands. *Energy and Buildings* 114 (2016): 27-37. https://doi.org/10.1016/j.enbuild.2015.06.038

Postprint-Version, page 35-50 in this dissertation:

HOELSCHER, M.-T., NEHLS, T., JÄNICKE, B. and G. WESSOLEK (2015). Quantifying cooling effects of facade greening: Shading, transpiration and insulation. *Energy and Buildings* 114 (2016): 283-290. https://doi.org/10.1016/j.enbuild.2015.06.047

Postprint-Version, page 51-65 in this dissertation:

HOELSCHER, M.-T., KERN, M.A., WESSOLEK, G. and T. NEHLS (2018). A new consistent sap flow baseline-correction approach for the stem heat balance method using nocturnal water vapour pressure deficits and its application in the measurements of urban climbing plant transpiration. *Agricultural and Forest Meteorology* 248: 169-176. https://doi.org/10.1016/j.agrformet.2017.09.014

Postprint-Version, page 11-34 in this dissertation:

JÄNICKE, B., MEIER, F., HOELSCHER, M.-T. and D. SCHERER (2015). Evaluating the effects of façade greening on human bioclimate in a complex urban environment. *Advances in Meteorology* 2015: 15 pp. https://doi.org/10.1155/2015/747259